Supporting Information

A novel access to phosphanylidene-phosphorane complexes via P-donor substitution and a detailed bonding analysis

David Biskup,[a] Gregor Schnakenburg,[a] René T. Boeré,[b] Arturo Espinosa Ferao*[c] and Rainer Streubel*[a]

[a]*Institut für Anorganische Chemie, Rheinische Friedrich-Wilhelms-Universität Bonn, Gerhard-Domagk-Str. 1, 53121 Bonn, Germany.*

[b]*Department of Chemistry and Biochemistry, University of Lethbridge, Lethbridge, AB T1K3M4, Canada.*

[c]*Departamento de Química Orgánica, Facultad de Química, Campus Espinardo, Universidad de Murcia, 30100 Murcia, Spain.*

Table of contents

1 General methods

All reactions were performed under dried and deoxygenated argon atmosphere using Schlenk or glovebox techniques. The used argon (>99.998%) was purified by a system of three columns (deoxygenation by a BTS copper catalyst (BASF PuriStar® R3-15S) at ca. 100 °C, removing moisture with silica gel, phosphorus pentoxide desiccant with indicator (Sicapent®) and calcium chloride). Glassware, spatulae, cannulae as well as filter papers were dried in a compartment dryer at 110 °C for at least one hour. Additionally, the glassware was heated with a heat gun (up to 550 °C) under active vacuum (<0.02 mbar) and filled with argon three times. Sterile syringes were purged with argon three times before use. The solvents were dried by standard procedures[1] by refluxing over proper desiccants under an argon atmosphere (*n*-pentane over sodium wire (Ø = 2 mm); benzene of potassium mirror; diethyl ether stabilized with 3,5-di-*tert*-butyl-4-hydroxytoluene (BHT) and tetrahydrofuran over benzo-phenone and sodium wire; dichloromethane over calcium hydride) for several days and distilled before use. Alternatively, diethyl ether was dried using a MBraun SPS-800 solvent purification system. For filtration stainless steel cannulae (Ø = 1 mm and 2 mm) with Whatman® glass microfiber filters (grade GF/B) were used if not stated otherwise. After use, devices made of stainless steel were cleaned with acetone, water and diluted hydrochloric acid and glassware by storage in a concentrated solution of potassium hydroxide in isopropanol for at least two days and in diluted hydrochloric acid for one day. Afterwards, the glassware was washed with water and soap, acetone and petroleum ether 40/65. All joints were greased with OKS 1112 grease or with PTFE paste (Carl Roth). Vacuum was applied by a rotary vane pump (vacuubrand RZ6) enabling pressures of $<10^{-2}$ mbar.

NMR spectra were recorded on a Bruker Avance I 300 MHz, Bruker Avance I 400 MHz or Bruker Avance III HD Ascend 500 MHz spectrometer at the NMR department of the University of Bonn and subsequently analysed by the program *Mestrenova 14.2*. The calibration of the ^{1}H and ^{13}C NMR spectra was done via the solvent residual signals relative to tetramethylsilane (<1% in $CDCl_3$) (C_6D_6: $\delta(^{1}H)$ = 7.16 ppm and $\delta(^{13}C)$ = 128.06 ppm, CD_2Cl_2: $\delta(^{1}H)$ = 5.32 ppm and $\delta(^{13}C)$ = 53.84 ppm, and THF-d_8: $\delta(^{1}H)$ = 1.72 ppm or 3.58 ppm and $\delta(^{13}C)$ = 25.31 ppm or 67.21 ppm).[2] ^{31}P NMR spectra were measured relative to 85% H_3PO_4(aq) as external reference by using the ^{2}H frequency of the deuterated solvent (lock frequency) and the frequency ratio value $\Xi(^{31}P)$ = 40.480742%.[3] All lock frequencies were calibrated internally against the ^{1}H signals of solutions of tetramethylsilane with a volume fraction of $\Phi \leq 1\%$ in the corresponding deuterated solvent. The used deuterated solvents were purified by distillation over proper desiccants (C_6D_6 and THF-d_8 over a potassium mirror and CD_2Cl_2 over CaH_2), trap-to-trap recondensation and degassing by three freeze-pump-thaw cycles. The purified solvent was stored over 3 Å or 4 Å molecular sieves. The chemical shift (δ) is given in parts per million (ppm) and the coupling constant ($^{n}J_{X,Y}$) in Hertz (Hz) as absolute values neglecting the sign where *n* is the number of bonds between the coupling nuclei X and Y. For assigning the multiplicity following

abbreviations were used: s = singlet, d = doublet, dd = doublet of doublets, dm = doublet of multiplets, t = triplet, q = quartet m = multiplet, sat = satellites and br = broad. For ^{1}H NMR spectra additionally the number of nuclei is given accordingly which is determined via integration. The ^{1}H and ^{13}C NMR signals of compounds were assigned by a combination of COSY, HSQC and HMBC experiments to unequivocally assign protons and carbon resonances if necessary. All measurements were performed at ambient temperature (298 K) if not stated otherwise.

Mass spectra using liquid injection field desorption ionisation (LIFDI) were recorded on a Thermo Finnigan MAT 90 sector field instrument equipped with a LIFDI ion source (Linden CMS). The samples were dissolved in toluene or tetrahydrofuran. The solutions were prepared in a glovebox using dried, recondensed and degassed solvents. Only selected data are given for detected ions. The peaks are given in mass-to-charge ratio (*m/z*) while only the isotopomer with the highest relative abundance is represented. Additionally, the relative intensities of the peaks are given in parentheses and the proposed molecule fragments in square brackets if not stated otherwise.

ATR-IR spectra of solids were recorded in the spectral range of 4000–400 cm^{-1} on a Bruker Alpha FTIR spectrometer with a single-reflection ATR measurement attachment (Platinum-ATR Diamond) or a Shimadzu IRSpirit FTIR spectrometer with a single-reflection ATR measurement attachment (QATR-S) in a glovebox at ambient temperature. For apodization the Happ-Genzel function was used. All analyses were performed using the programs *EZ OMNIC 7.3* of Fisher Scientific, *OPUS* of Bruker and *LabSolutions IR 2.26* of Shimadzu. Only selected wavenumbers of the absorption bands are given using reciprocal centimetres (cm^{-1}). The intensities of the bands are marked as strong (s), medium (m) or weak (w).

Elemental analyses were performed on a Elementar Vario Micro analysis device in quadruplicate or triplicate for each sample. All samples were prepared and weighed up in tin or silver sample containers using a micro-analytical balance in a glovebox. The mean C and H values are given for each compound.

Melting points were measured using an SRS DigiMelt device or a Büchi melting point determination device according to Dr. Tottoli. The samples were flame-sealed in a glass capillary (Ø = 0.1 mm) *in vacuo* (<0.02 mbar) and heated quickly (ca. 5 K/min) for a rough determination of the melting point or decomposition temperature. Afterwards, a heating rate of approximately 2 K/min was used until the sample melted or decomposed. The thermally treated samples were cooled to ambient temperature and studied by ^{1}H and/or ^{31}P NMR spectroscopy to confirm whether decomposition had occurred. No internal or external temperature corrections were performed.

Single crystal X-ray diffraction analyses were performed on a Bruker D8 Venture diffractometer, a STOE IPDS-2T diffractometer or a STOE STADIVARI diffractometer equipped with a low-temperature device

(Oxford Cryostream 700 series or 800 series) at 100(2) K or 120(2) K by using graphite monochromated Mo-K_α (λ = 0.71073 Å) or Cu-K_α radiation (λ = 1.54186 Å). Intensities were measured by fine-slicing Φ and ω scans and corrected background, polarization and Lorentz effects. A semi-empirical absorption correction was applied for the data sets following Blessing's method.[4] The structure was solved by direct methods and refined anisotropically by the least-squares procedure implemented in ShelX program system.[5] All non-hydrogen atoms were refined anisotropically. The hydrogen atoms were included isotropically refined using a riding model at the bound carbon atoms. The program *Olex2 1.5*[6] of *OlexSys* was used for analyses and the ellipsoid representations of the molecular structures with the probability level set to 50%. Crystallographic data for the structures reported in this paper have been deposited with the Cambridge Crystallographic Data Centre as supplementary publication no. CCDC-2282404 (**3a**), CCDC-2282405 (**3a-Cr**) and CCDC-2282406 (**3b**) which can be obtained free of charge via www.ccdc.cam.ac.uk/data_request/cif.

2 Experimental procedures and characterisation

Synthesis of complex 3a

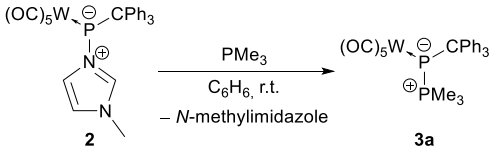

0.08 mL (0.78 mmol, 5.4 eq.) of trimethylphosphane was added dropwise to a solution of 0.098 g (0.14 mmol, 1.0 eq.) of complex **2**[7] in 5.0 mL of benzene at ambient temperature. The solution was stirred for 17 hours. The supernatant of the obtained yellow suspension was filtered off using a filter cannula (Ø = 1 mm). The product was obtained as yellow solid after drying for 80 minutes *in vacuo* at ambient temperature. Yield: 0.079 g (0.12 mmol, 81%). Mp 168 °C (dec.). Elemental analysis calcd (%) for $C_{27}H_{24}O_5P_2W$: C 48.10, H 3.59; found: C 48.16, H 3.80. IR (ATR Diamond): ν_{max} / cm^{-1} = 1911 (s) (CO), 1975 (m) (CO), 2059 (m) (CO). ^{1}H NMR (500.04 MHz, THF-d_8, 298 K): δ / ppm = 7.69–7.67 (m, 6H; CPh_3), 7.24–7.21 (m, 6H; CPh_3), 7.14–7.11 (m, 3H; CPh_3), 1.28 (dd, $^2J_{P,H}$ = 12.14 Hz, $^3J_{P,H}$ = 2.48 Hz, 9H; C*H*$_3$). ^{13}C{^{1}H} NMR (125.75 MHz, THF-d_8, 298 K): δ / ppm = 200.8 (d, $^2J_{P,C}$ = 15.5 Hz; *trans*-*C*O), 200.0 (dd_{sat}, $^2J_{P,C}$ = 4.3 Hz, $^3J_{P,C}$ = 4.3 Hz, $^1J_{W,C}$ = 125.4 Hz; *cis*-*C*O), 148.5 (br s; *ipso*-*C*), 131.6 (d, $J_{P,C}$ = 10.4 Hz; Ph), 128.8 (s; Ph), 126.8 (d, $J_{P,C}$ = 0.9 Hz; Ph), 59.3 (dd, $^1J_{P,C}$ = 33.5 Hz, $^2J_{P,C}$ = 3.2 Hz; P-*C*Ph_3), 15.4 (dd, $^1J_{P,C}$ = 42.6 Hz, $^2J_{P,C}$ = 8.7 Hz; P(*C*H_3)$_3$). ^{31}P{^{1}H} NMR (202.44 MHz, THF-d_8, 298 K): δ / ppm = 16.9 (d_{sat}, $^1J_{P,P}$ = 456.3 Hz, $^1J_{P,C}$ = 42.6 Hz; *P*Me_3), −20.9 (d_{sat}, $^1J_{P,P}$ = 456.3 Hz, $^1J_{W,P}$ = 120.6 Hz; W-*P*CPh_3). ^{31}P NMR (202.44 MHz, THF-d_8, 298 K): δ / ppm = 16.9 (dm_{sat}, $^1J_{P,P}$ = 456.3 Hz, $^1J_{P,C}$ = 42.6 Hz; *P*Me_3), −20.9 (d_{sat}, $^1J_{P,P}$ = 456.3 Hz, $^1J_{W,P}$ = 120.6 Hz; W-*P*CPh_3). MS (LIFDI, selected data): *m/z* (%) = 674.0 (100) $[M]^+$, 243.1 (91) $[CPh_3]^+$.

Synthesis of complex 3a-Cr

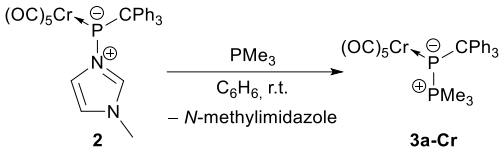

0.24 mL (2.33 mmol, 5.2 eq.) of trimethylphosphane was added to a solution of 0.246 g (0.45 mmol, 1.0 eq.) of complex **2-Cr**[7] in 10 mL of benzene at ambient temperature. The solution was stirred for 22 hours. The supernatant of the obtained yellow suspension was filtered off using a filter cannula (Ø = 1 mm). The solid residue was redissolved in 15 mL of dichloromethane. After addition of 15 mL of *n*-pentane to form a yellow precipitate. The product was washed three times with 4 mL of *n*-pentane and obtained as yellow solid after drying for 1.5 hours *in vacuo* at ambient temperature. Yield: 0.191 g (0.35 mmol, 79%). Mp 150 °C (dec.). Elemental analysis calcd (%) for $C_{27}H_{24}O_5P_2Cr$: C 59.79, H 4.46; found: C 59.53, H 4.75. IR (ATR Diamond): ν_{max} / cm^{-1} = 1875 (s) (CO), 1918 (s) (CO), 1974 (w) (CO), 2048 (m) (CO). ^1H NMR (400.13 MHz, CD_2Cl_2, 298 K): δ / ppm = 7.66–7.64 (m, 6H; CPh_3), 7.30–7.25 (m, 6H; CPh_3), 7.19–7.14 (m, 3H; CPh_3), 1.25 (dd, $^2J_{P,H}$ = 10.36 Hz, $^3J_{P,H}$ = 10.36 Hz, 9H; C*H*$_3$). $^{13}C\{^1H\}$ NMR (125.75 MHz, CD_2Cl_2, 298 K): δ / ppm = 224.0 (s; *trans*-*C*O), 218.5 (d, $^2J_{P,C}$ = 5.2 Hz; *cis*-*C*O), 147.8 (br s; *ipso*-*C*), 130.8 (d, $J_{P,C}$ = 9.2 Hz; Ph), 128.3 (s; Ph), 126.3 (s; Ph), 59.3 (d, $^1J_{P,C}$ = 41.7 Hz; P-*C*Ph_3), 16.0 (dd, $^1J_{P,C}$ = 39.4 Hz, $^2J_{P,C}$ = 11.2 Hz; P(*C*H_3)$_3$). $^{31}P\{^1H\}$ NMR (162.00 MHz, CD_2Cl_2, 298 K): δ / ppm = 17.3 (d, $^1J_{P,P}$ = 484.1 Hz; *P*Me_3), 12.5 (d, $^1J_{P,P}$ = 484.1 Hz; Cr-*P*CPh_3). ^{31}P NMR (162.00 MHz, CD_2Cl_2, 298 K): δ / ppm = 17.3 (dm, $^1J_{P,P}$ = 484.1 Hz; *P*Me_3), 12.5 (d, $^1J_{P,P}$ = 484.1 Hz; Cr-*P*CPh_3). MS (LIFDI, selected data): *m/z* (%) = 542.0 (100) $[M]^+$, 243.1 (85) $[CPh_3]^+$.

Synthesis of complex 3b

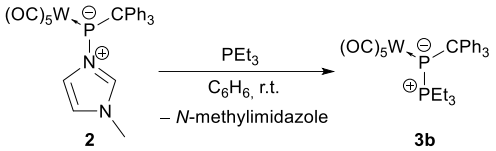

0.13 mL (0.88 mmol, 5.0 eq.) of triethylphosphane was added to a solution of 0.119 g (0.18 mmol, 1.0 eq.) of complex **2**[7] in 5.0 mL of benzene at ambient temperature. The solution was stirred for 16 hours. All volatiles were removed *in vacuo* at ambient temperature. The product was obtained as yellow-orange solid after drying for 3.5 hours *in vacuo*. Yield: 0.112 g (0.16 mmol, 89%). Mp 122 °C (dec.). Elemental analysis calcd (%) for $C_{30}H_{30}O_5P_2W$: C 50.30, H 4.22; found: C 50.39, H 4.34. IR (ATR Diamond): ν_{max} / cm^{-1} = 1905 (s) (CO), 1978 (m) (CO), 2056 (m) (CO). ^1H NMR (300.13 MHz, C_6D_6, 298 K): δ / ppm = 7.84–7.80 (m, 6H; CPh_3), 7.10–7.04 (m, 6H; CPh_3), 6.95–6.90 (m, 3H; CPh_3), 1.26–1.15 (m, 6H; C*H*$_2$), 0.56–0.46 (m, 9H; C*H*$_3$). $^1H\{^{31}P\}$ NMR (300.13 MHz, C_6D_6, 298 K): δ / ppm = 7.84–7.80 (m, 6H; CPh_3), 7.10–7.04 (m, 6H; CPh_3), 6.95–6.90 (m, 3H; CPh_3), 1.21 (q, $^3J_{H,H}$ = 7.63 Hz, 6H; C*H*$_2$), 0.51 (t, $^3J_{H,H}$

= 7.63 Hz, 9H; CH_3). $^{13}C\{^1H\}$ NMR (75.48 MHz, C_6D_6, 298 K): δ / ppm = 200.0 (s; *trans*-*C*O), 199.5 (dd, $^2J_{P,C}$ = 3.9 Hz, $^3J_{P,C}$ = 3.9 Hz; *cis*-*C*O), 148.2 (dd, $J_{P,C}$ = 7.9 Hz, $J_{P,C}$ = 5.1 Hz; *ipso*-*C*), 130.8 (dd, $J_{P,C}$ = 14.3 Hz, $J_{P,C}$ = 10.8 Hz; Ph), 128.7 (s; Ph), 126.1 (s; Ph), 58.5 (dd, $^1J_{P,C}$ = 35.4 Hz, $^2J_{P,C}$ = 3.5 Hz; P-*C*Ph_3), 16.6 (dd, $^1J_{P,C}$ = 36.4 Hz, $^2J_{P,C}$ = 6.6 Hz; P(*C*$H_2CH_3)_3$), 7.6 (br s; P(CH_2*C*$H_3)_3$). $^{31}P\{^1H\}$ NMR (121.51 MHz, C_6D_6, 298 K): δ / ppm = 33.3 (d, $^1J_{P,P}$ = 476.9 Hz; *P*Et_3), −28.6 (d_{sat}, $^1J_{P,P}$ = 476.9 Hz, $^1J_{W,P}$ = 123.9 Hz; W-*P*CPh_3). ^{31}P NMR (121.51 MHz, C_6D_6, 298 K): δ / ppm = 33.3 (dm, $^1J_{P,P}$ = 476.9 Hz; *P*Et_3), −28.6 (d_{sat}, $^1J_{P,P}$ = 476.9 Hz, $^1J_{W,P}$ = 123.9 Hz; W-*P*CPh_3). MS (LIFDI, selected data): *m/z* (%) = 716.3 (56) $[M]^+$, 474.1 (17) $[M-CPh_3+H]^+$, 243.2 (100) $[CPh_3]^+$.

Synthesis of complex 3c

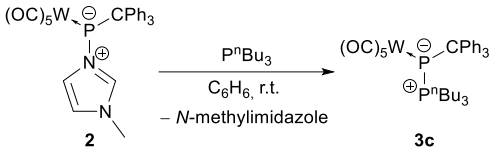

0.20 mL (0.81 mmol, 5.0 eq.) of tri-*n*-butylphosphane was added to a solution of 0.109 g (0.16 mmol, 1.0 eq.) of complex **2**[7] in 5.0 mL of benzene at ambient temperature. The solution was stirred for 20 hours. All volatiles were removed *in vacuo* at ambient temperature and the obtained yellow solid was dried under the same conditions for 2 hours. The product was recrystallized in 10 mL of a 7:1 *n*-pentane/diethyl ether mixture at −40 °C. The supernatant was filtered off using a filter cannula (Ø = 1 mm) at −40 °C and the yellow needle-shaped crystals were washed three times with 1 mL of *n*-pentane at −40 °C. The product was obtained as yellow solid after drying for 1.5 hours *in vacuo* at ambient temperature. Yield: 0.076 g (0.09 mmol, 59%). Mp 120 °C (dec.). Elemental analysis calcd (%) for $C_{36}H_{42}O_5P_2W$: C 54.01, H 5.29; found: C 53.97, H 5.47. IR (ATR Diamond): ν_{max} / cm^{-1} = 1905 (s) (CO), 1968 (m) (CO), 2056 (m) (CO). ^{1}H NMR (500.04 MHz, THF-d_8, 298 K): δ / ppm = 7.75–7.73 (m, 6H; CPh_3), 7.24–7.20 (m, 6H; CPh_3), 7.13–7.10 (m, 3H; CPh_3) 1.62–1.56 (m, 6H; PCH_2), 1.48–1.41 (m, 6H; PCH_2CH_2), 1.29–1.22 (m, 6H; CH_2CH_3), 0.86 (t, $^3J_{H,H}$ = 7.36 Hz, 9H; CH_3). ^{13}C{^{1}H} NMR (125.75 MHz, THF-d_8, 298 K): δ / ppm = 200.7 (d, $^1J_{P,C}$ = 15.4 Hz; *trans*-CO), 200.2 (dd_{sat}, $^2J_{P,C}$ = 3.9 Hz, $^3J_{P,C}$ = 3.9 Hz, $^1J_{W,C}$ = 125.6 Hz; *cis*-CO), 148.9 (dd, $J_{P,C}$ = 7.9 Hz, $J_{P,C}$ = 5.1 Hz; *ipso*-C), 131.5 (d, $J_{P,C}$ = 10.6 Hz; Ph), 128.8 (s; Ph), 126.7 (s; Ph), 59.4 (dd, $^1J_{P,C}$ = 36.1 Hz, $^2J_{P,C}$ = 3.7 Hz; P-CPh_3), 26.5 (dd, $J_{P,C}$ = 6.5 Hz, $J_{P,C}$ = 3.5 Hz; PCH_2CH_2), 25.0 (d, $J_{P,C}$ = 13.7 Hz; CH_2CH_3), 24.7 (dd, $^1J_{P,C}$ = 35.2 Hz, $^2J_{P,C}$ = 5.8 Hz; PCH_2CH_2), 13.8 (s; CH_3). ^{31}P{^{1}H} NMR (202.44 MHz, THF-d_8, 298 K): δ / ppm = 28.8 (d_{sat}, $^1J_{P,P}$ = 471.6 Hz, $^1J_{P,C}$ = 35.3 Hz; P^nBu_3), −25.0 (d_{sat}, $^1J_{P,P}$ = 471.6 Hz, $^1J_{W,P}$ = 122.1 Hz; W-$PCPh_3$). ^{31}P NMR (202.44 MHz, THF-d_8, 298 K): δ / ppm = 28.8 (dm, $^1J_{P,P}$ = 471.6 Hz; P^nBu_3), −25.0 (d_{sat}, $^1J_{P,P}$ = 471.6 Hz, $^1J_{W,P}$ = 122.1 Hz; W-$PCPh_3$). MS (LIFDI, selected data): *m/z* (%) = 800 (18) $[M]^+$, 243 (100) $[CPh_3]^+$.

Preparation of complexes 3a–c via Li/Cl phosphinidenoid complex 1

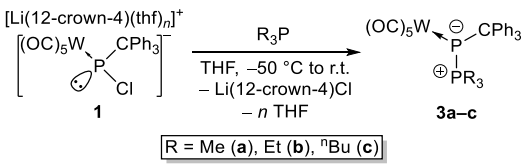

A solution of a Li/Cl phosphinidenoid tungsten(0) complex **1** was prepared using 1.0 eq. of $[W(CO)_5\{P(CPh_3)Cl_2\}]$, 1.0 eq. of 12-crown-4 and 1.0 eq. of *tert*-butyl lithium in THF at −80 °C. Afterwards, 1.5 eq. of the phosphane was added to the solution of **1** *in situ* dropwise at −50 °C. The reaction mixture was slowly warmed up to ambient temperature within circa 16 h. All volatiles were

removed *in vacuo* and the product was extracted three times using diethyl ether. The products were obtained after removing the solvent *in vacuo* at ambient temperature and drying under the same conditions.

3 NMR spectra

Compound 3a

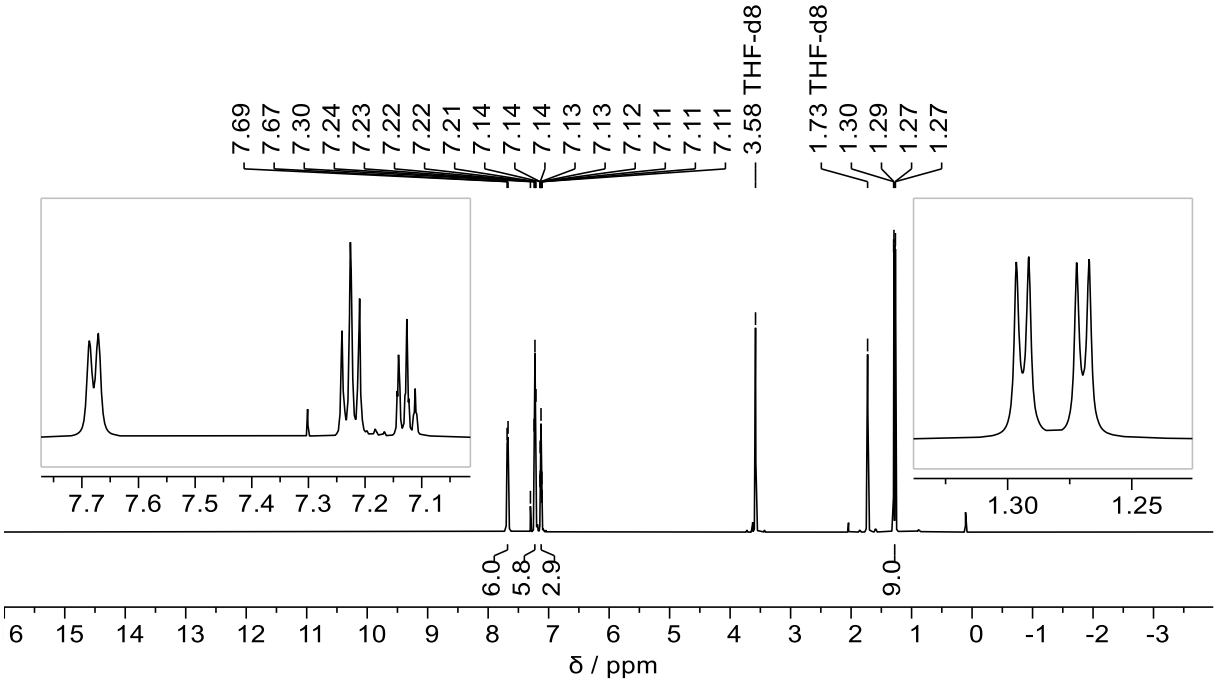

Fig. S1 ^{1}H NMR spectrum (500.04 MHz, THF-d_8, 298 K) of compound **3a**.

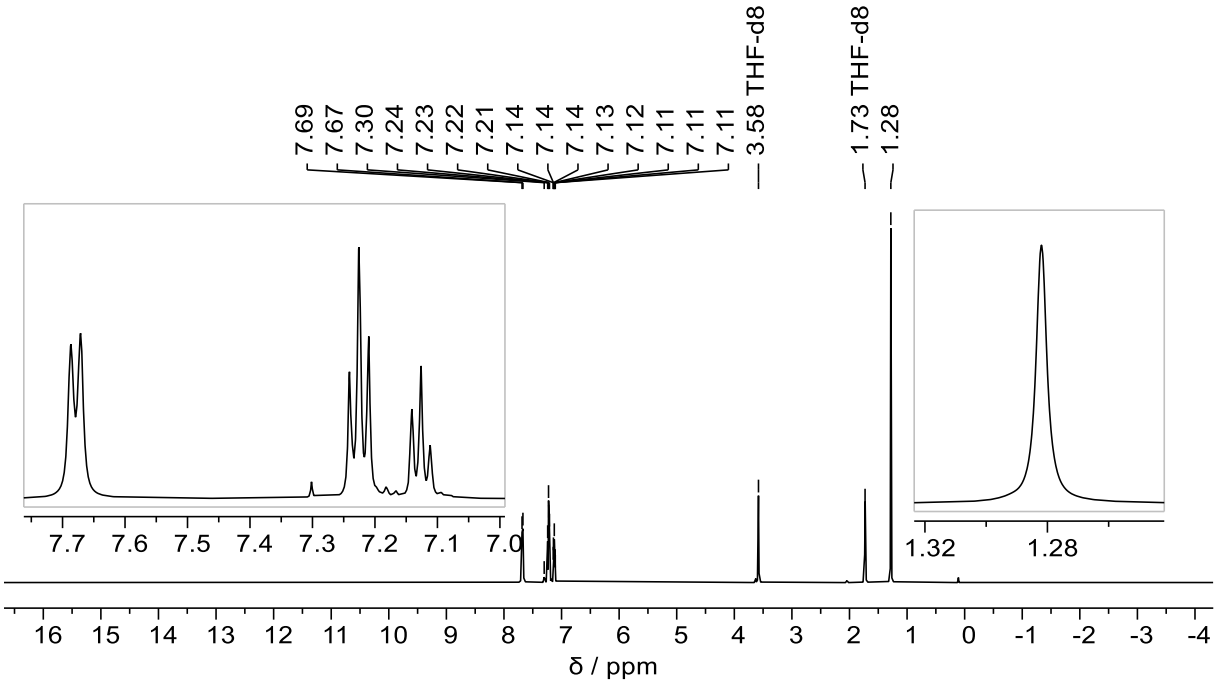

Fig. S2 ^{1}H{^{31}P} NMR spectrum (500.04 MHz, THF-d_8, 298 K) of compound **3a**.

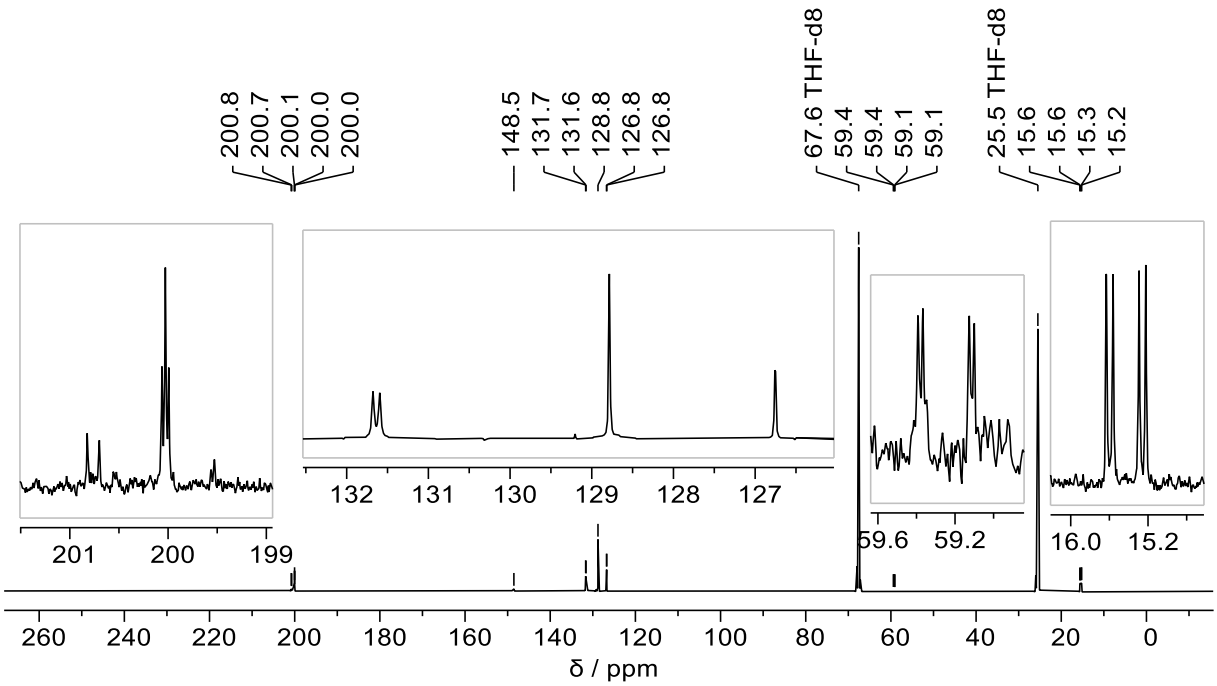

Fig. S3 $^{13}C\{^{1}H\}$ NMR spectrum (125.75 MHz, THF-d_8, 298 K) of compound **3a**.

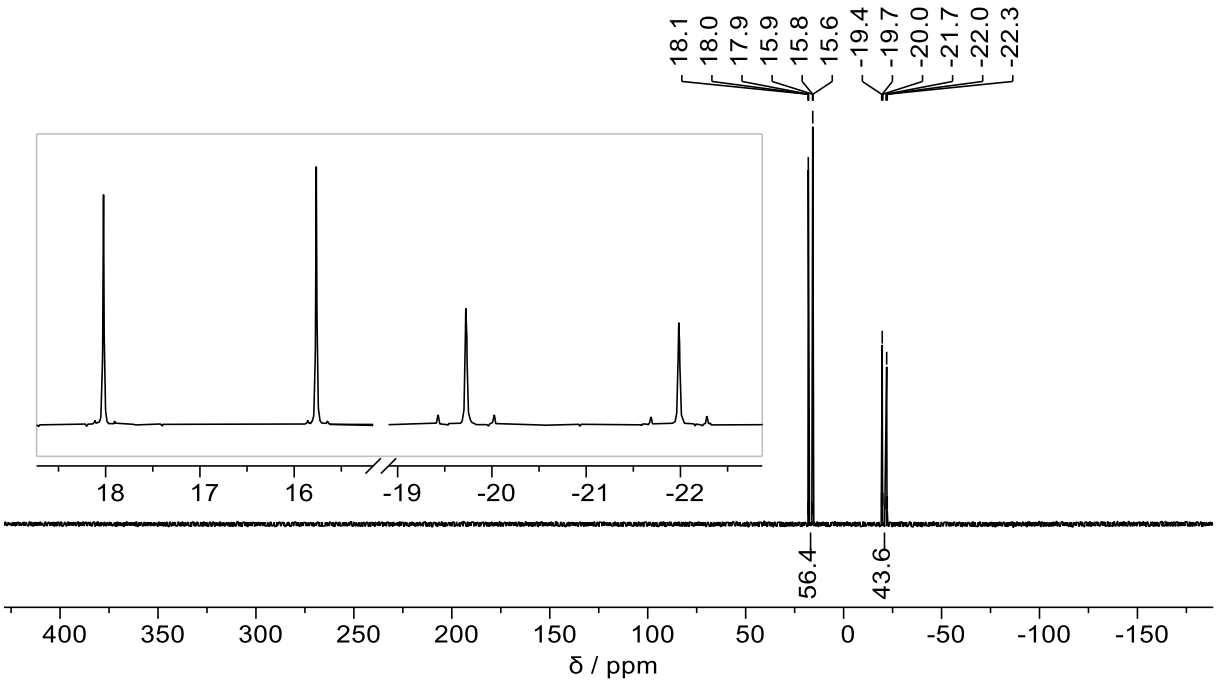

Fig. S4 $^{31}P\{^{1}H\}$ NMR spectrum (202.44 MHz, THF-d_8, 298 K) of compound **3a**.

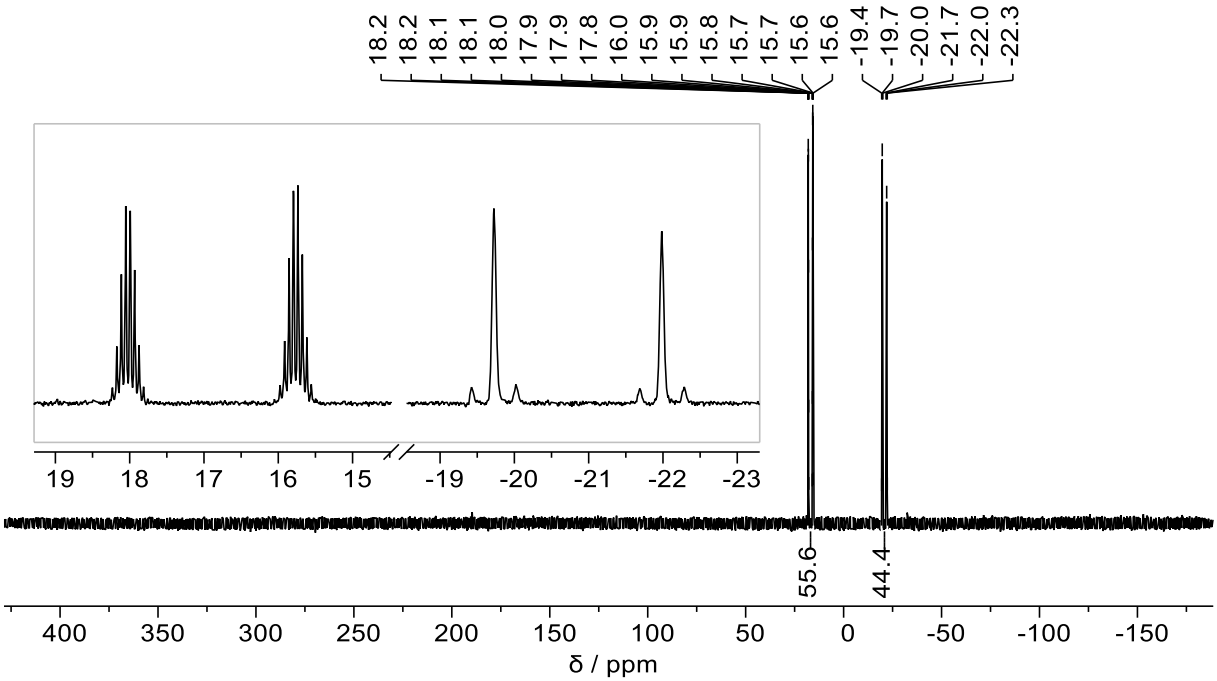

Fig. S5 ^{31}P NMR spectrum (202.44 MHz, THF-d_8, 298 K) of compound **3a**.

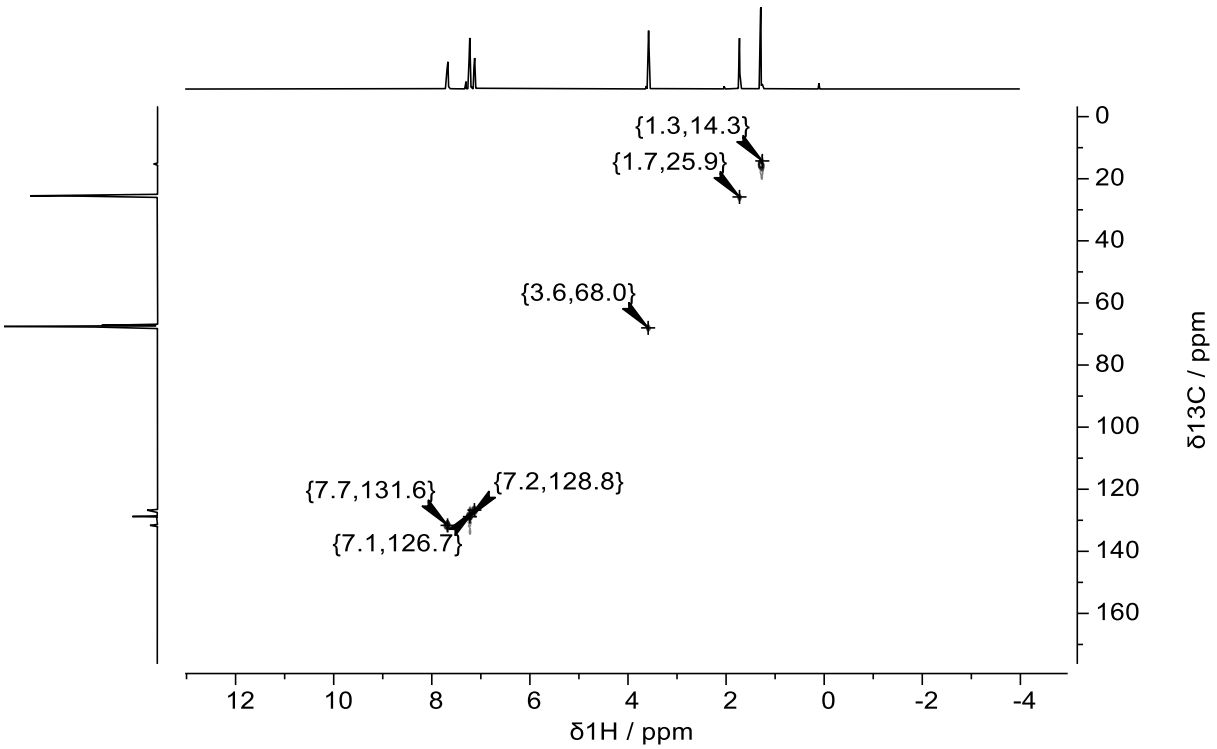

Fig. S6 ^{1}H,^{13}C HSQC NMR spectrum (500.04 MHz, 125.75 MHz, THF-d_8, 298 K) of compound **3a**.

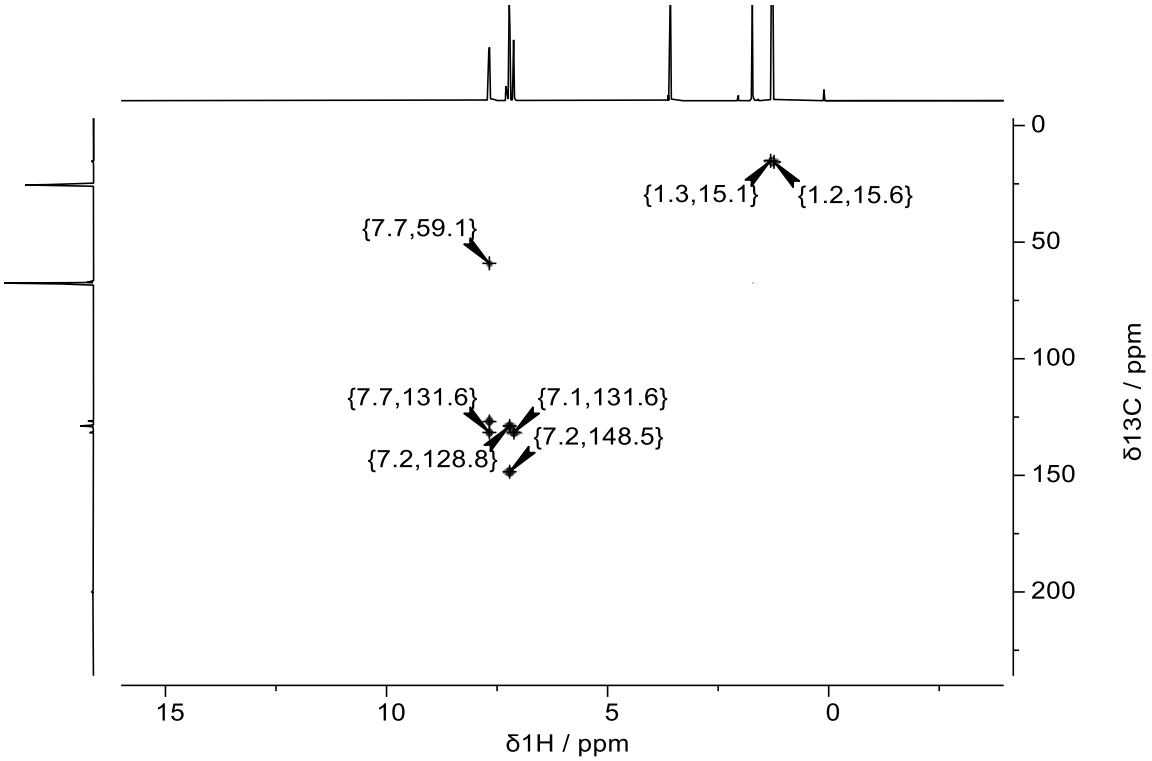

Fig. S7 ^{1}H,^{13}C HMBC NMR spectrum (500.04 MHz, 125.75 MHz, THF-d_8, 298 K) of compound **3a**.

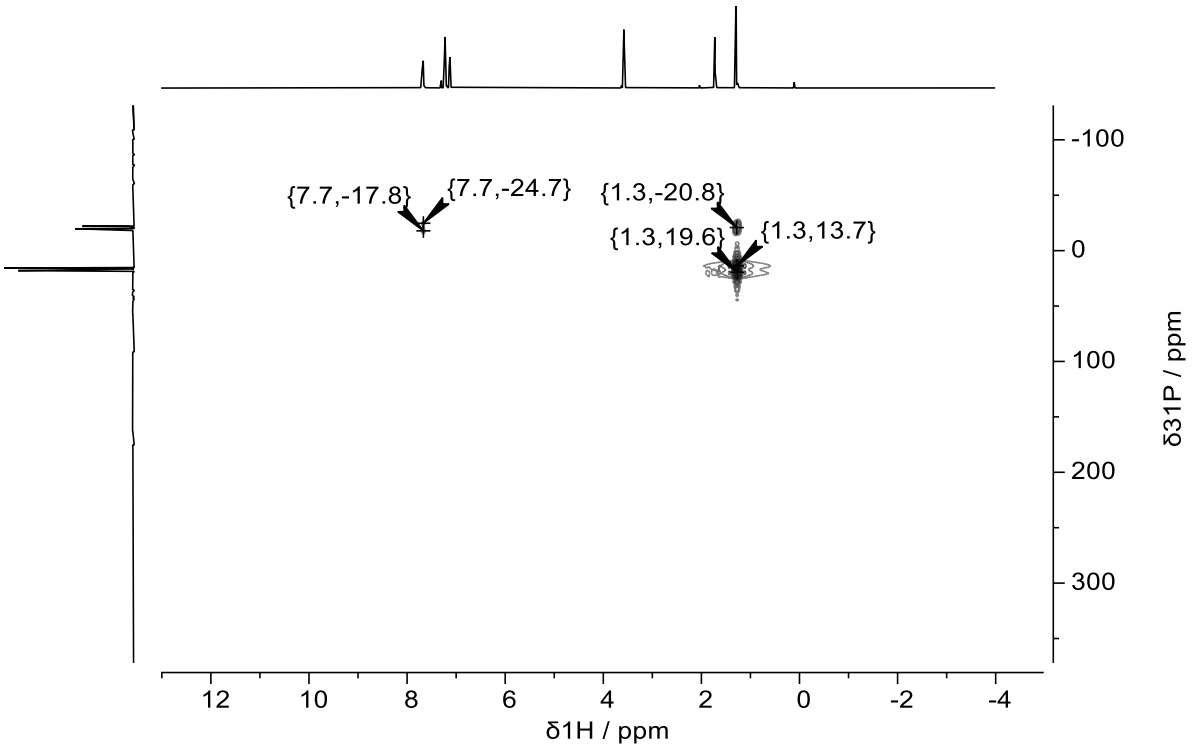

Fig. S8 ^{1}H,^{31}P HMBC NMR spectrum (500.04 MHz, 202.44 MHz, THF-d_8, 298 K) of compound **3a**.

Compound 3a-Cr

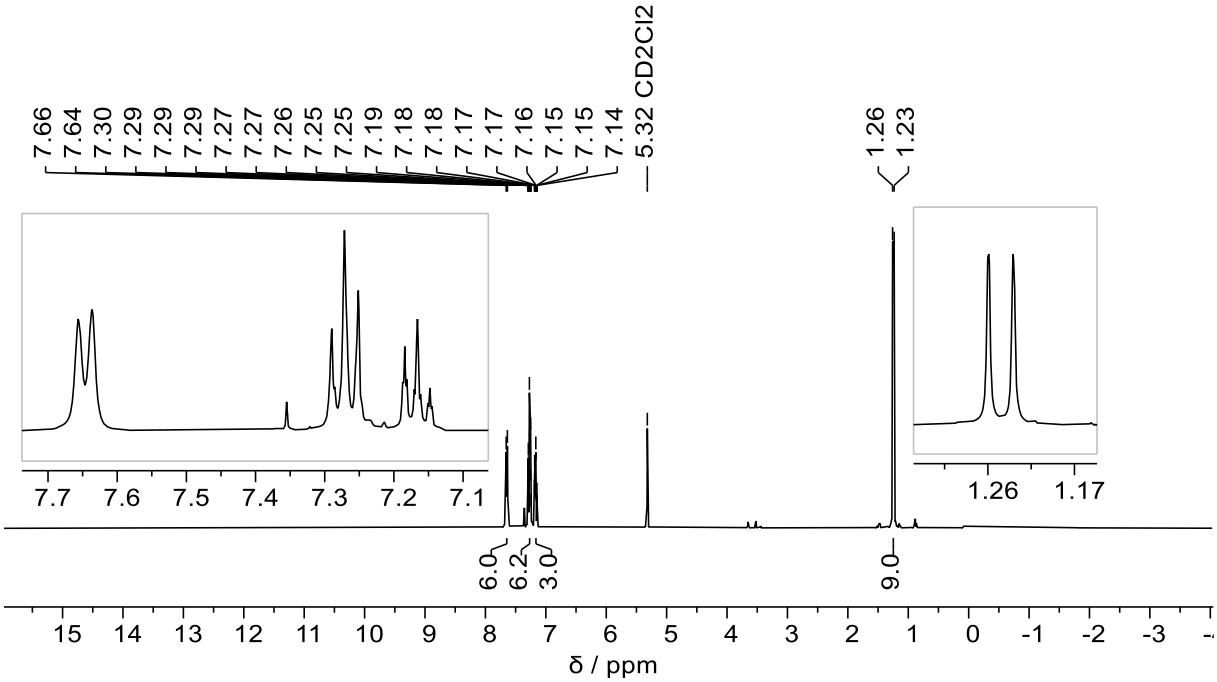

Fig. S9 ^{1}H NMR spectrum (400.13 MHz, CD_2Cl_2, 298 K) of compound **3a-Cr**.

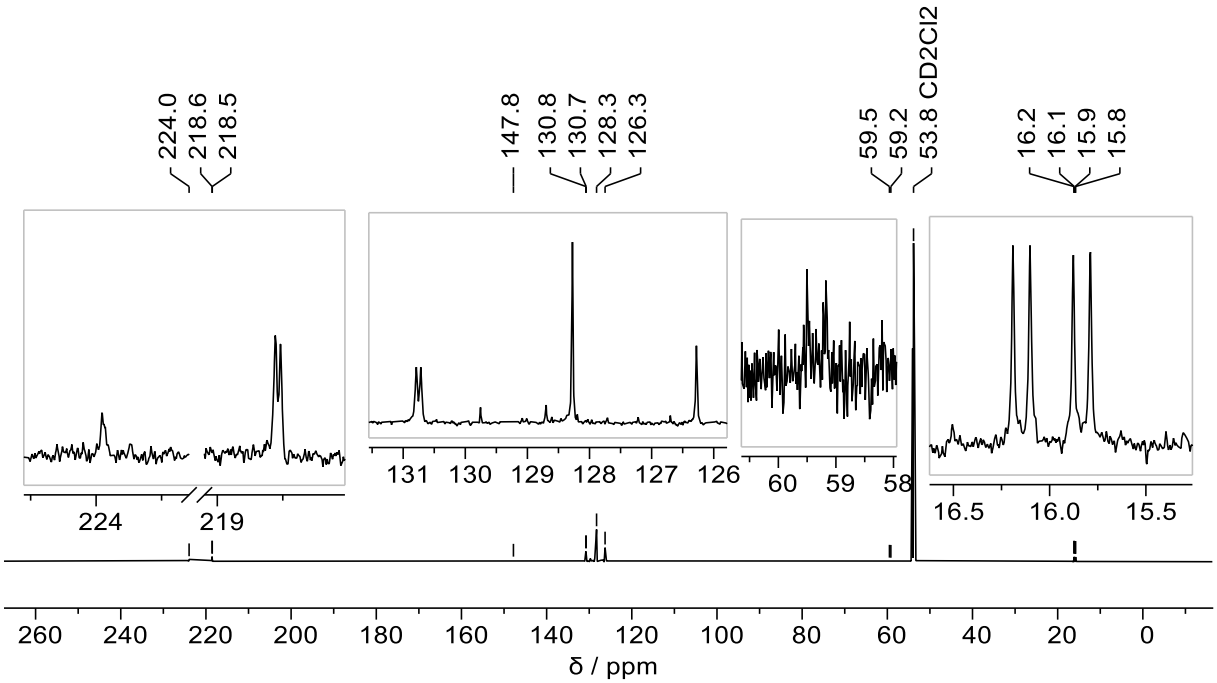

Fig. S10 $^{13}C\{^{1}H\}$ NMR spectrum (125.75 MHz, CD_2Cl_2, 298 K) of compound **3a-Cr**.

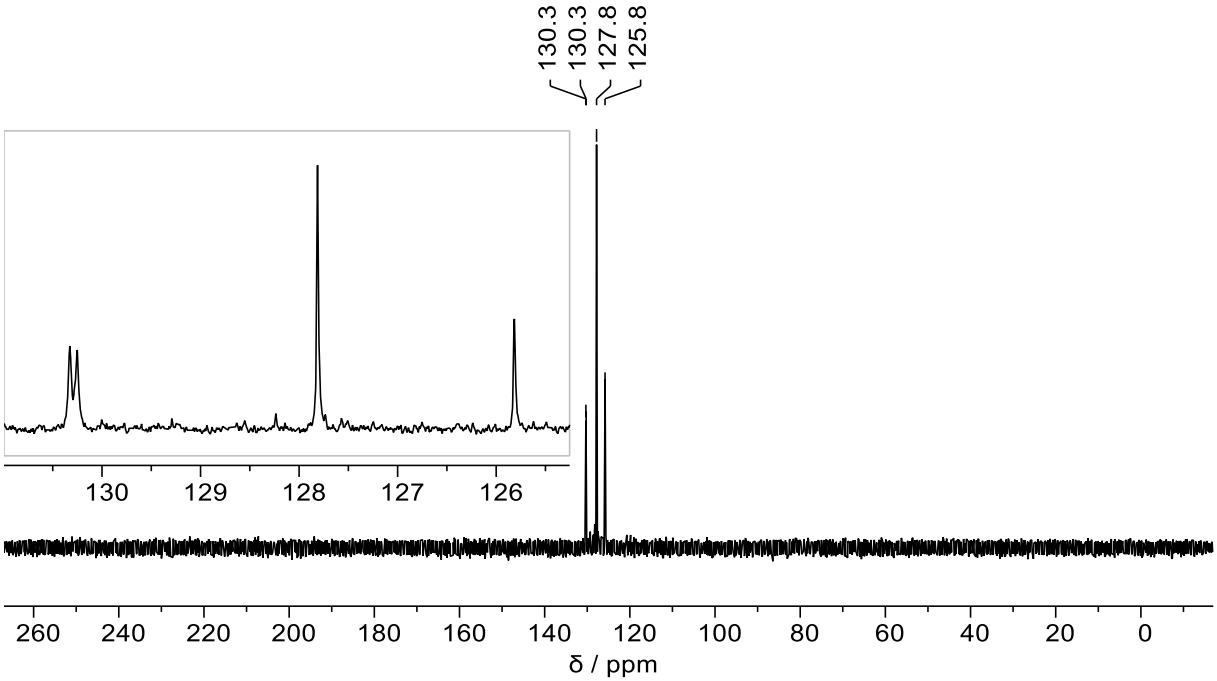

Fig. S11 ^{13}C DEPT90 NMR spectrum (125.75 MHz, CD_2Cl_2, 298 K) of compound **3a-Cr**.

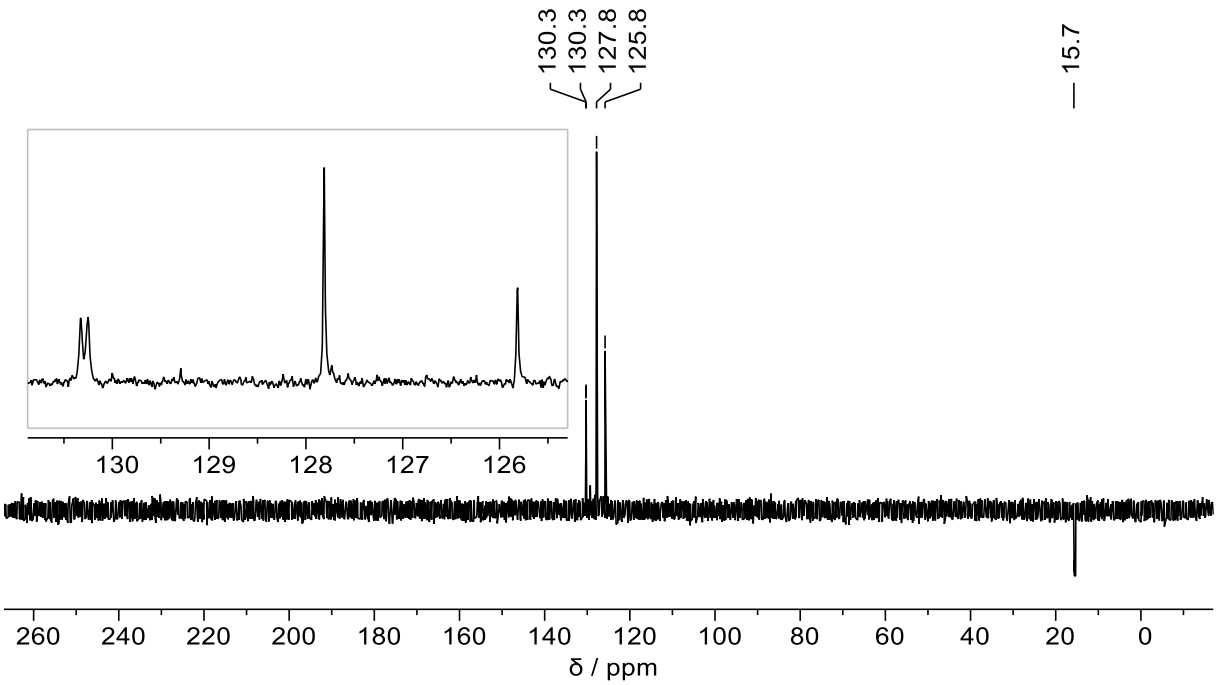

Fig. S12 ^{13}C DEPT135 NMR spectrum (125.75 MHz, CD_2Cl_2, 298 K) of compound **3a-Cr**.

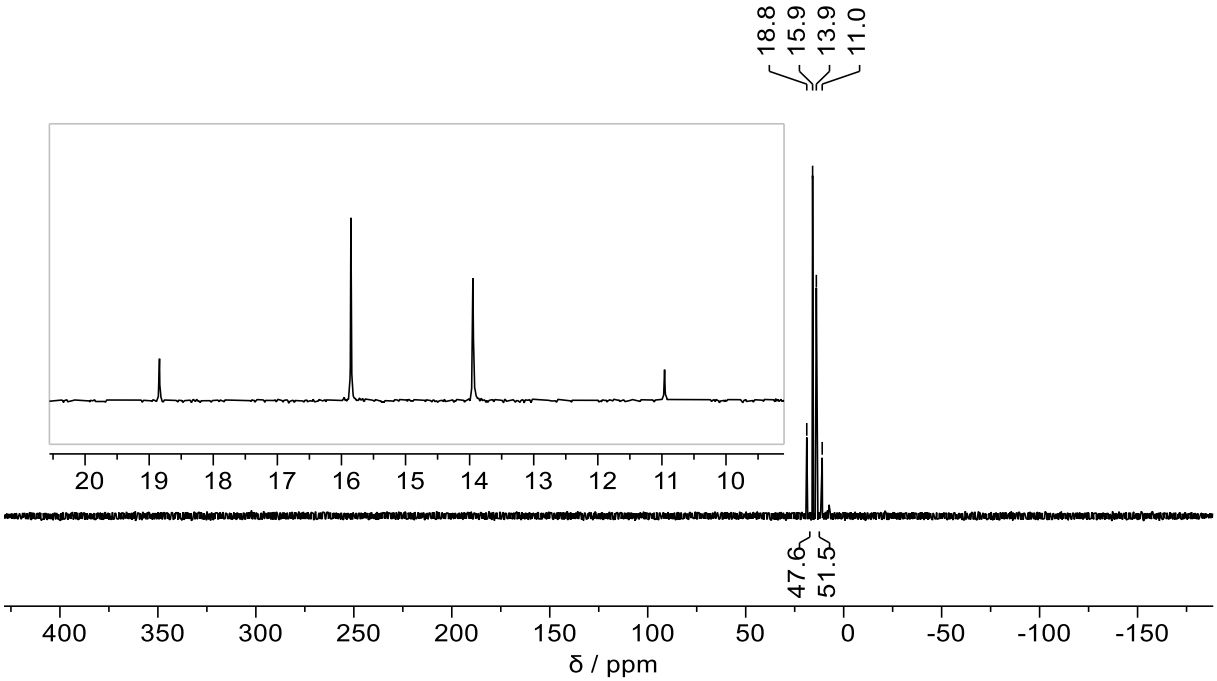

Fig. S13 $^{31}P\{^{1}H\}$ NMR spectrum (162.00 MHz, CD_2Cl_2, 298 K) of compound **3a-Cr**.

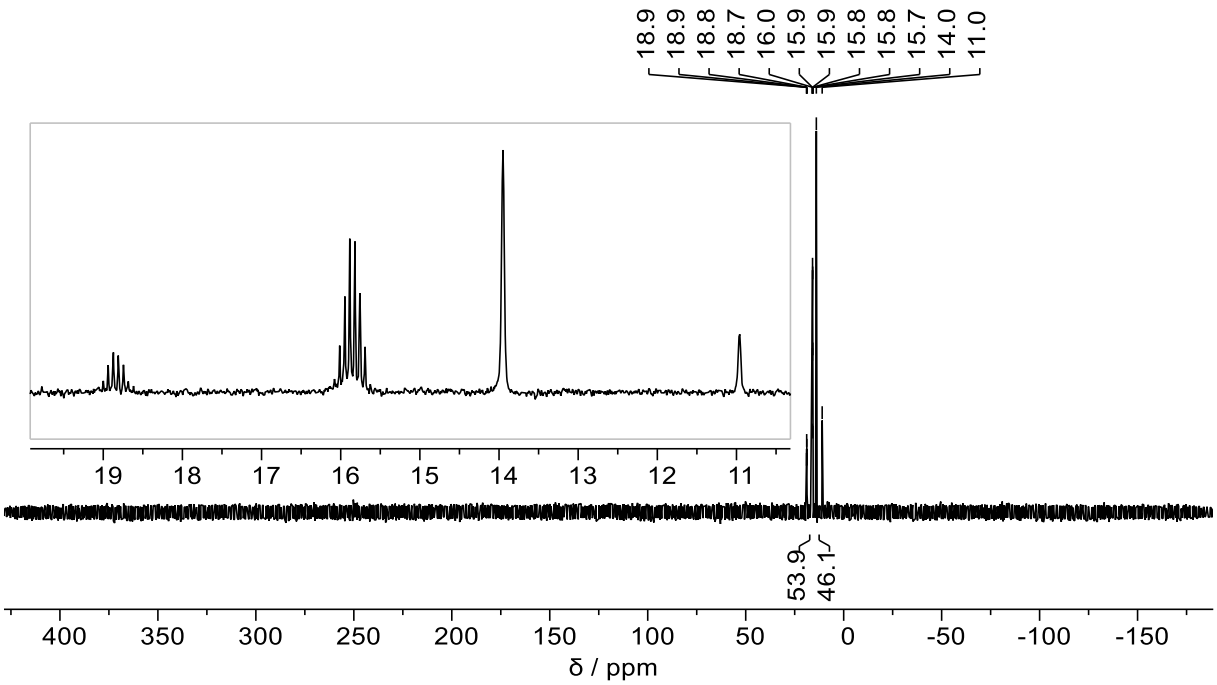

Fig. S14 ^{31}P NMR spectrum (162.00 MHz, CD_2Cl_2, 298 K) of compound **3a-Cr**.

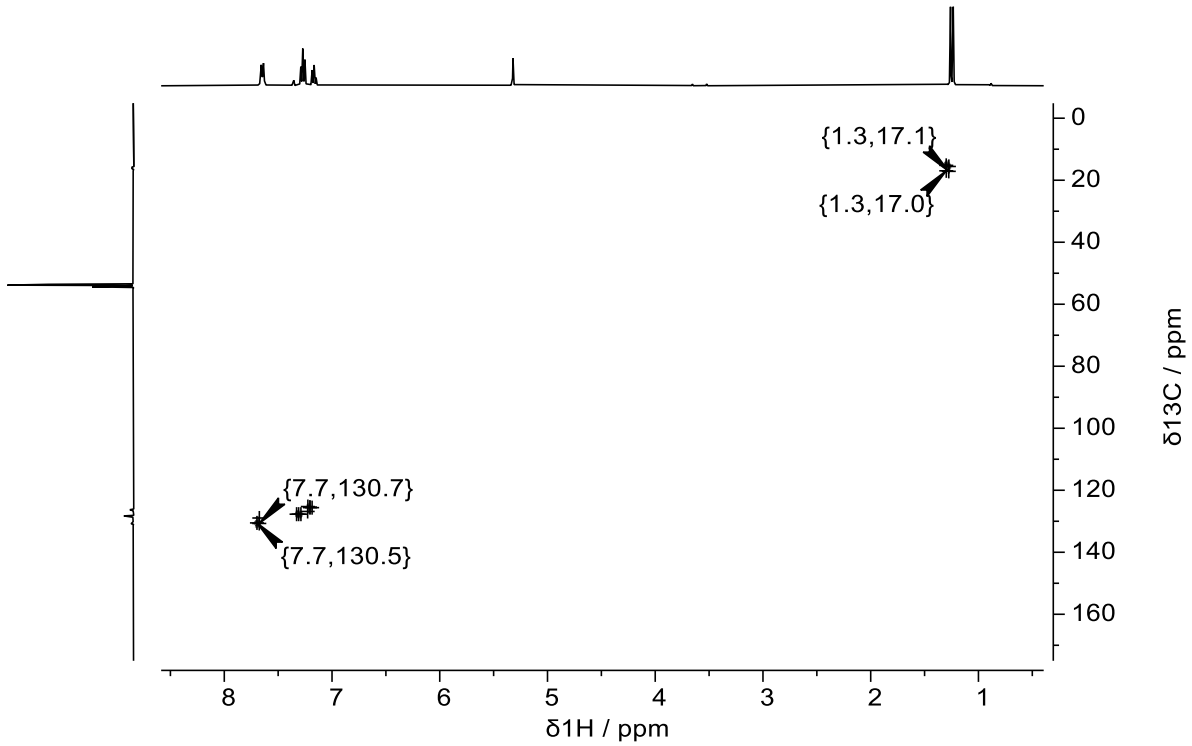

Fig. S15 $^{1}H,^{13}C$ HSQC NMR spectrum (400.13 MHz, 100.62 MHz, CD_2Cl_2, 298 K) of compound **3a-Cr**.

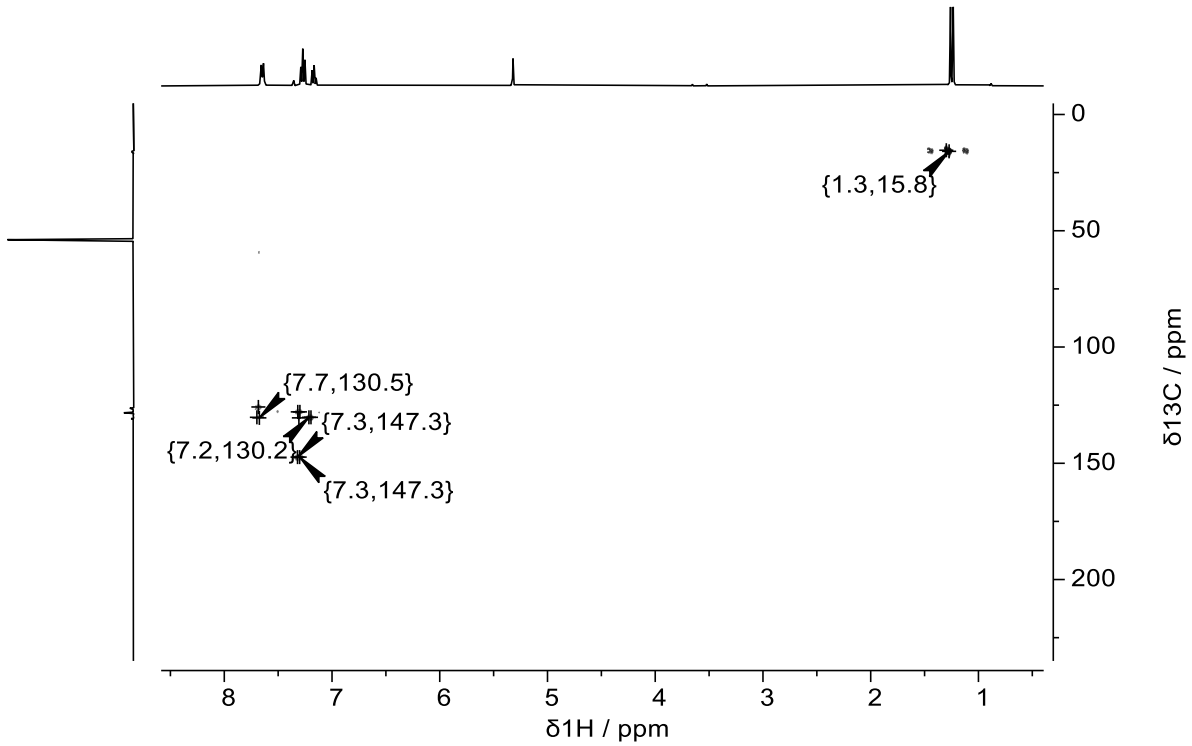

Fig. S16 $^{1}H,^{13}C$ HMBC NMR spectrum (400.13 MHz, 100.62 MHz, CD_2Cl_2, 298 K) of compound **3a-Cr**.

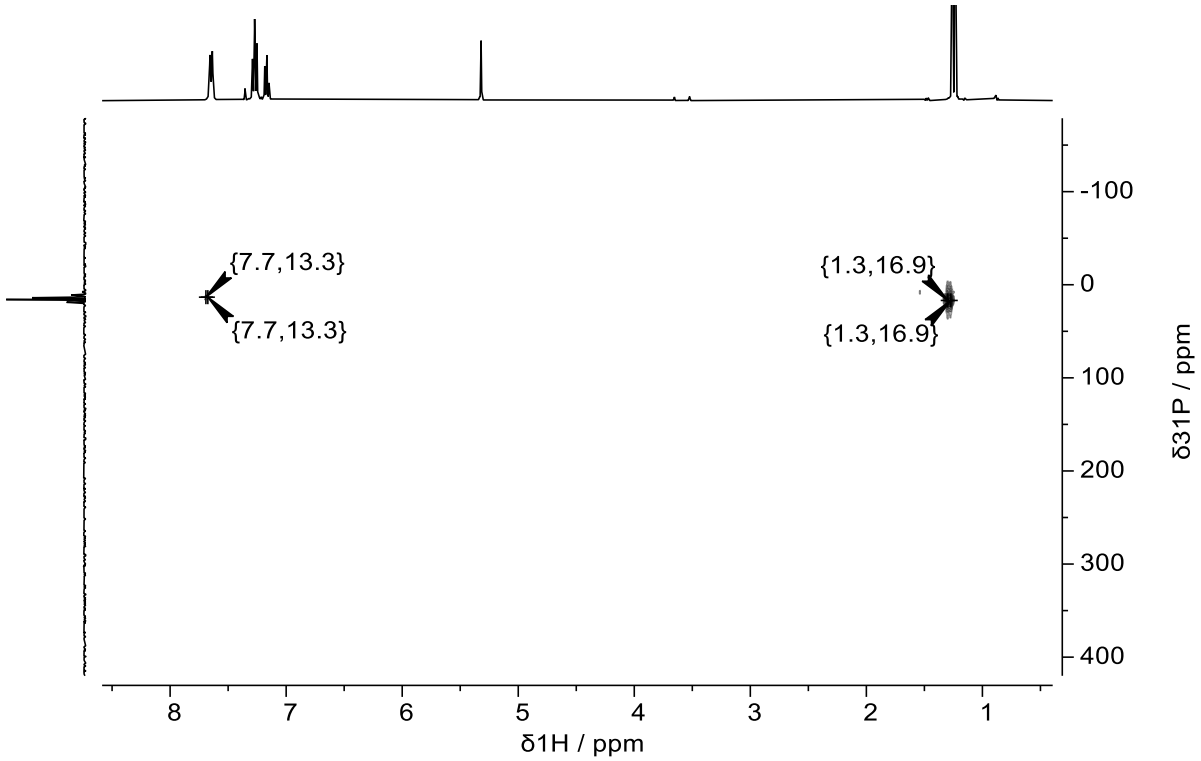

Fig. S17 $^{1}H,^{31}P$ HMBC NMR spectrum (400.13 MHz, 162.00 MHz, CD_2Cl_2, 298 K) of compound **3a-Cr**.

Compound 3b

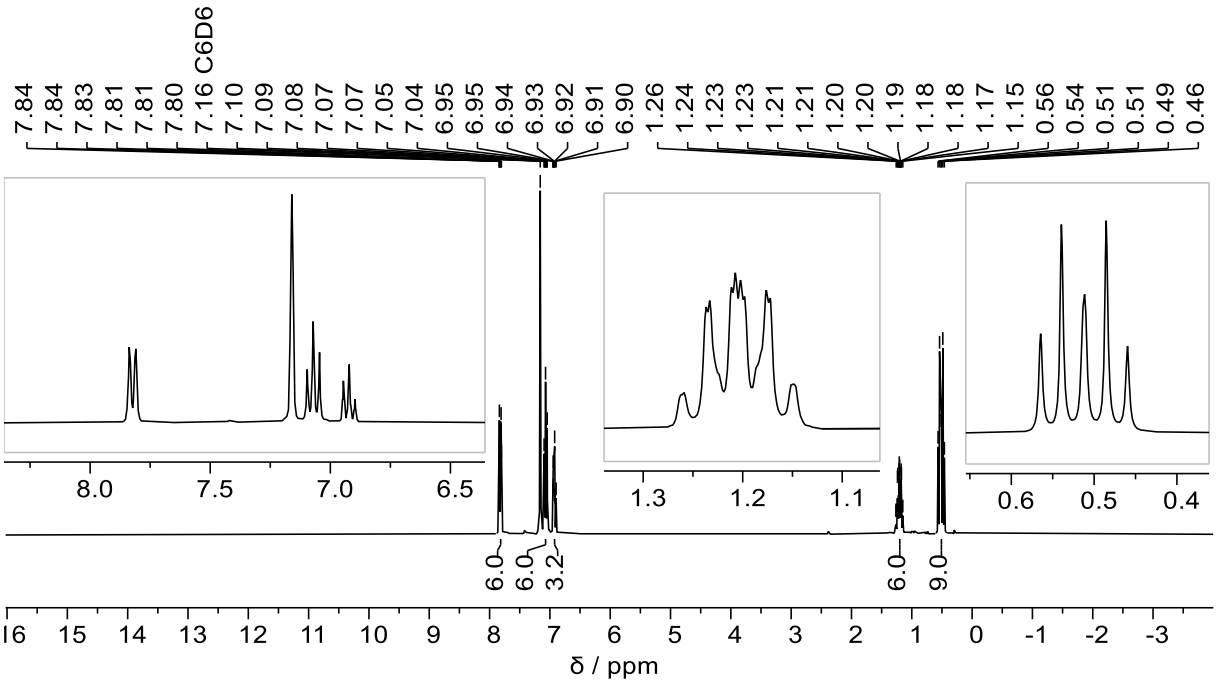

Fig. S18 ^{1}H NMR spectrum (300.13 MHz, C_6D_6, 298 K) of compound **3b**.

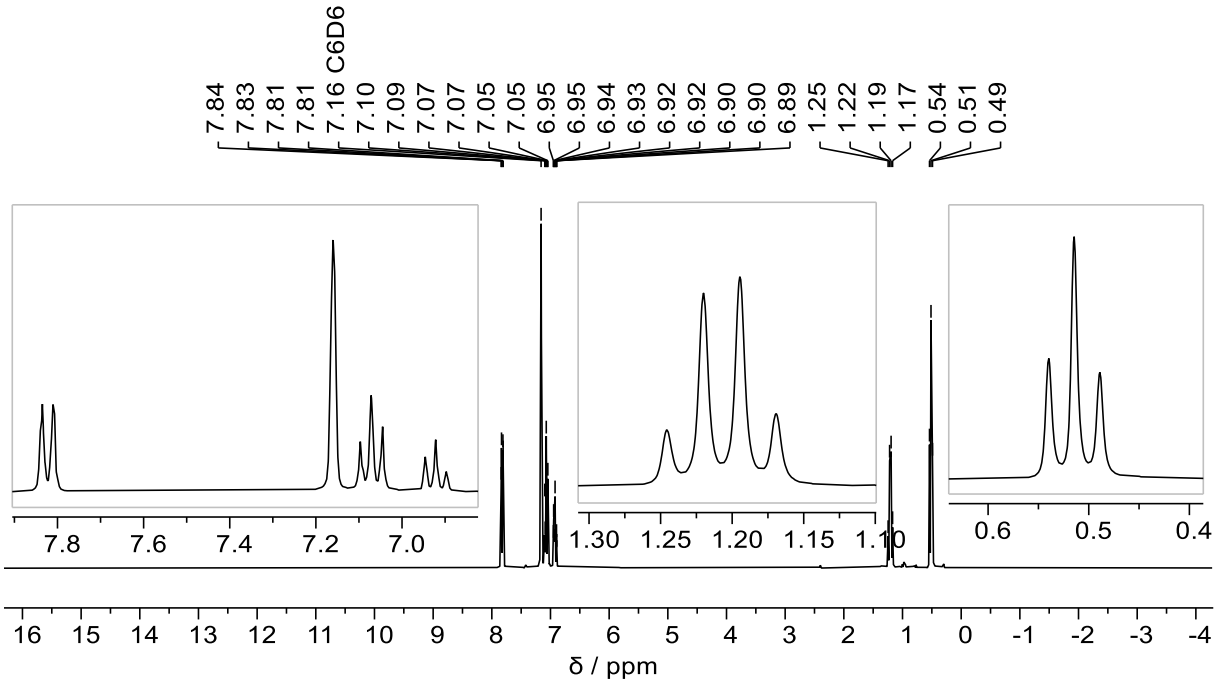

Fig. S19 $^{1}H\{^{31}P\}$ NMR spectrum (300.13 MHz, C_6D_6, 298 K) of compound **3b**.

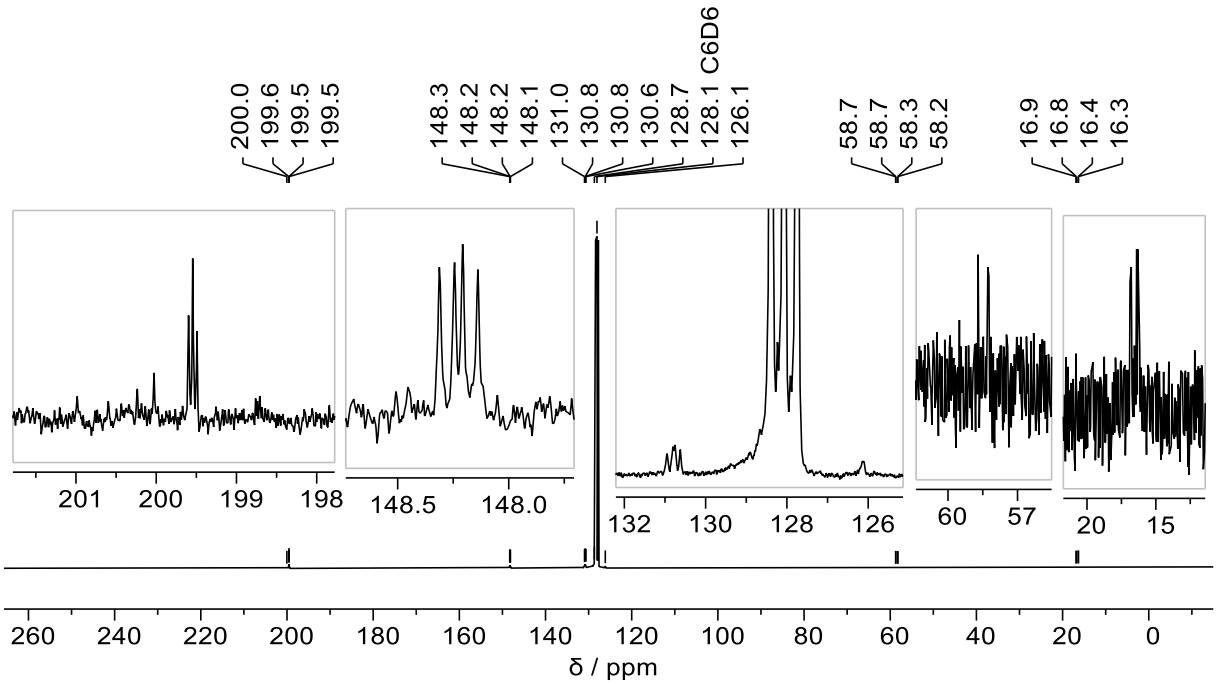

Fig. S20 $^{13}C\{^{1}H\}$ NMR spectrum (75.48 MHz, C_6D_6, 298 K) of compound **3b**.

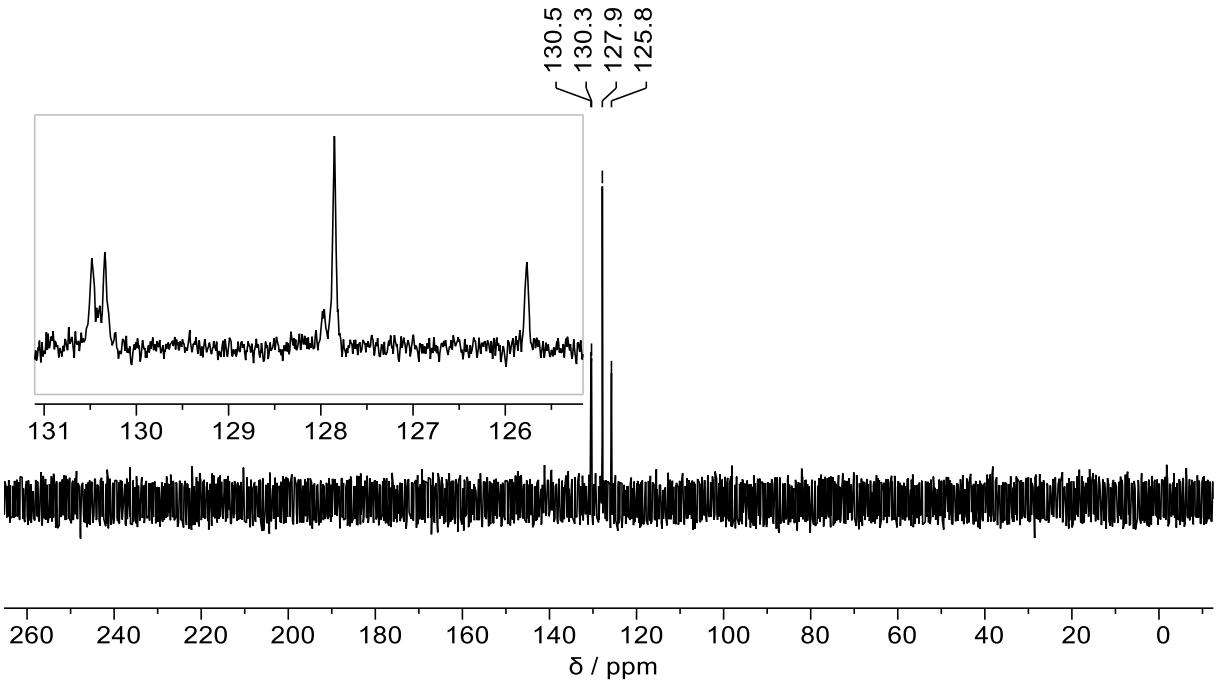

Fig. S21 ^{13}C DEPT135 NMR spectrum (75.48 MHz, C_6D_6, 298 K) of compound **3b**.

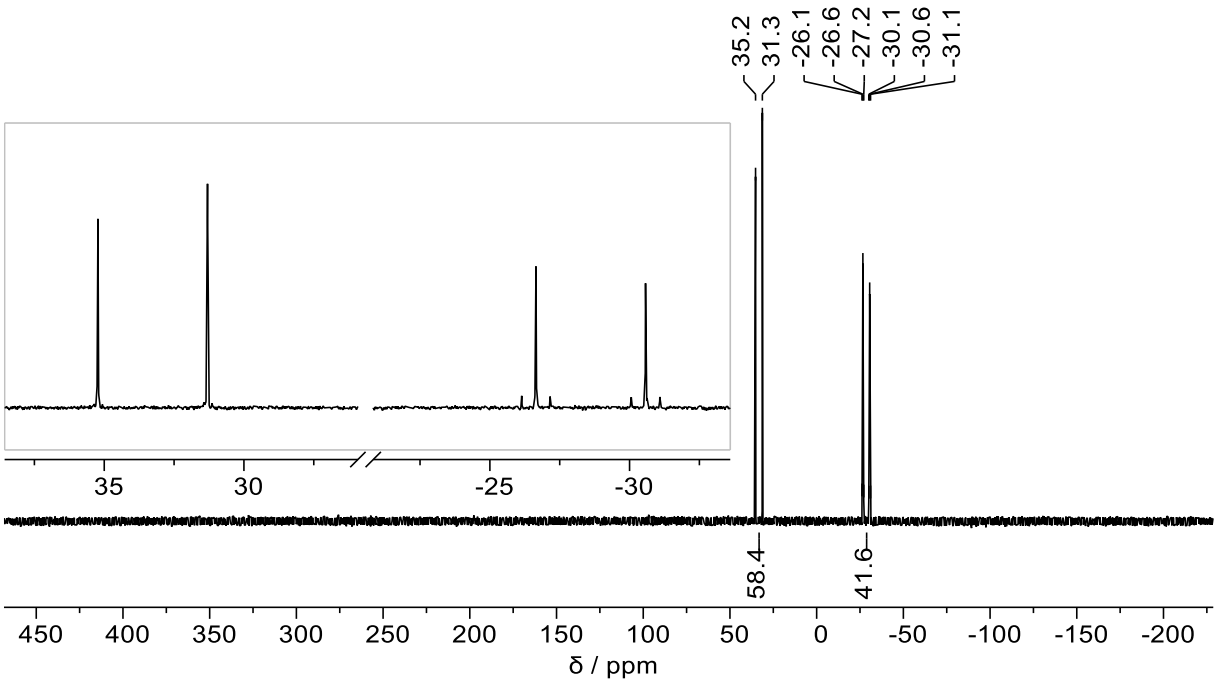

Fig. S22 $^{31}P\{^1H\}$ NMR spectrum (121.51 MHz, C_6D_6, 298 K) of compound **3b**.

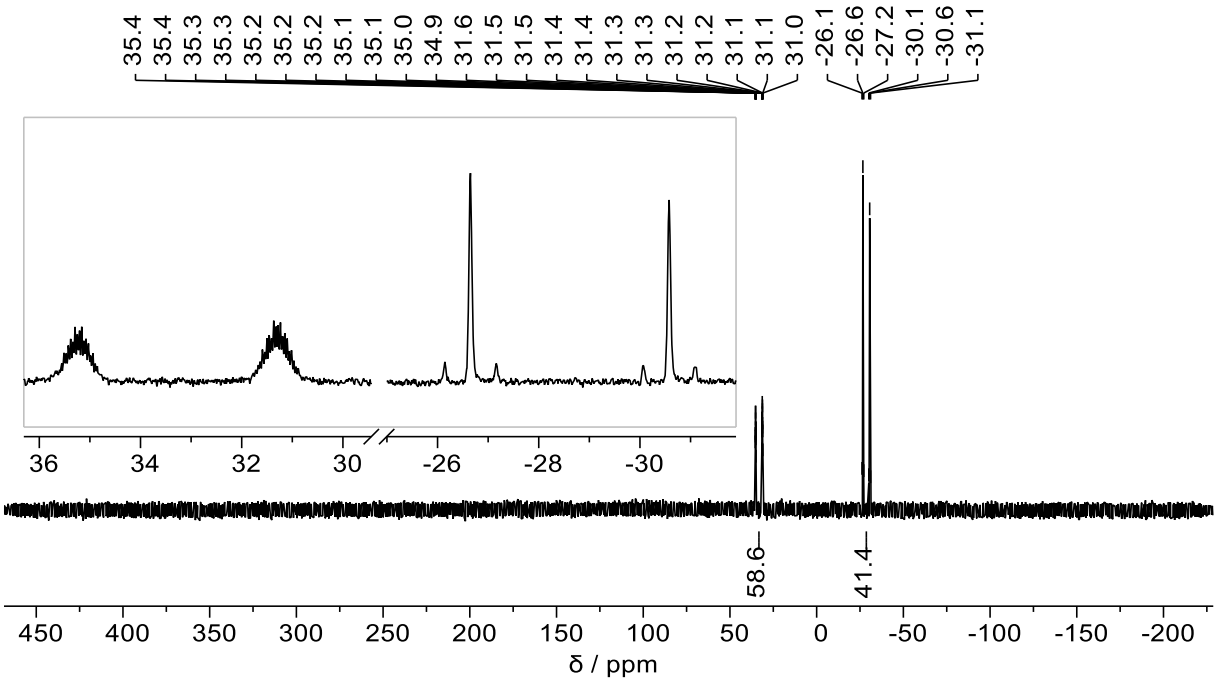

Fig. S23 ^{31}P NMR spectrum (121.51 MHz, C_6D_6, 298 K) of compound **3b**.

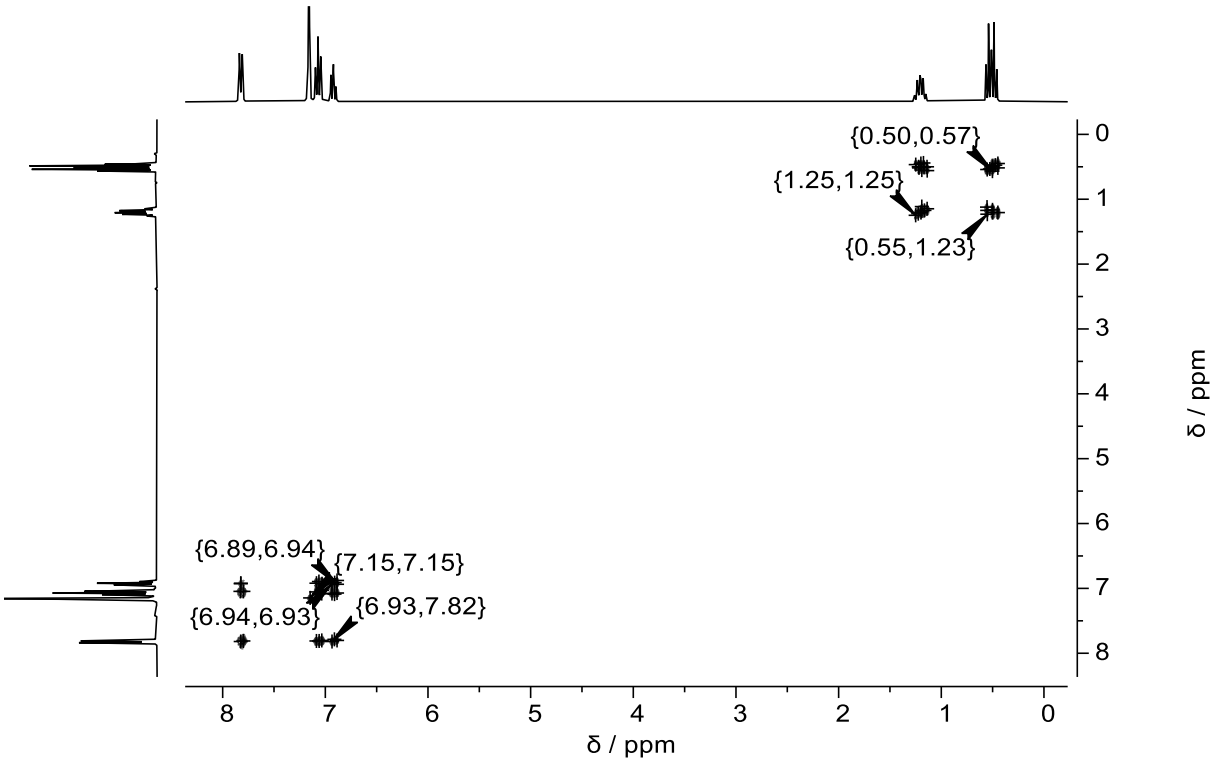

Fig. S24 ^{1}H,^{1}H COSY NMR spectrum (300.13 MHz, 300.13 MHz, C_6D_6, 298 K) of compound **3b**.

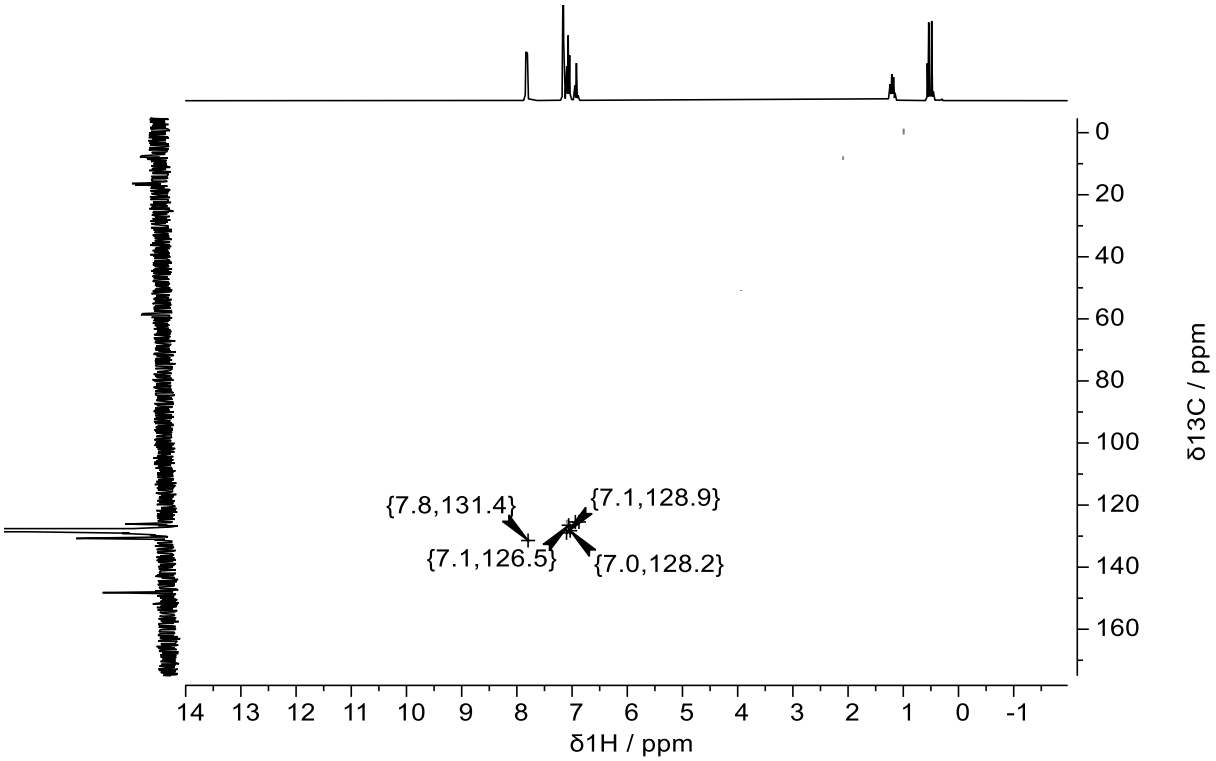

Fig. S25 $^{1}H,^{13}C$ HSQC NMR spectrum (300.13 MHz, 75.47 MHz, C_6D_6, 298 K) of compound **3b**.

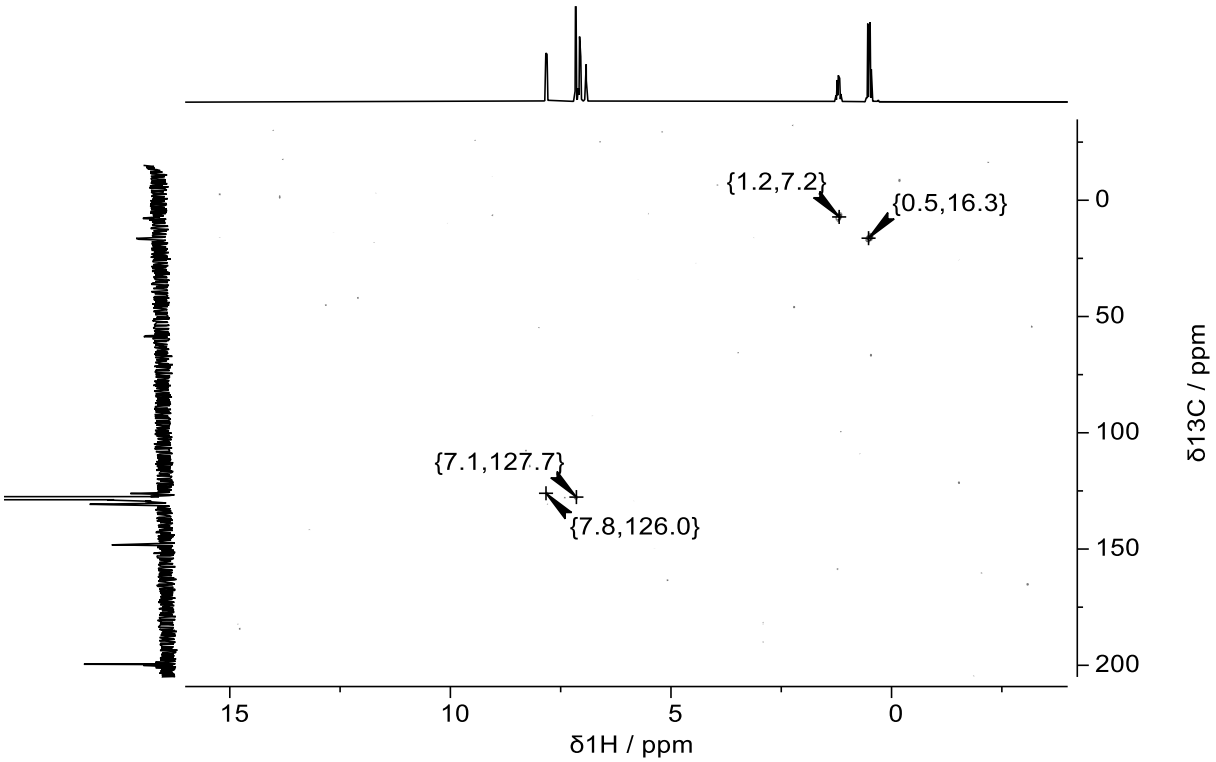

Fig. S26 $^{1}H,^{13}C$ HMBC NMR spectrum (300.13 MHz, 75.47 MHz, C_6D_6, 298 K) of compound **3b**.

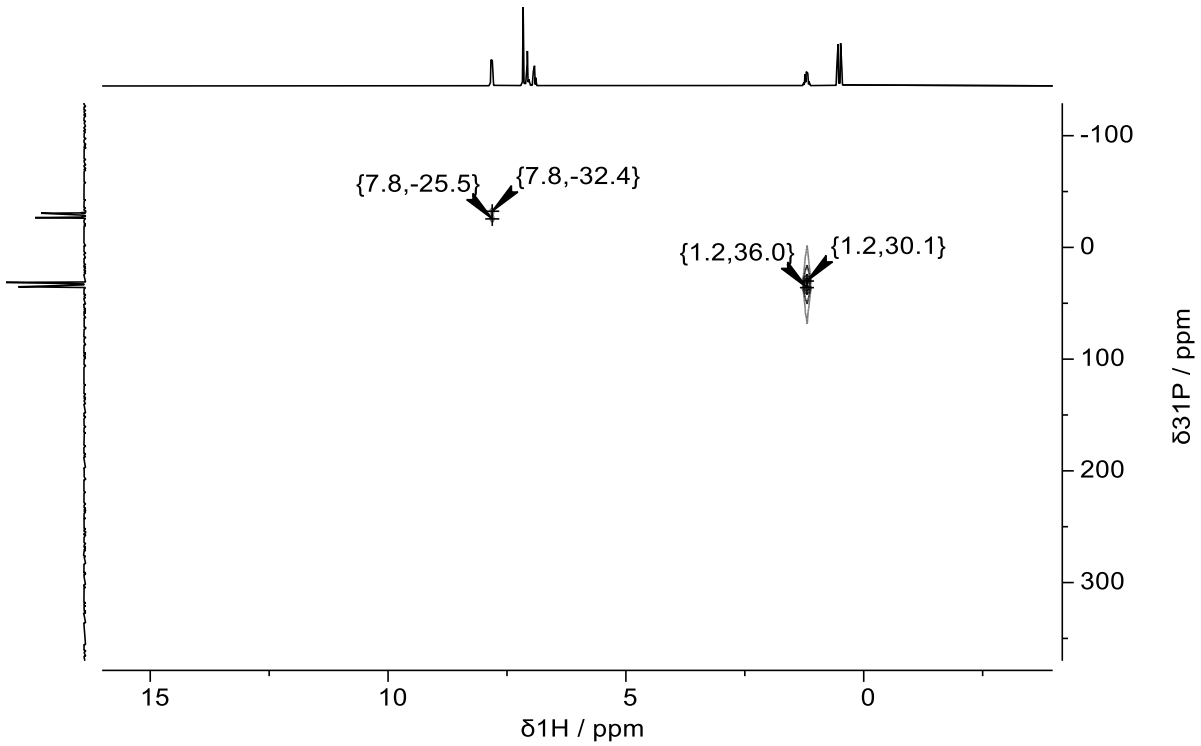

Fig. S27 $^{1}H,^{31}P$ HMBC NMR spectrum (300.13 MHz, 121.51 MHz, C_6D_6, 298 K) of compound **3b**.

Compound 3c

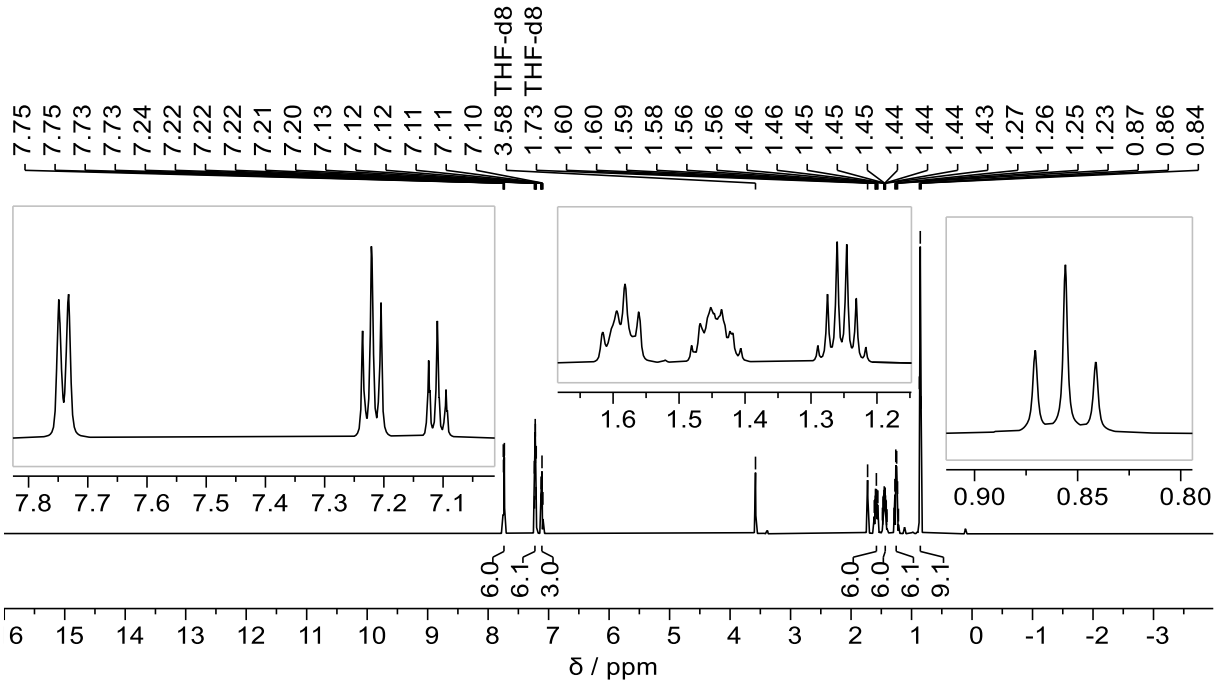

Fig. S28 ^{1}H NMR spectrum (500.04, THF-d_8, 298 K) of compound **3c**.

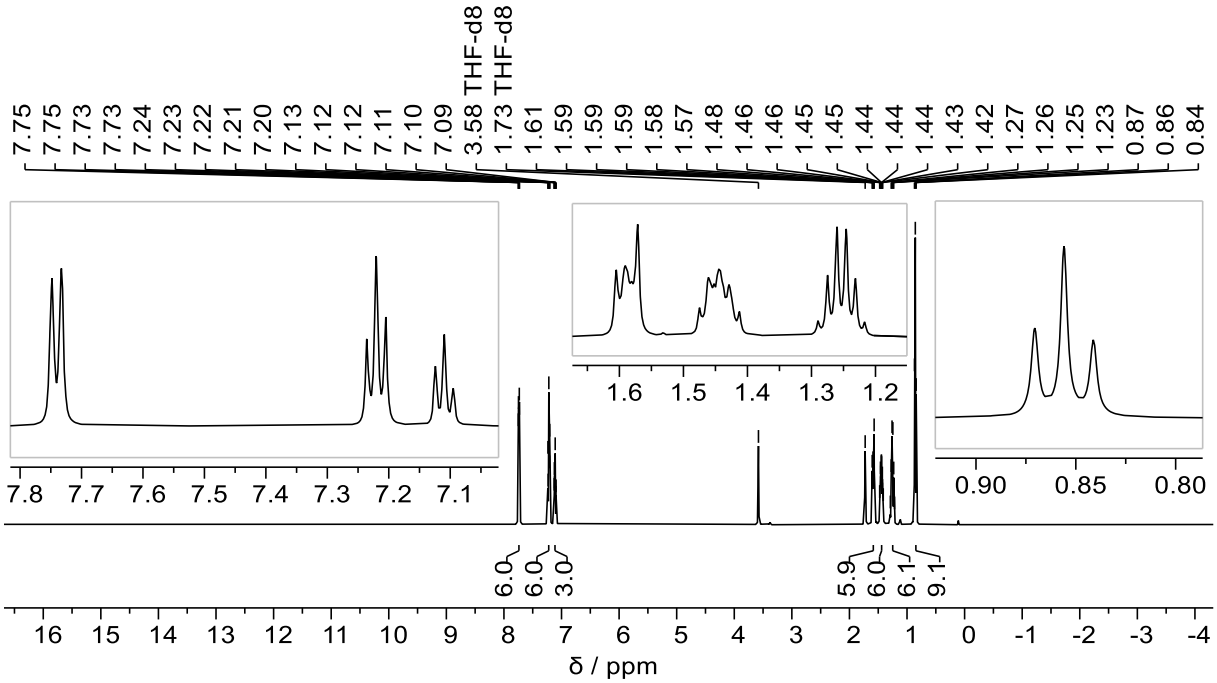

Fig. S29 $^{1}H\{^{31}P\}$ NMR spectrum (500.04 MHz, THF-d_8, 298 K) of compound **3c**.

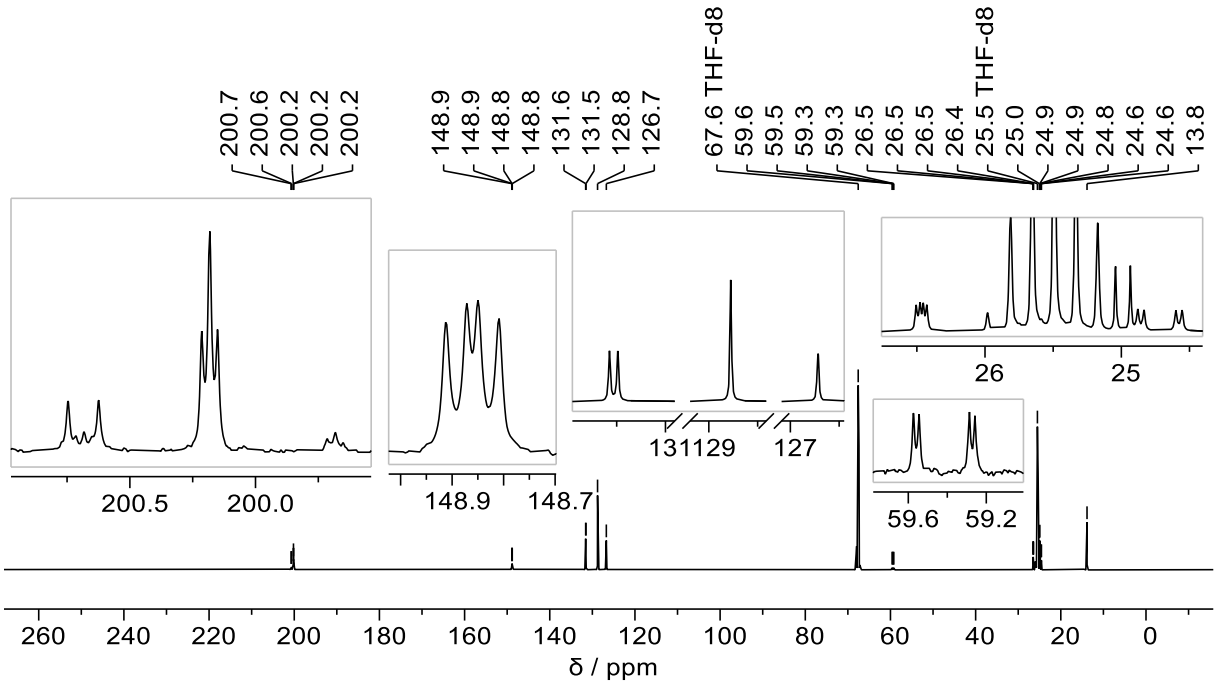

Fig. S30 $^{13}C\{^{1}H\}$ NMR spectrum (125.75 MHz, THF-d_8, 298 K) of compound **3c**.

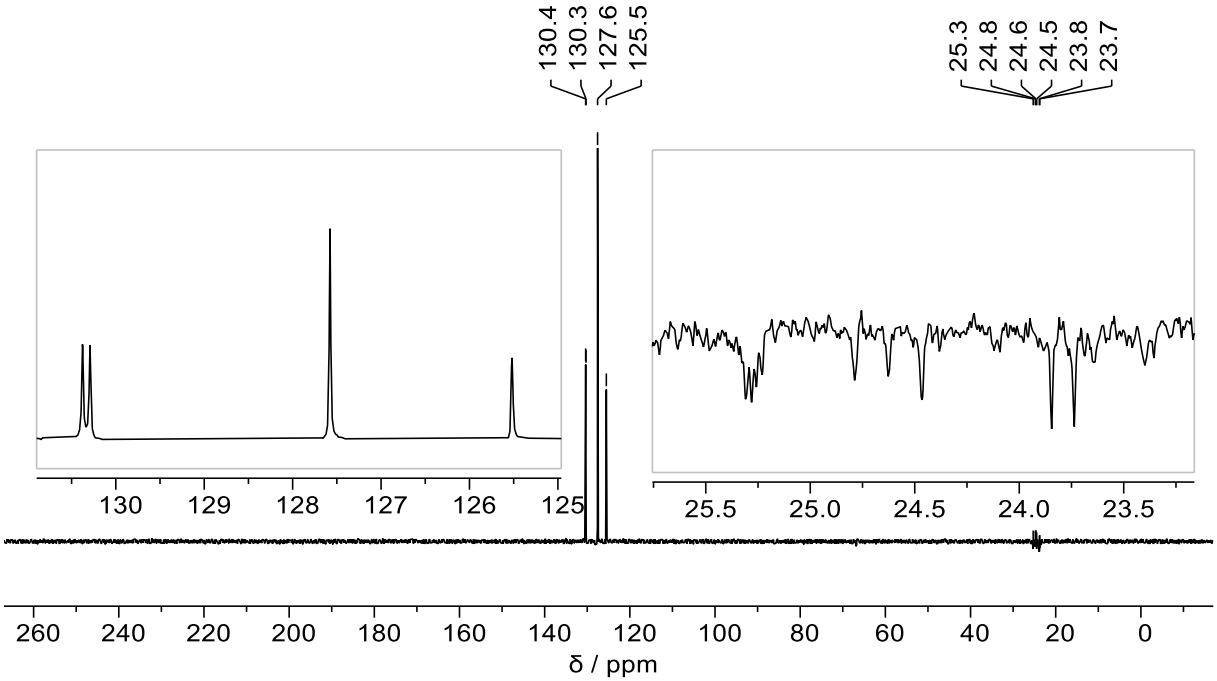

Fig. S31 ^{13}C DEPT90 NMR spectrum (125.75 MHz, THF-d_8, 298 K) of compound **3c**.

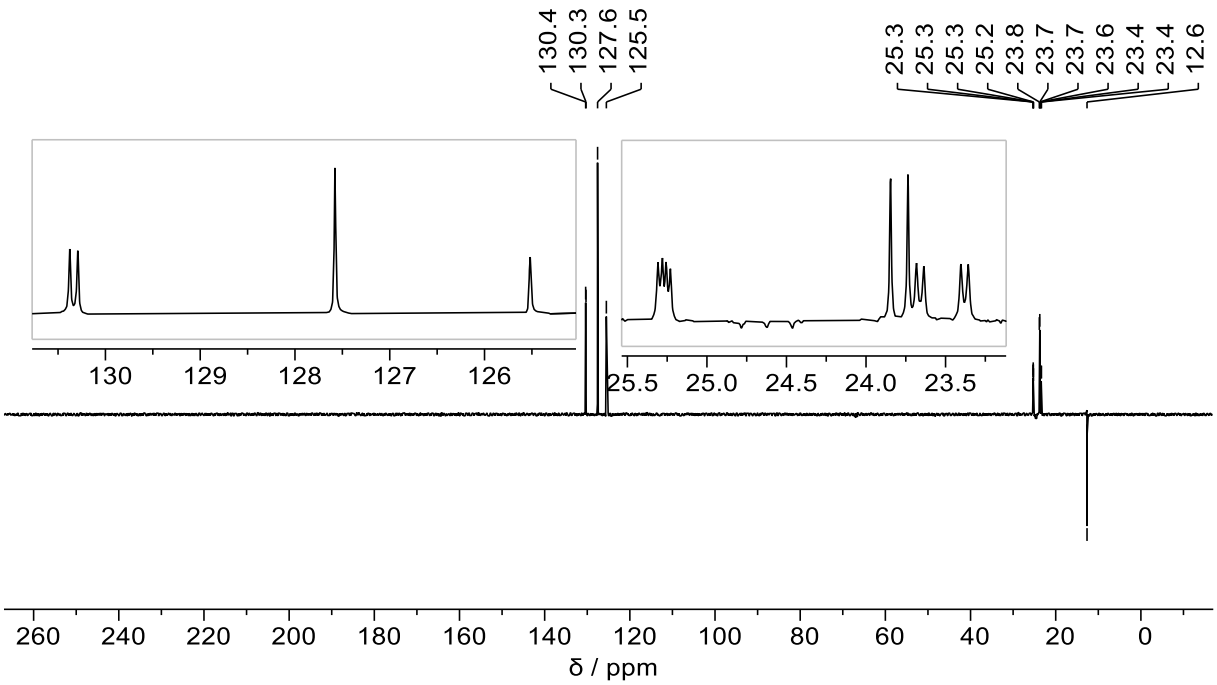

Fig. S32 ^{13}C DEPT135 NMR spectrum (125.75 MHz, THF-d_8, 298 K) of compound **3c**.

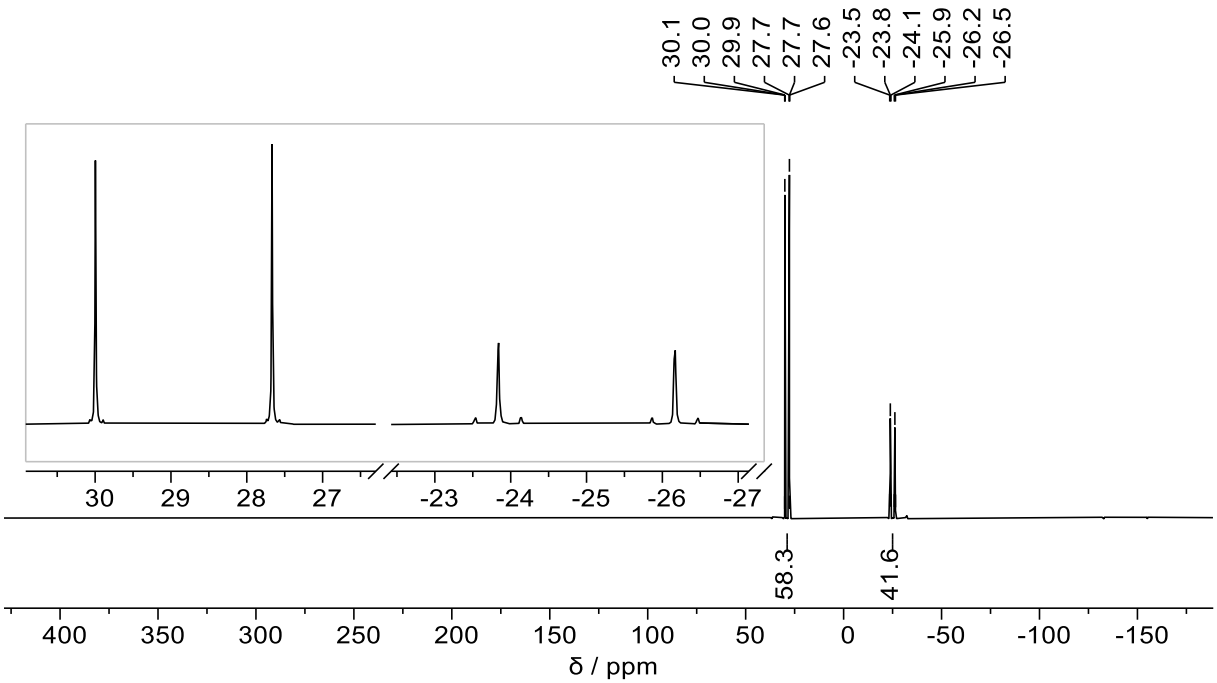

Fig. S33 $^{31}P\{^{1}H\}$ NMR spectrum (202.44 MHz, THF-d_8, 298 K) of compound **3c**.

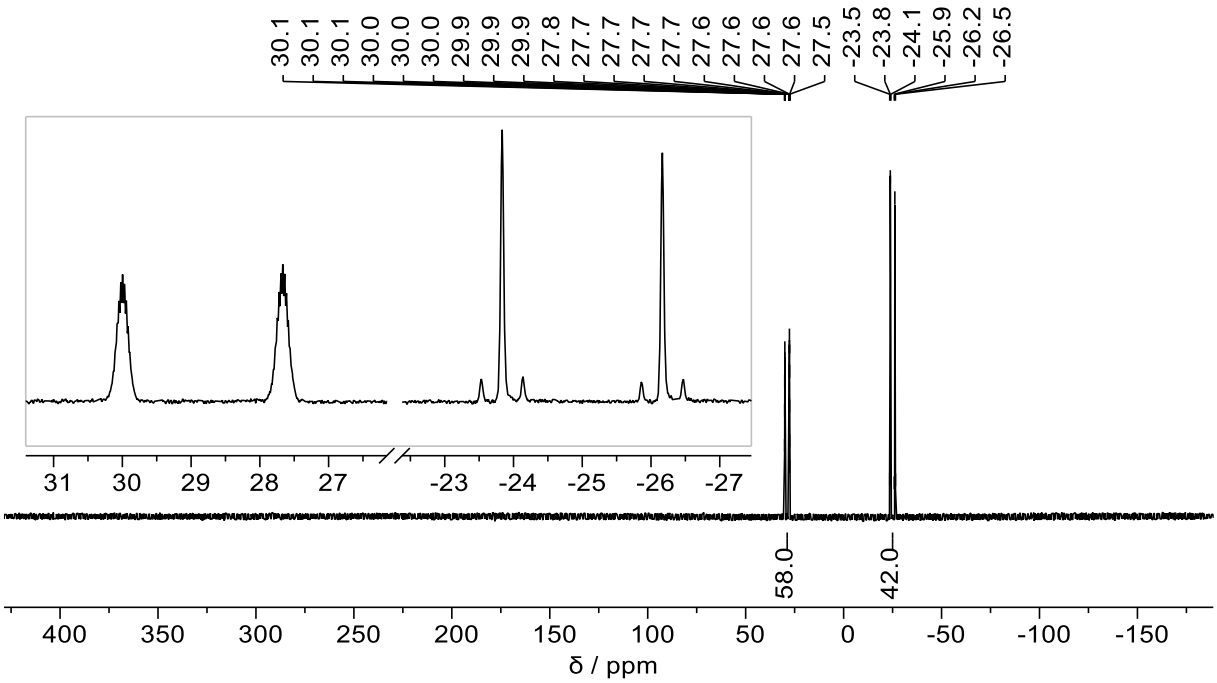

Fig. S34 ^{31}P NMR spectrum (202.44 MHz, THF-d_8, 298 K) of compound **3c**.

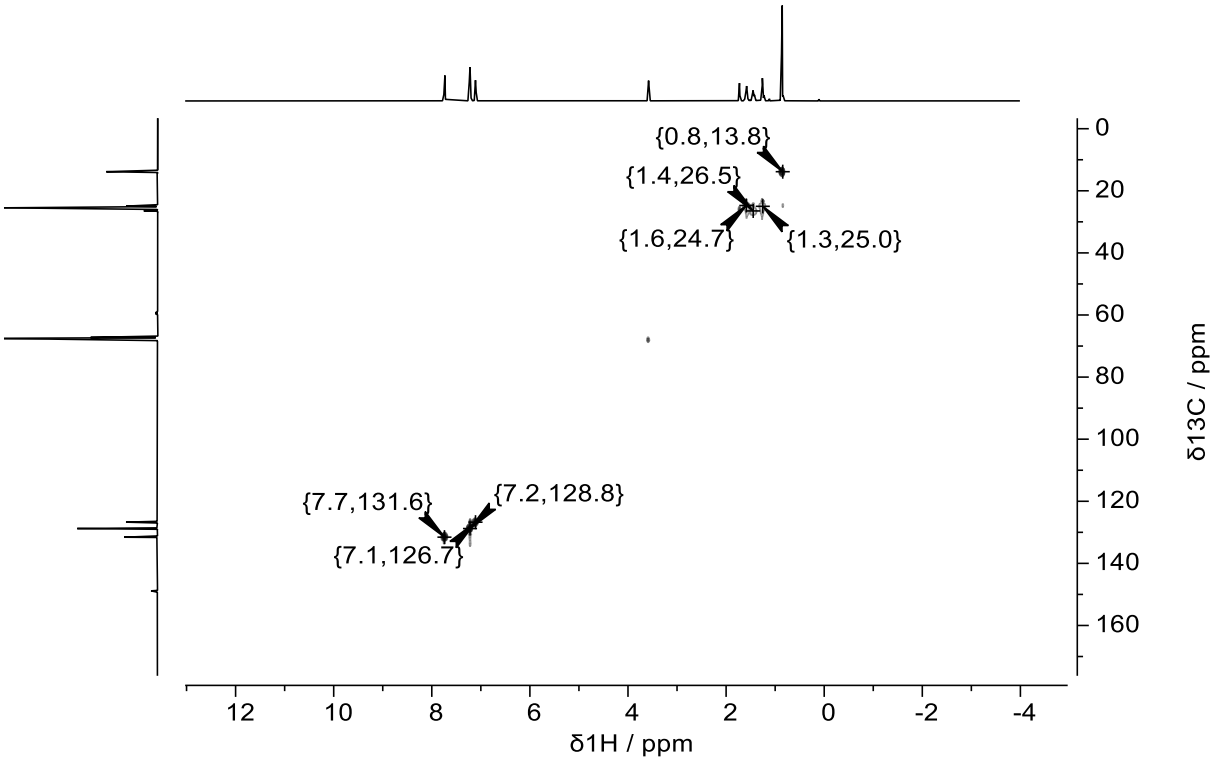

Fig. S35 $^{1}H,^{13}C$ HSQC NMR spectrum (500.04 MHz, 125.75 MHz, THF-d_8, 298 K) of compound **3c**.

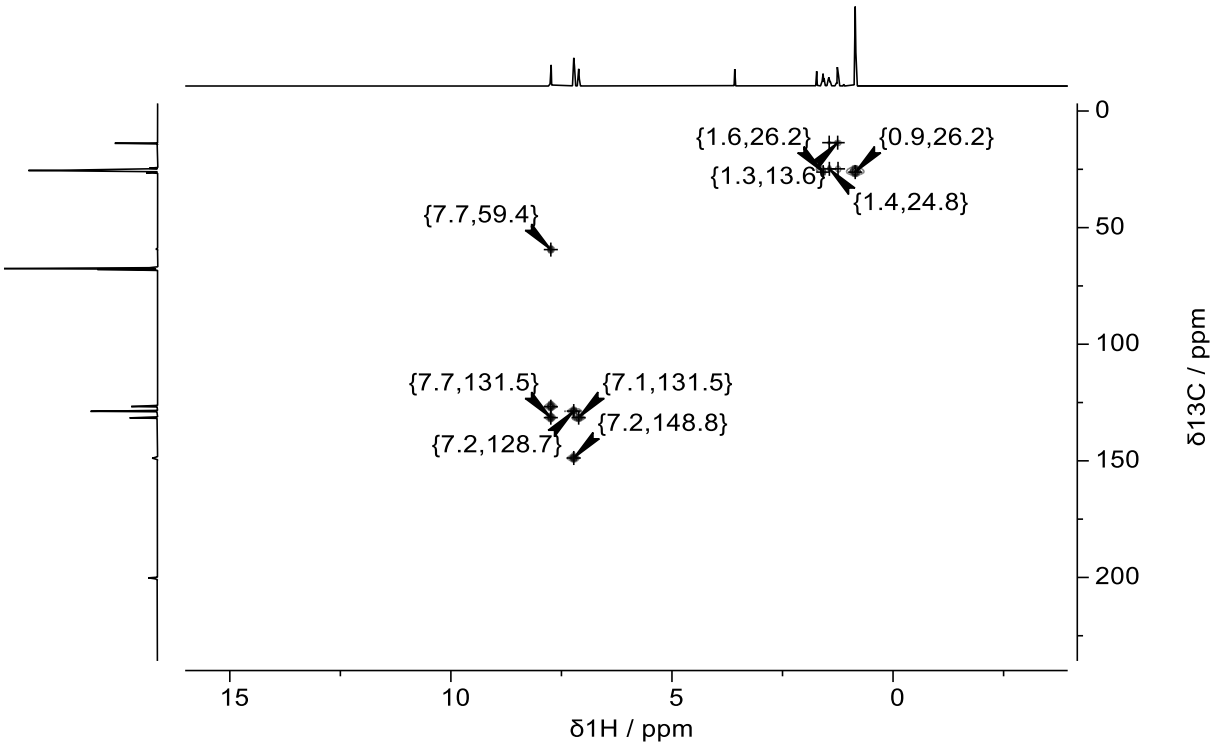

Fig. S36 $^{1}H,^{13}C$ HMBC NMR spectrum (500.04 MHz, 125.75 MHz, THF-d_8, 298 K) of compound **3c**.

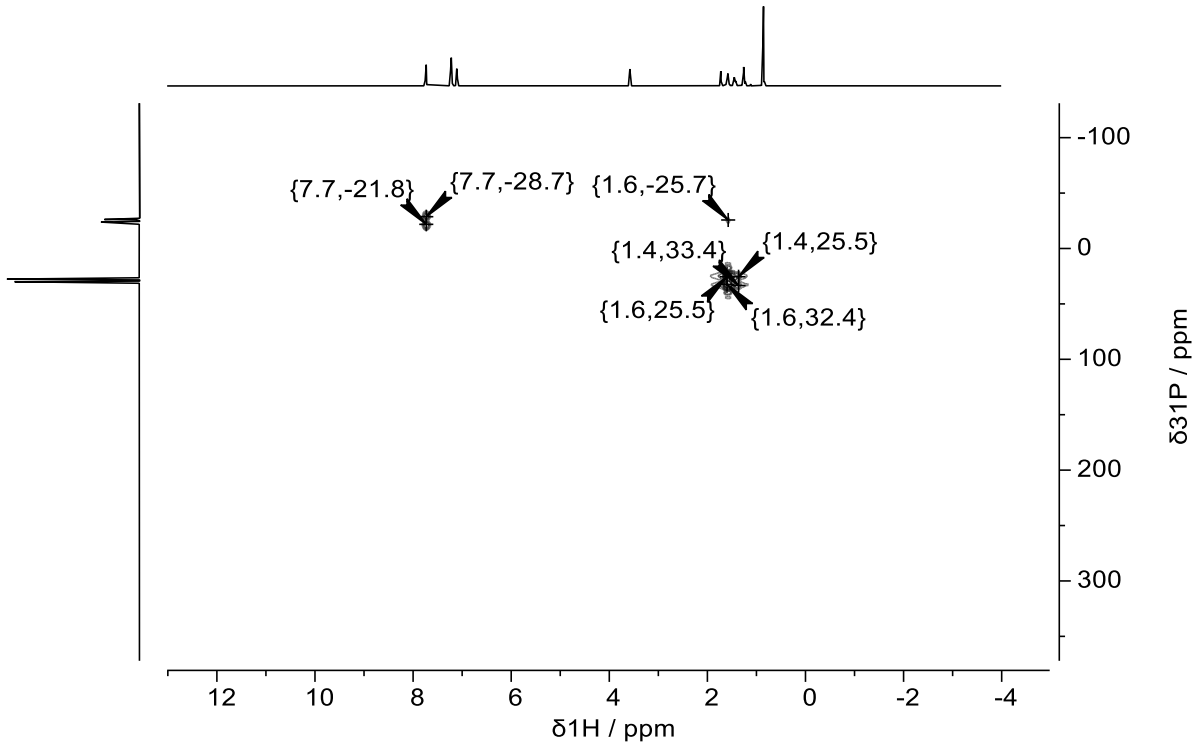

Fig. S37 $^{1}H,^{31}P$ HMBC NMR spectrum (500.04 MHz, 202.44 MHz, THF-d_8, 298 K) of compound **3c**.

4 Electrochemical experiments

The measurements of cyclic voltammograms were performed using the potentiostat and galvanostat system WaveNowXV® of Pine Research with scan rates of 20–10000 mV/s. For all CV measurements Pine research ceramic screen-printed platinum electrodes containing an Ag/AgCl reference electrode were used. These electrodes combine working, counter and reference electrodes on one ceramic plate. A low volume glass cell with a special PTFE insert at the bottom that features a narrow slit for the ceramic screen-printed electrodes was used. The internal volume of the slit is approximately 1 mL. For the experiments a 0.2 M electrolyte solution of $[^{n}Bu_4N]PF_6$ in tetrahydrofuran was freshly prepared and used. The electrolyte was dried *in vacuo* (<0.02 mbar) at 80 °C for 24 h. Tetrahydrofuran was freshly purified by drying over a potassium mirror, trap-to-trap recondensation and degassing by three freeze-pump-thaw cycles. The used analyte was prepared with a concentration of 1 mM if not stated otherwise. All sample preparations and measurements were performed in a glovebox under argon atmosphere at ambient temperature. After background scans on the electrolyte solution were measured, the analyte was added. Background scans established an electrochemical window from −3.2 V to 0.6 V (3.8 V wide; potentials referenced to $Fc^{+/0}$) and identified the anodic and cathodic limits with respect to the nominal voltage of the solid silver reference. Next, open circuit potential measurements were performed to establish the starting potential of the cyclic voltammetry experiments. Careful cyclic voltammetry scans were then measured in the anodic and cathodic directions to encounter the most accessible processes, and only after these were investigated thoroughly, further scans to higher positive and negative potentials were measured. After all measurements were completed, cobaltocenium hexafluorophosphate $[(\eta^5\text{-}C_5H_5)_2Co]PF_6$ was added to a concentration of 1 mM and served as internal reference using the cobaltocenium/cobaltocene ($Cc^{+/0}$) redox couple, set to −1.35 V.[8] See Figs. S38, S44, S50, S56 for examples of referencing; sometimes showing both Cc waves. Thus, the cyclic voltammograms could be indirectly referenced to the ferrocene/ferrocenium ($Fc^{+/0}$) redox couple, set to 0 V, according to IUPAC recommendations.[9] A thorough investigation was undertaken for each sample, and scan rate dependences were measured, which show increased chemical reversibility with scan rates for the first anodic processes. Plots of the peak currents against the square root of the scan rate $\nu^{1/2}$ for these are linear, indicative of diffusion-based voltammetric behavior (*i.e.* occurring in solution at the interface between the solid electrode and the bulk solutions). For measurement and data processing the program *Aftermath* of Pine Research was used. All plots of the cyclic voltammograms were obtained using the program *OriginPro 8G* of OrginLab.

Table S1 Cyclic voltammetry measurement details for complexes **3a–c**.

Compound	*m* / mg	*M* / g/mol	*n* / μmol	*c* / mmol/L
3a	5.4	674.272	8	2.0
3a-Cr	1.6	542.428	3	1.0
3b	2.1	716.353	3	1.0
3c	2.4	800.515	3	1.0

Compound 3a

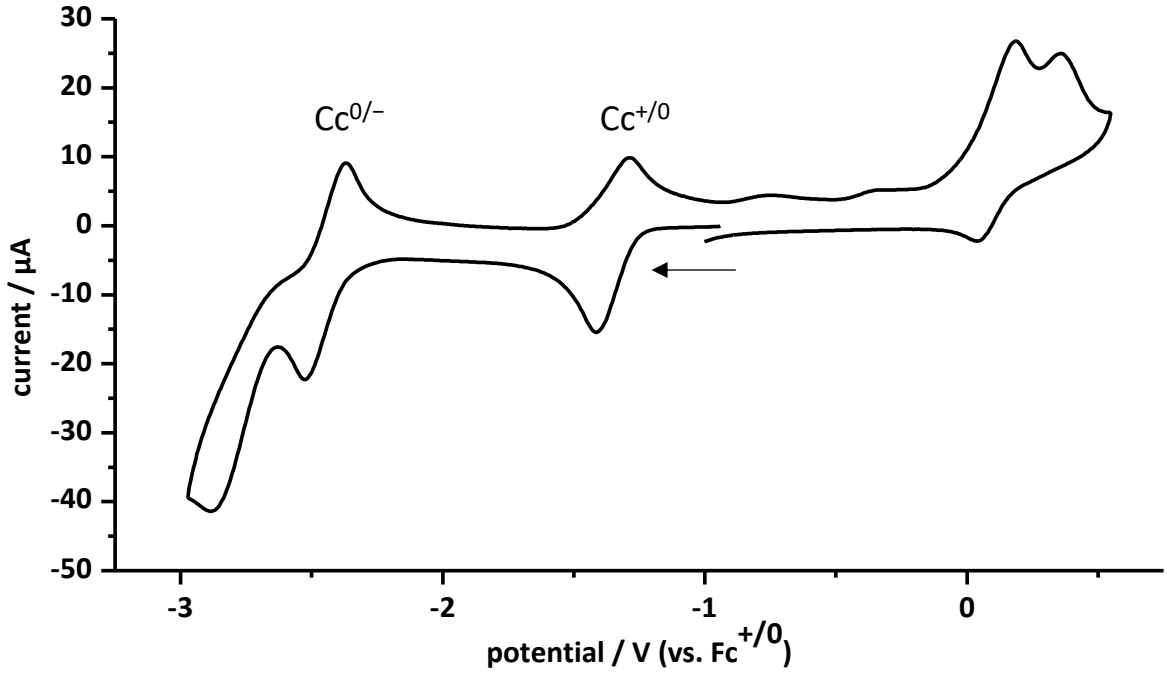

Fig. S38 Cyclic voltammogram of complex **3a** (2 mM) at a Pt electrode in a 0.2 M $^{n}Bu_4PF_6$/THF solution with cobaltocenium hexafluorophosphate as internal reference; measurement with cathodic initial scan direction (denoted with an arrow); scan rate: 200 mV/s; potentials are referenced against $Fc^{+/0}$.

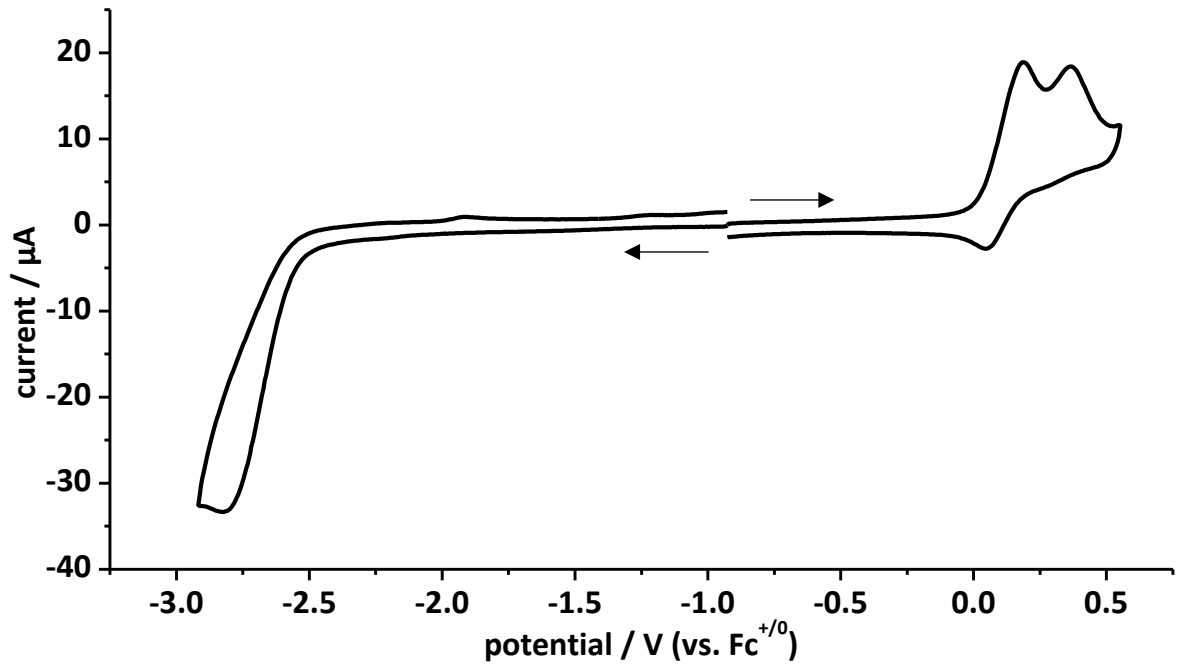

Fig. S39 Overlay of cyclic voltammograms of complex **3a** (2 mM) at a Pt electrode in a 0.2 M $^{n}Bu_4PF_6$/THF solution; oxidation parts with anodic initial scan direction and reduction parts with cathodic initial scan direction as denoted with arrows; scan rate: 200 mV/s; potentials are referenced against $Fc^{+/0}$.

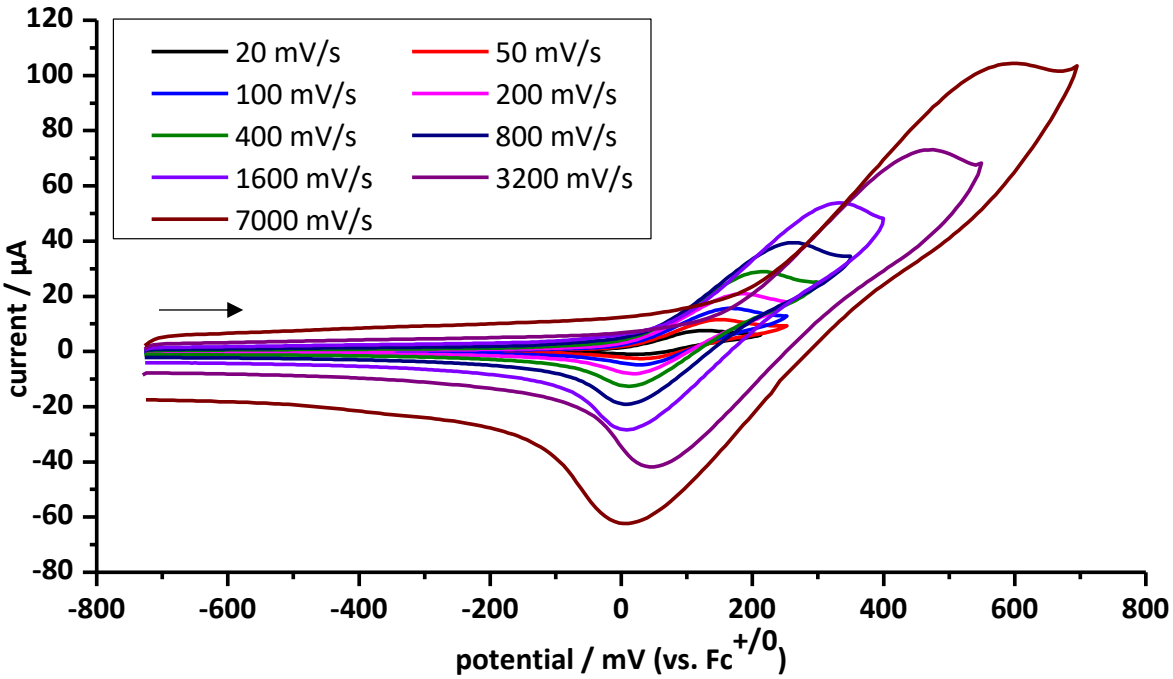

Fig. S40 Cyclic voltammogram of complex **3a** (2 mM) at a Pt electrode in a 0.2 M $^{n}Bu_4PF_6$/THF solution at various scan rates; measurement with anodic initial scan direction (denoted with an arrow) of the first redox process; potentials are referenced against $Fc^{+/0}$.

Table S2 Selected results of the cyclic voltametric studies of **3a** in 0.2 M $^{n}Bu_4NPF_6$/THF solution at ambient temperature. Potentials are referenced against $Fc^{+/0}$.

ν / mV/s	E_p^{Ia} / V	i_p^{Ia} / µA	E_p^{Ic} / V	i_p^{Ic} / µA	$E_{1/2}^{I}$ / V	ΔE_p^{I} / mV	$\lvert i_p^{c}/i_p^{a} \rvert$
20	0.13	4.22	0.02	−1.01	0.08	105	0.24
50	0.15	6.69	0.03	−4.88	0.09	125	0.73
100	0.17	8.98	0.03	−7.83	0.10	140	0.87
200	0.19	11.0	0.02	−11.7	0.10	170	1.07
400	0.22	16.1	0.01	−17.2	0.11	206	1.07
800	0.26	22.1	0.01	−24.5	0.14	256	1.11
1600	0.34	30.6	0.01	−34.8	0.17	327	1.14
3200	0.48	44.8	0.04	−49.2	0.26	432	1.10
7000	0.60	66.8	0.00	−73.9	0.30	593	1.11

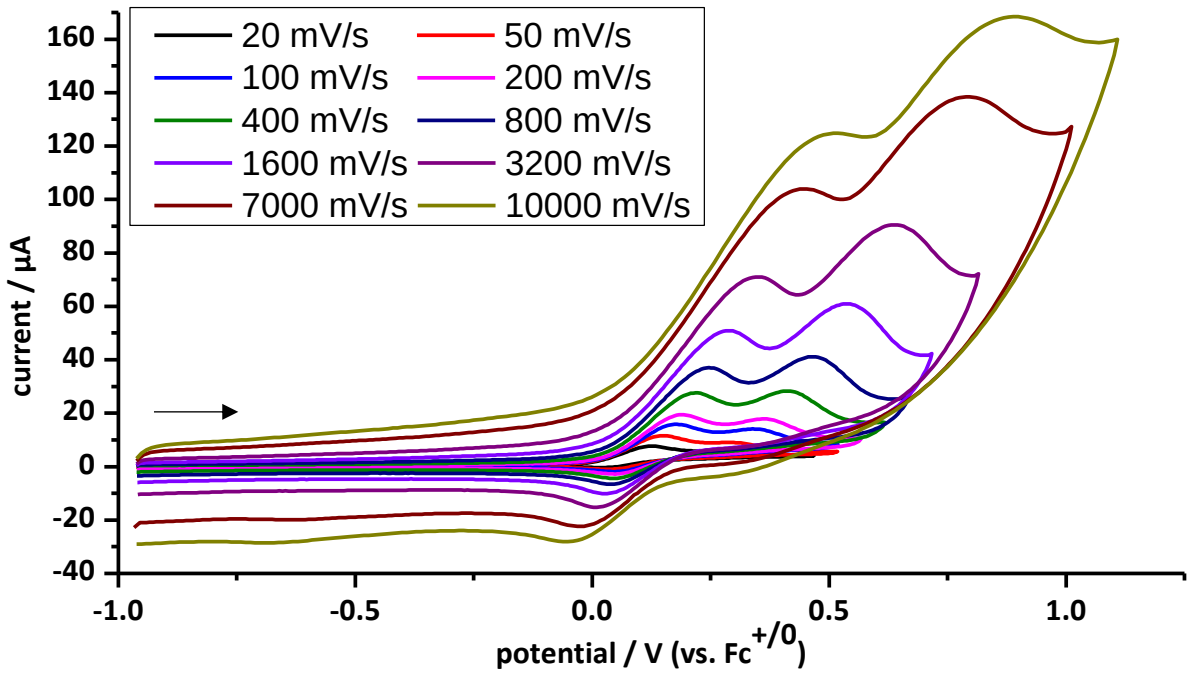

Fig. S41 Cyclic voltammogram of complex **3a** (2 mM) at a Pt electrode in a 0.2 M $^{n}Bu_4PF_6$/THF solution at various scan rates; measurement with anodic initial scan direction (denoted with an arrow) of the first and second redox process; potentials are referenced against $Fc^{+/0}$.

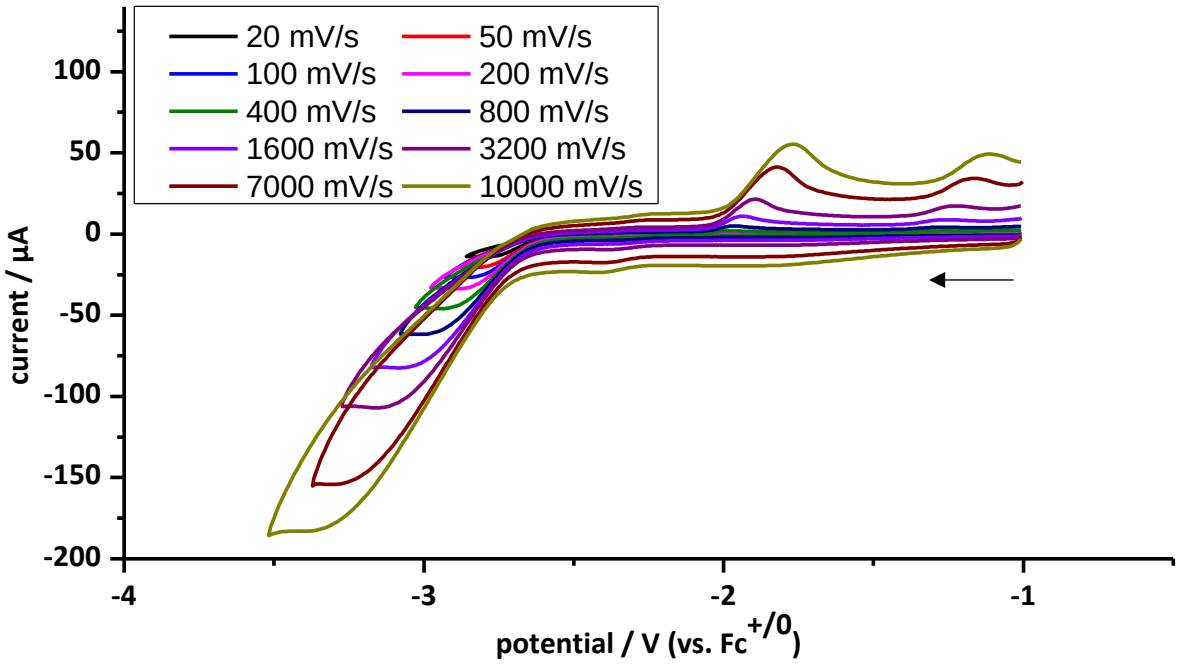

Fig. S42 Cyclic voltammogram of complex **3a** (2 mM) at a Pt electrode in a 0.2 M $^{n}Bu_4PF_6$/THF solution at various scan rates; measurement with cathodic initial scan direction (denoted with an arrow) of the third redox process; potentials are referenced against $Fc^{+/0}$.

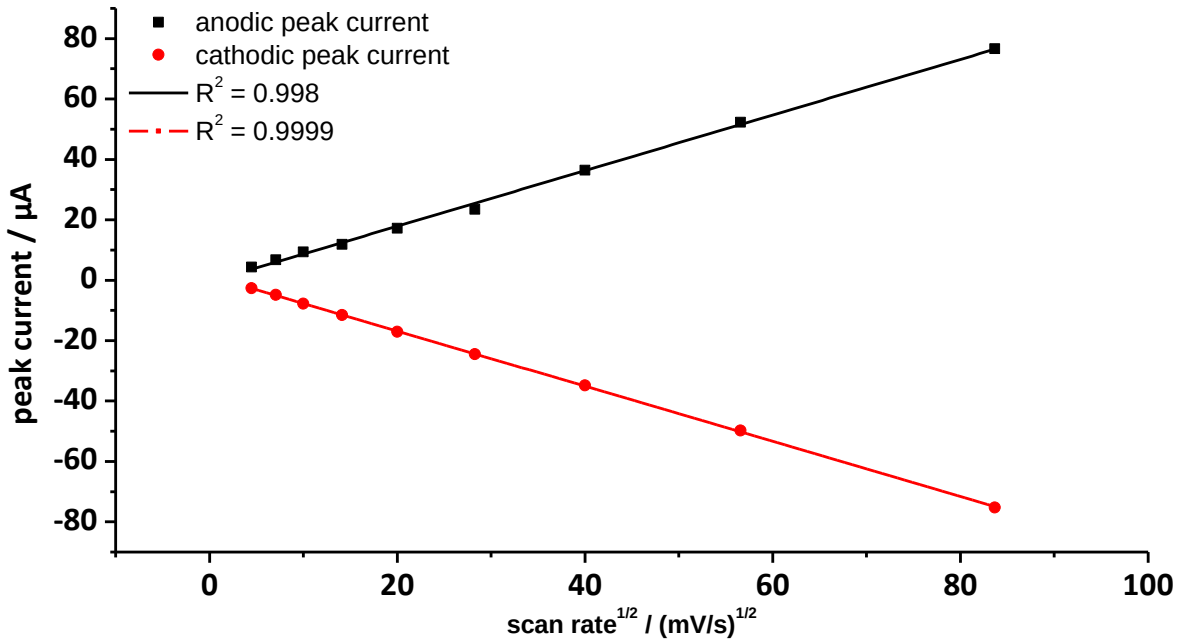

Fig. S43 Plot of the peak currents against the square root of the scan rate $\nu^{1/2}$ for the first redox process of complex **3a**.

Compound 3a-Cr

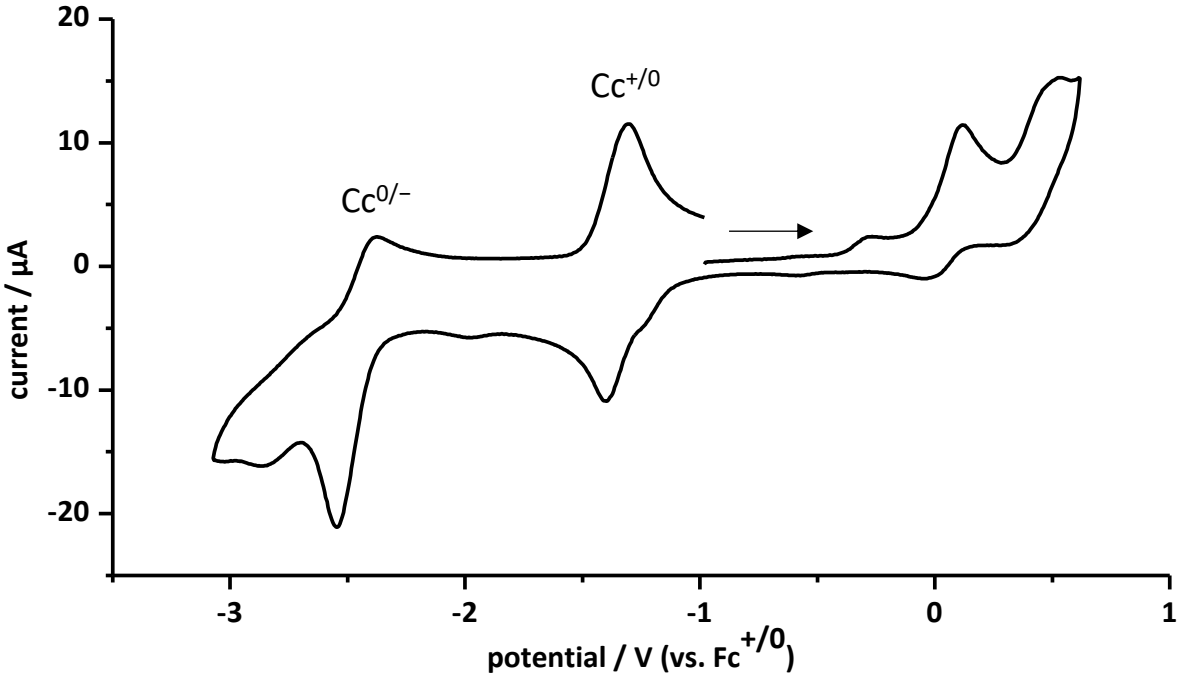

Fig. S44 Cyclic voltammogram of complex **3a-Cr** (1 mM) at a Pt electrode in a 0.2 M $^{n}Bu_4PF_6$/THF solution with cobaltocenium hexafluorophosphate as internal reference; measurement with anodic initial scan direction (denoted with an arrow); scan rate: 200 mV/s; potentials are referenced against $Fc^{+/0}$.

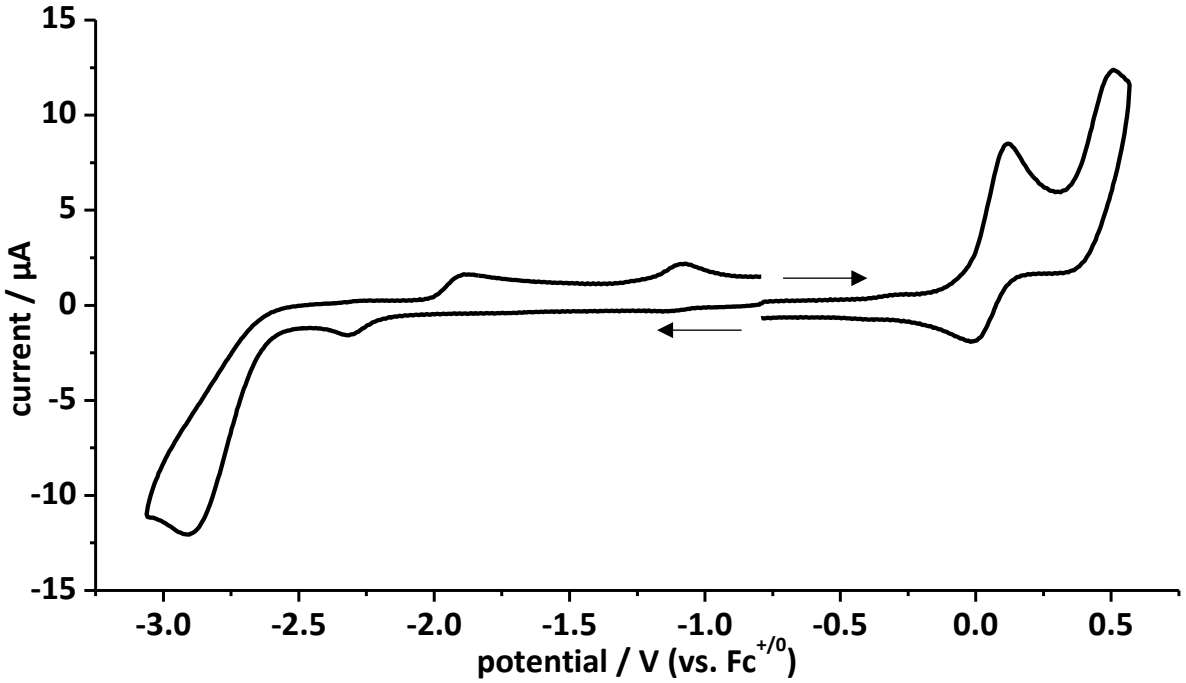

Fig. S45 Overlay of cyclic voltammograms of complex **3a-Cr** (1 mM) at a Pt electrode in a 0.2 M $^{n}Bu_4PF_6$/THF solution; oxidation parts with anodic initial scan direction and reduction parts with cathodic initial scan direction as denoted with arrows; scan rate: 200 mV/s; potentials are referenced against $Fc^{+/0}$.

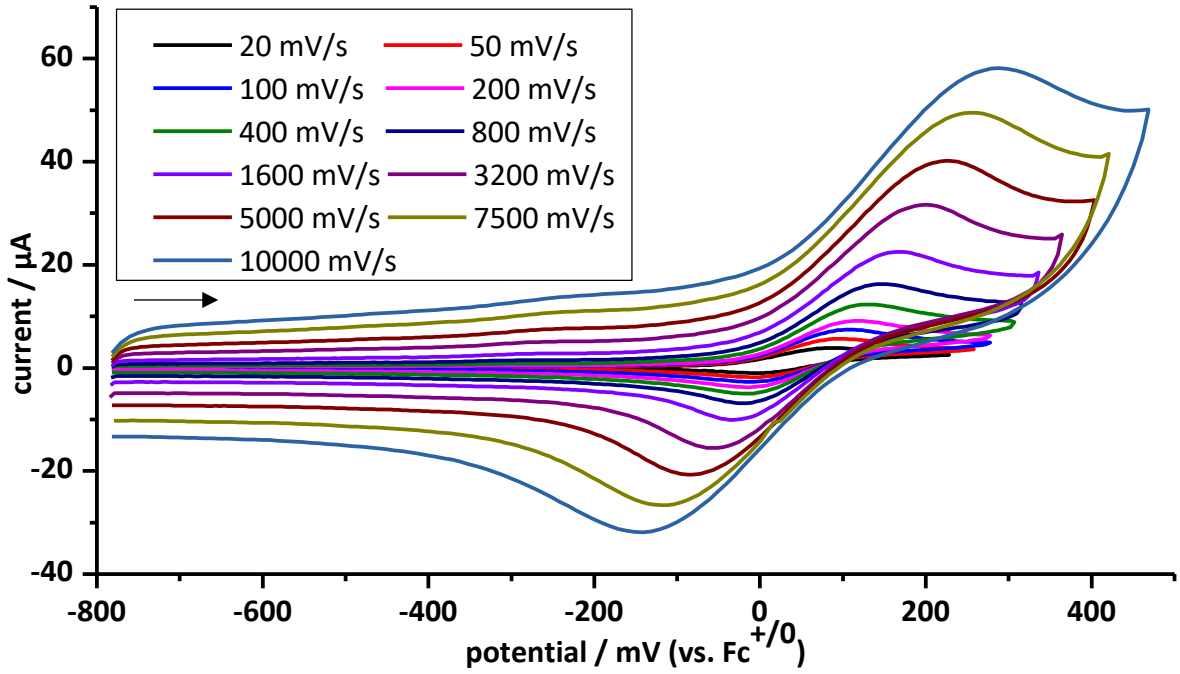

Fig. S46 Cyclic voltammogram of complex **3a-Cr** (1 mM) at a Pt electrode in a 0.2 M $^{n}Bu_4PF_6$/THF solution at various scan rates; measurement with anodic initial scan direction (denoted with an arrow) of the first redox process; potentials are referenced against $Fc^{+/0}$.

Table S3 Selected results of the cyclic voltametric studies of **3a-Cr** in 0.2 M $^{n}Bu_4NPF_6$/THF solution at ambient temperature. Potentials are referenced against $Fc^{+/0}$.

ν / mV/s	E_p^{Ia} / V	i_p^{la} / µA	E_p^{Ic} / V	i_p^{lc} / µA	$E_{1/2}^{I}$ / V	ΔE_p^{I} / mV	$\lvert i_p^c/i_p^a \rvert$
20	0.09	2.29	−0.01	−1.94	0.04	95	0.85
50	0.10	3.53	−0.01	−3.02	0.05	105	0.86
100	0.11	4.77	−0.01	−4.19	0.05	119	0.88
200	0.12	5.72	−0.01	−5.55	0.05	131	0.97
400	0.13	7.70	−0.02	−7.49	0.06	151	0.97
800	0.14	10.1	−0.02	−10.3	0.06	163	1.02
1600	0.17	14.5	−0.03	−14.8	0.07	202	1.02
3200	0.20	21.3	−0.06	−22.3	0.07	257	1.04
5000	0.22	30.0	−0.08	−29.1	0.07	306	0.97
7500	0.25	36.0	−0.12	−38.1	0.07	373	1.06
10000	0.29	39.6	−0.14	−45.8	0.07	430	1.16

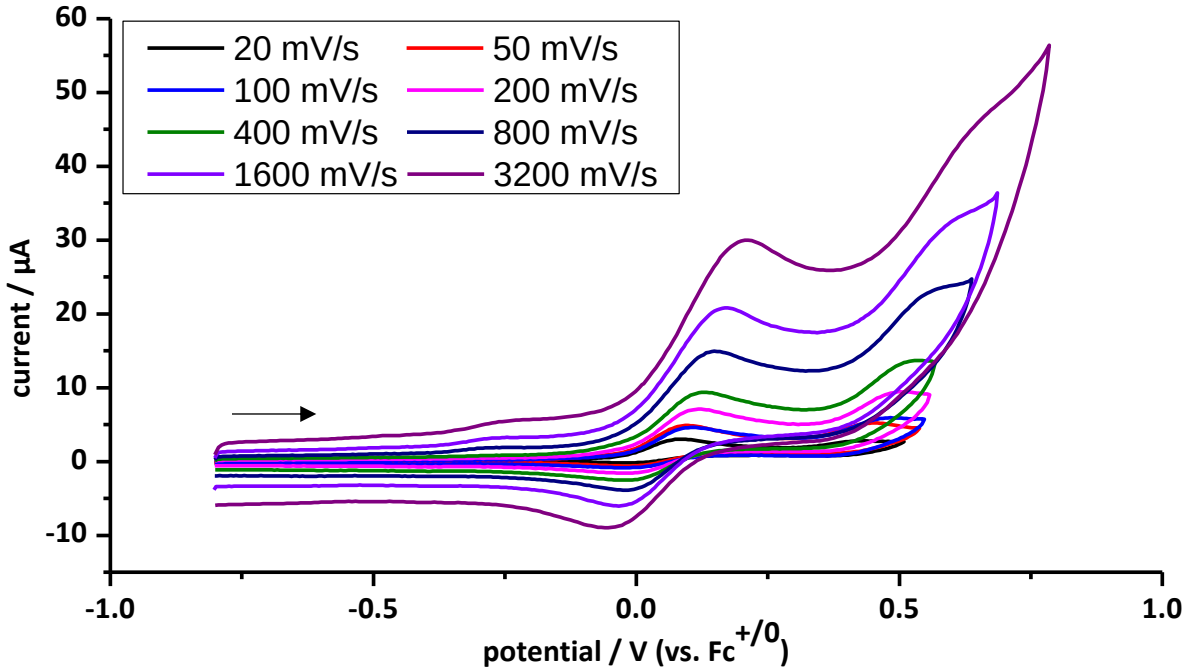

Fig. S47 Cyclic voltammogram of complex **3a-Cr** (1 mM) at a Pt electrode in a 0.2 M $^{n}Bu_4PF_6$/THF solution at various scan rates; measurement with anodic initial scan direction (denoted with an arrow) of the first and second redox process; potentials are referenced against $Fc^{+/0}$.

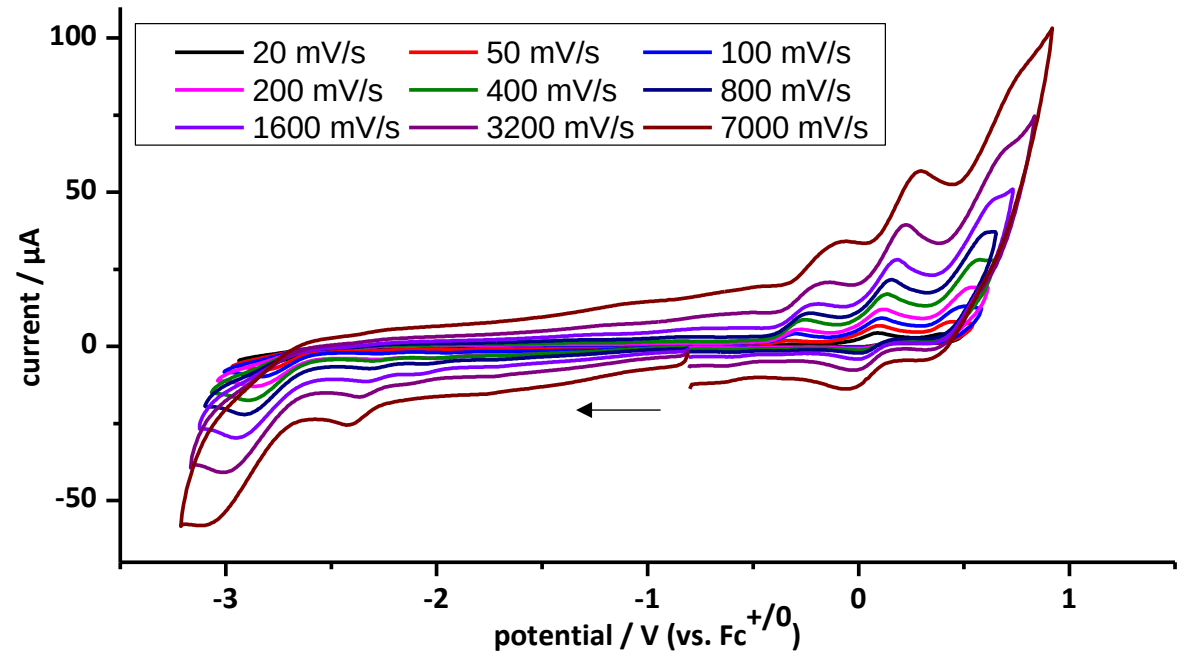

Fig. S48 Cyclic voltammogram of complex **3a-Cr** (1 mM) at a Pt electrode in a 0.2 M $^{n}Bu_4PF_6$/THF solution at various scan rates; measurement with cathodic initial scan direction (denoted with an arrow) of the first, second and third redox process; potentials are referenced against $Fc^{+/0}$.

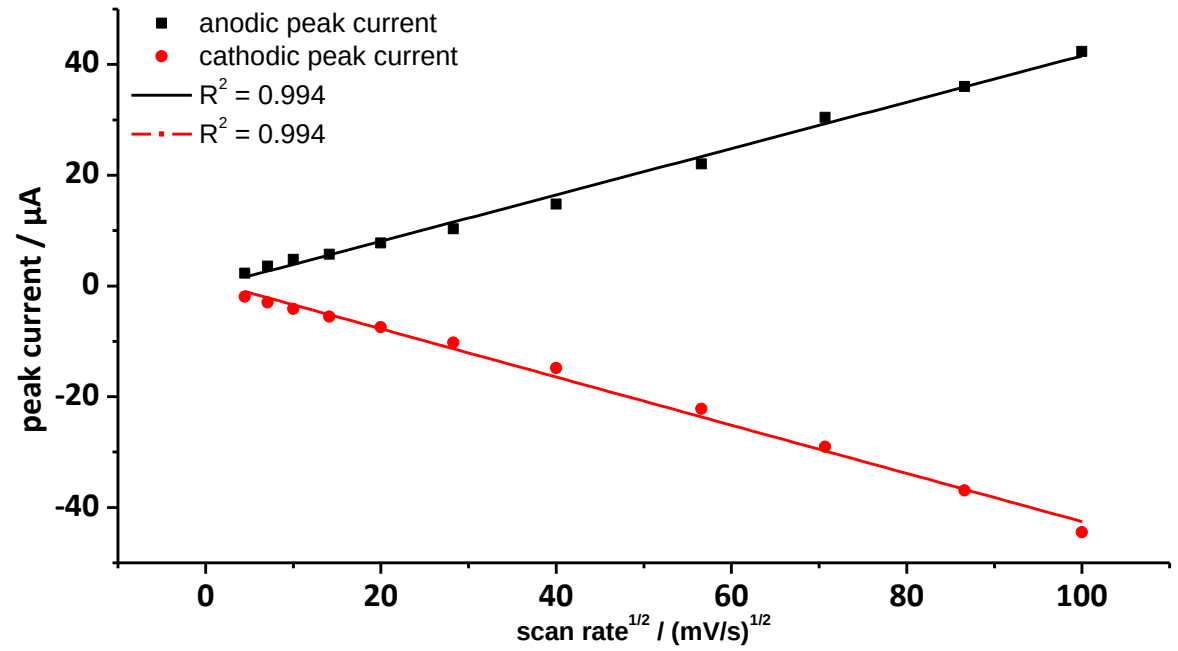

Fig. S49 Plot of the peak currents against the square root of the scan rate $\nu^{1/2}$ for the first redox process of complex **3a-Cr**.

Compound 3b

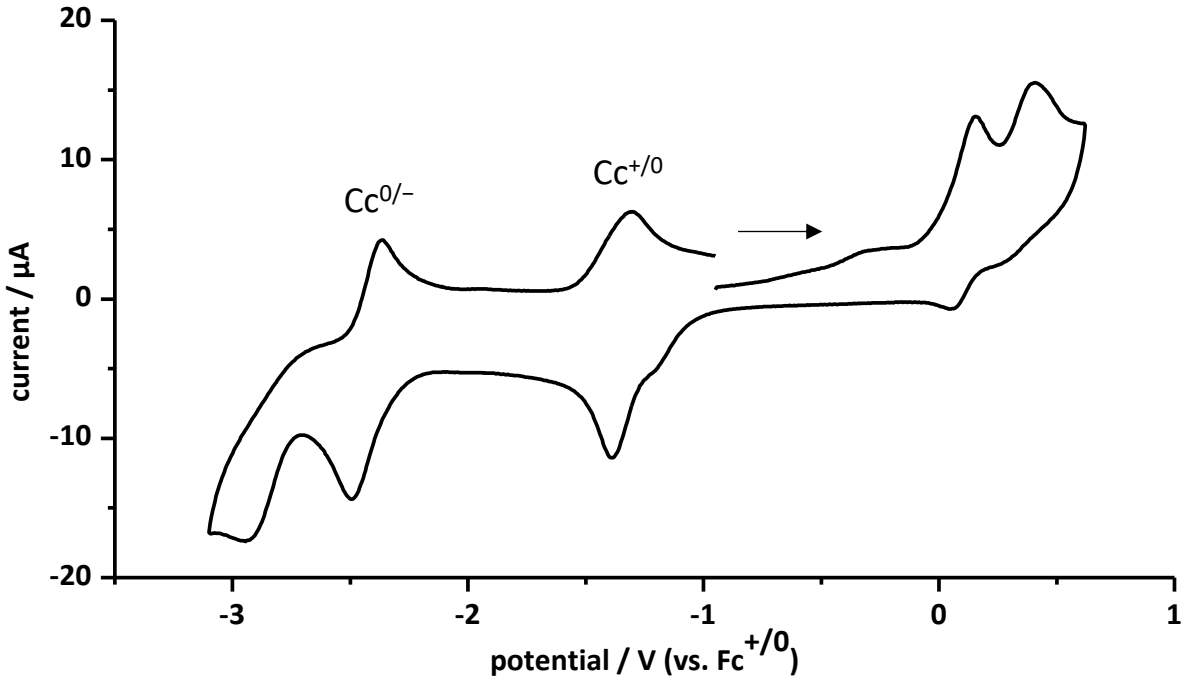

Fig. S50 Cyclic voltammogram of complex **3b** (1 mM) at a Pt electrode in a 0.2 M $^{n}Bu_4PF_6$/THF solution with cobaltocenium hexafluorophosphate as internal reference; measurement with anodic initial scan direction (denoted with an arrow); scan rate: 200 mV/s; potentials are referenced against $Fc^{+/0}$.

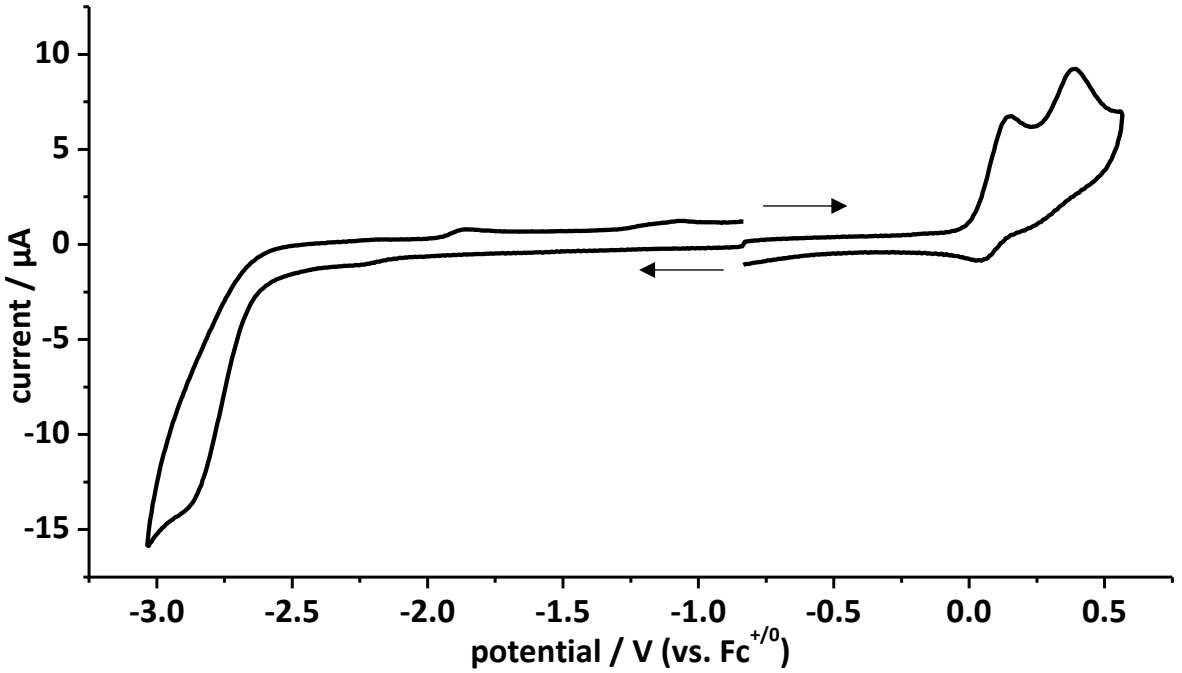

Fig. S51 Overlay of cyclic voltammograms of complex **3b** (1 mM) at a Pt electrode in a 0.2 M $^{n}Bu_4PF_6$/THF solution; oxidation part with anodic initial scan direction and reduction part with cathodic initial scan direction as denoted with arrows; scan rate: 200 mV/s; potentials are referenced against $Fc^{+/0}$.

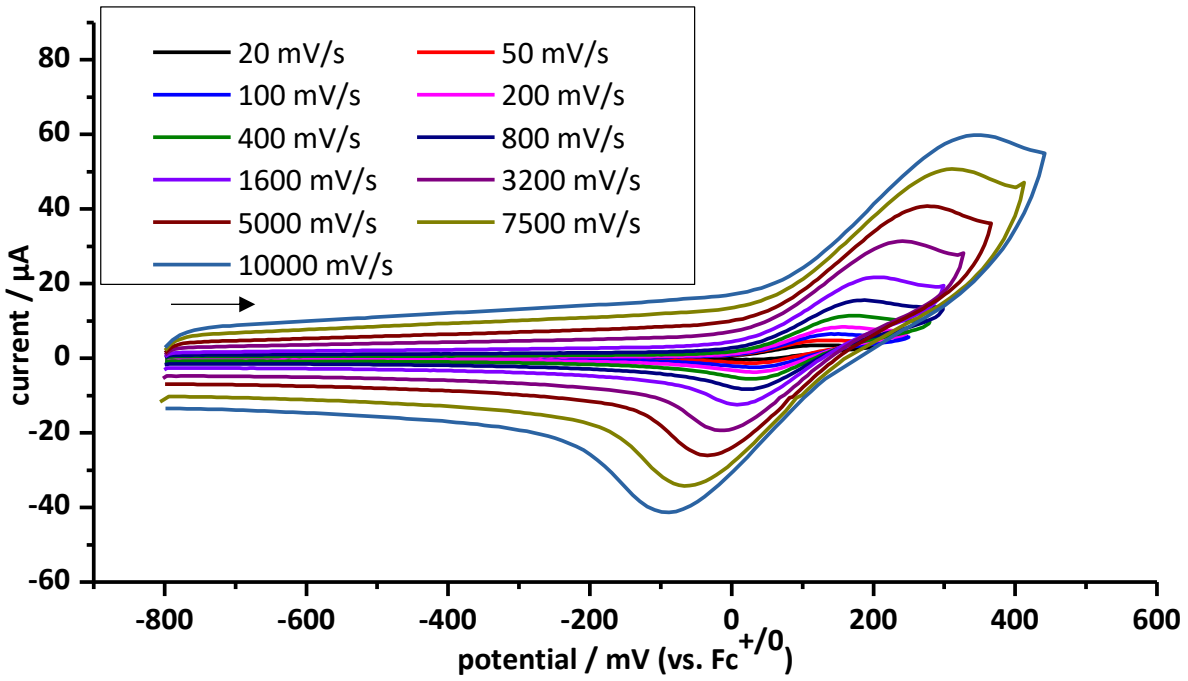

Fig. S52 Cyclic voltammogram of complex **3b** (1 mM) at a Pt electrode in a 0.2 M $^{n}Bu_4PF_6$/THF solution at various scan rates; measurement with anodic initial scan direction (denoted with an arrow) of the first redox process; potentials are referenced against $Fc^{+/0}$.

Table S4 Selected results of the cyclic voltametric studies of **3b** in 0.2 M $^{n}Bu_4NPF_6$/THF solution at ambient temperature. Potentials are referenced against $Fc^{+/0}$.

ν / mV/s	E_p^{Ia} / V	i_p^{Ia} / µA	E_p^{Ic} / V	i_p^{Ic} / µA	$E_{1/2}^{I}$ / V	ΔE_p^{I} / mV	$\lvert i_p^{c}/i_p^{a} \rvert$
20	0.12	1.74	0.02	−1.18	0.07	105	0.68
50	0.14	2.41	0.03	−2.47	0.08	105	1.03
100	0.15	3.60	0.03	−3.84	0.09	115	1.07
200	0.16	4.76	0.03	−5.48	0.10	121	1.15
400	0.17	6.66	0.02	−7.77	0.10	146	1.17
800	0.19	9.60	0.02	−11.4	0.11	163	1.19
1600	0.20	14.2	0.01	−16.9	0.11	197	1.19
3200	0.24	21.5	−0.02	−25.8	0.11	258	1.20
5000	0.28	30.1	−0.03	−34.7	0.12	310	1.15
7500	0.31	36.1	−0.07	−46.0	0.12	378	1.27
10000	0.35	40.6	−0.09	−56.4	0.13	440	1.39

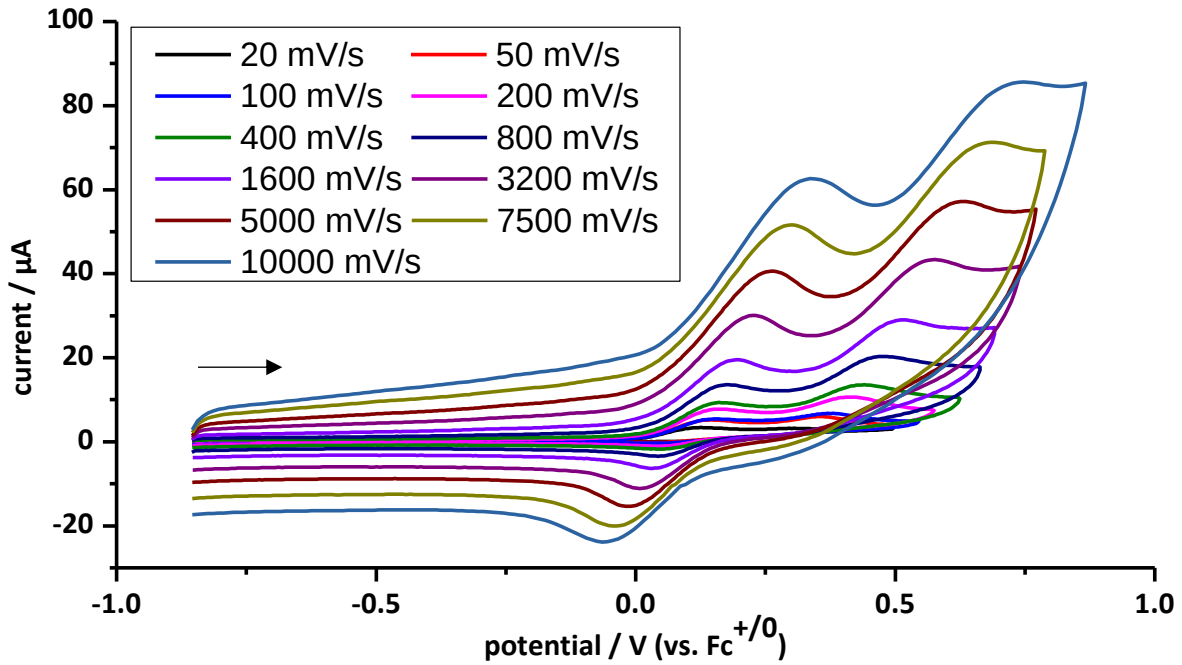

Fig. S53 Cyclic voltammogram of complex **3b** (1 mM) at a Pt electrode in a 0.2 M $^{n}Bu_4PF_6$/THF solution at various scan rates; measurement with anodic initial scan direction (denoted with an arrow) of the first and second redox process; potentials are referenced against $Fc^{+/0}$.

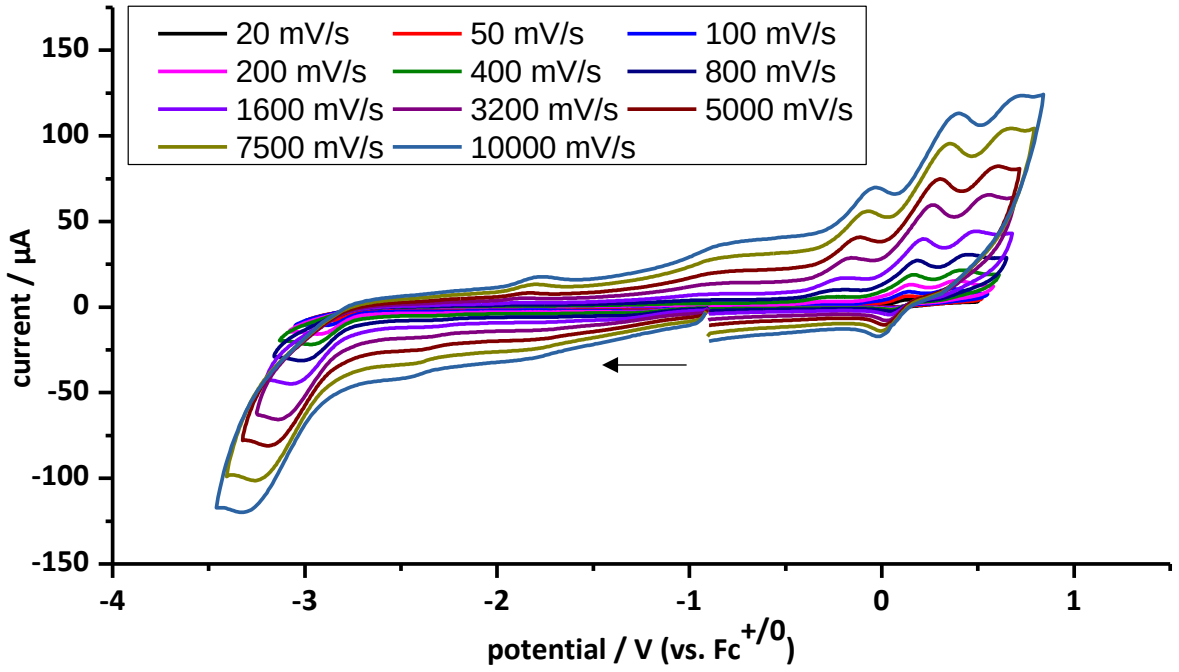

Fig. S54 Cyclic voltammogram of complex **3b** (1 mM) at a Pt electrode in a 0.2 M $^{n}Bu_4PF_6$/THF solution at various scan rates; measurement with cathodic initial scan direction (denoted with an arrow) of the first, second and third redox process; potentials are referenced against $Fc^{+/0}$.

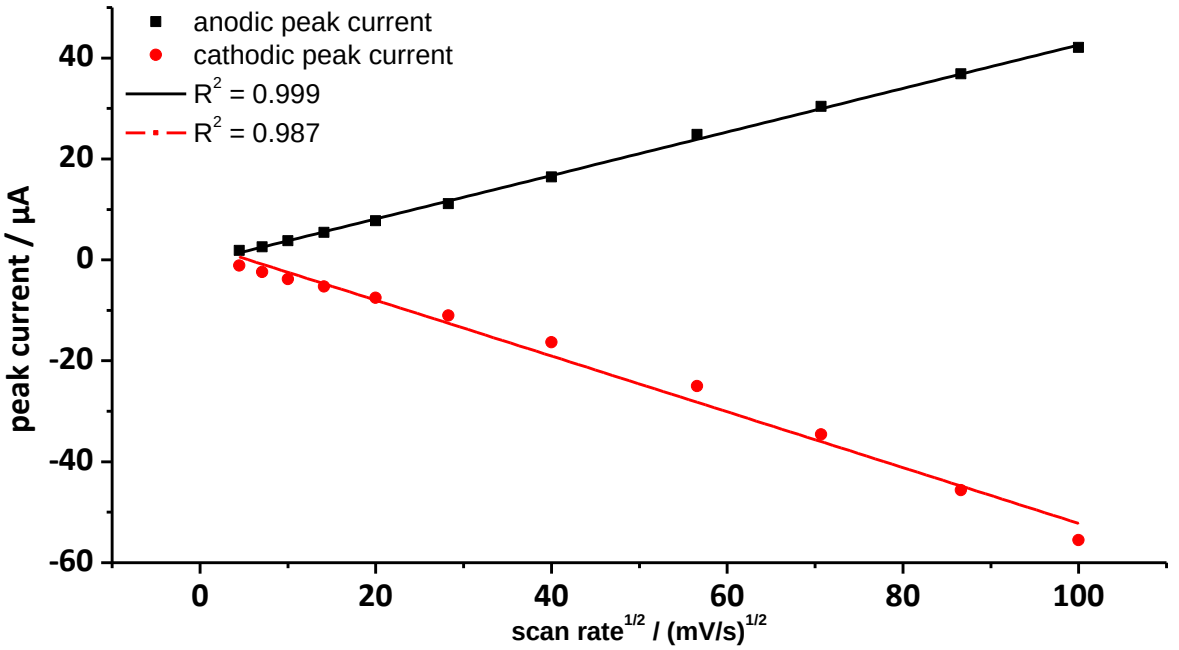

Fig. S55 Plot of the peak currents against the square root of the scan rate $\nu^{1/2}$ for the first redox process of complex **3b**.

Compound 3c

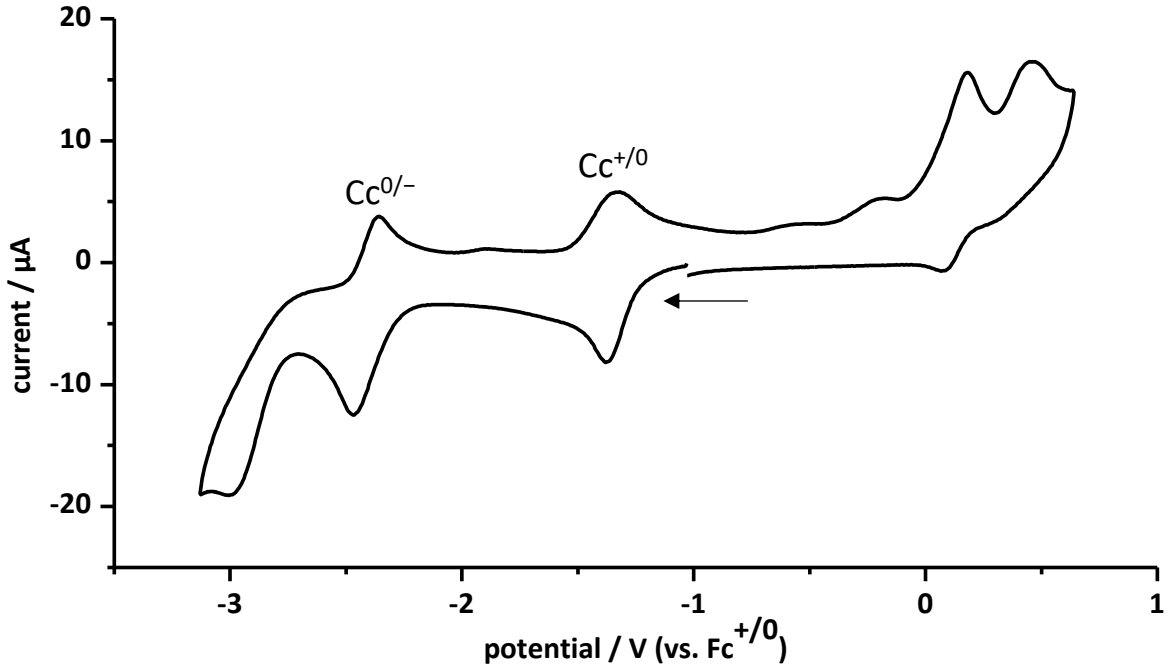

Fig. S56 Cyclic voltammogram of complex **3c** (1 mM) at a Pt electrode in a 0.2 M $^{n}Bu_4PF_6$/THF solution with cobaltocenium hexafluorophosphate as internal reference; measurement with cathodic initial scan direction (denoted with an arrow); scan rate: 200 mV/s; potentials are referenced against $Fc^{+/0}$.

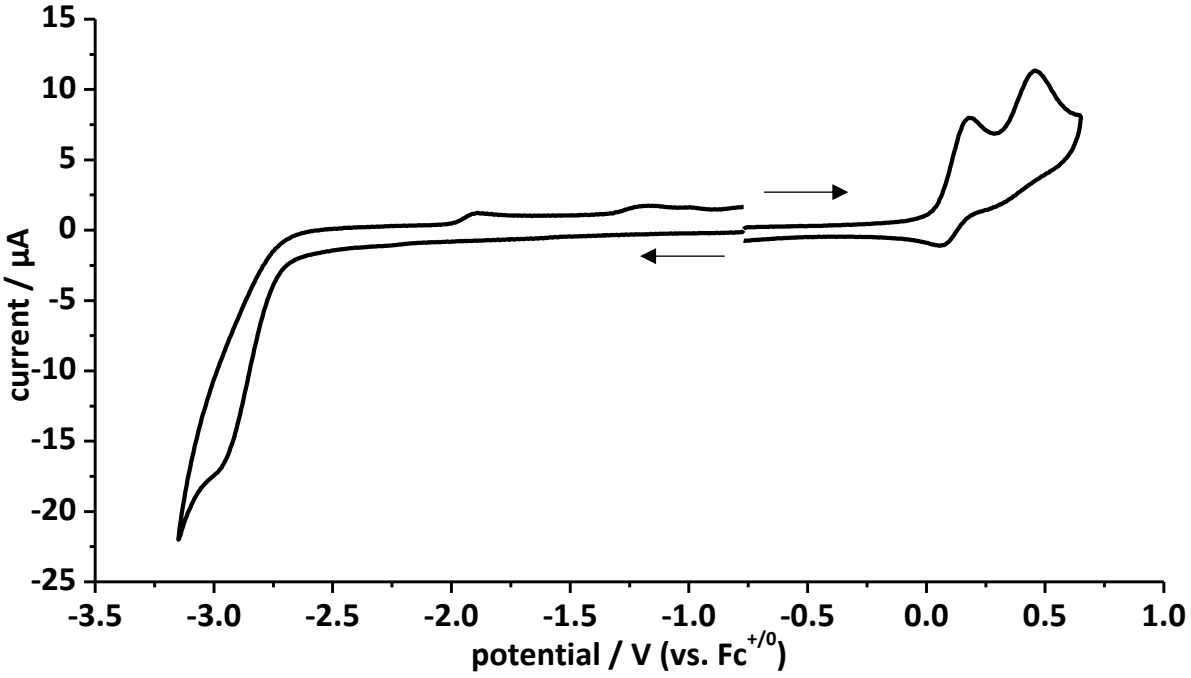

Fig. S57 Overlay of cyclic voltammograms of complex **3c** (1 mM) at a Pt electrode in a 0.2 M $^{n}Bu_4PF_6$/THF solution; oxidation part with anodic initial scan direction and reduction part with cathodic initial scan direction as denoted with arrows; scan rate: 200 mV/s; potentials are referenced against $Fc^{+/0}$.

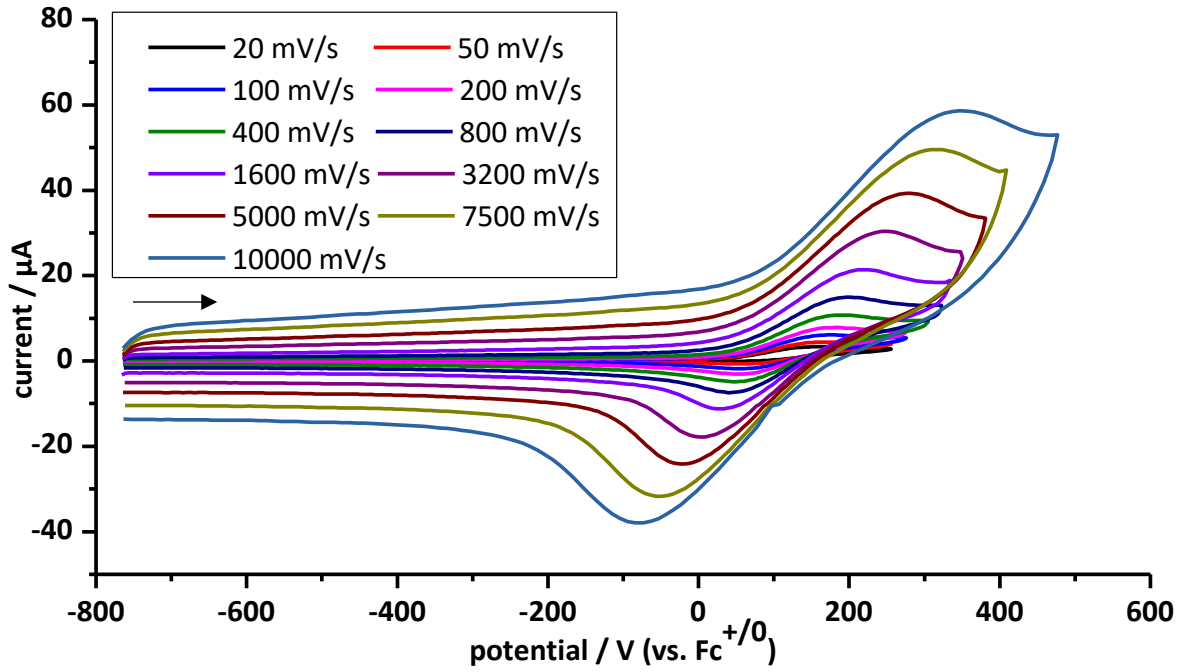

Fig. S58 Cyclic voltammogram of complex **3c** (1 mM) at a Pt electrode in a 0.2 M $^{n}Bu_4PF_6$/THF solution at various scan rates; measurement with anodic initial scan direction (denoted with an arrow) of the first redox process; potentials are referenced against $Fc^{+/0}$.

Table S5 Selected results of the cyclic voltametric studies of **3c** in 0.2 M $^{n}Bu_4NPF_6$/THF solution at ambient temperature. Potentials are referenced against $Fc^{+/0}$.

ν / mV/s	E_p^{Ia} / V	i_p^{Ia} / µA	E_p^{Ic} / V	i_p^{Ic} / µA	$E_{1/2}^{I}$ / V	ΔE_p^{I} / mV	$\lvert i_p^{c}/i_p^{a} \rvert$
20	0.16	1.97	0.05	−0.71	0.10	115	0.36
50	0.17	2.36	0.05	−1.59	0.11	121	0.68
100	0.18	3.17	0.06	−3.16	0.12	120	1.00
200	0.18	4.19	0.06	−4.72	0.12	125	1.13
400	0.19	6.44	0.05	−7.11	0.12	136	1.11
800	0.20	9.25	0.04	−10.6	0.12	162	1.14
1600	0.22	14.4	0.03	−15.8	0.12	192	1.10
3200	0.25	23.0	0.00	−24.0	0.13	248	1.04
5000	0.28	28.7	−0.02	−32.7	0.13	305	1.14
7500	0.32	35.0	−0.06	−43.4	0.13	373	1.24
10000	0.35	40.4	−0.08	−52.2	0.13	430	1.29

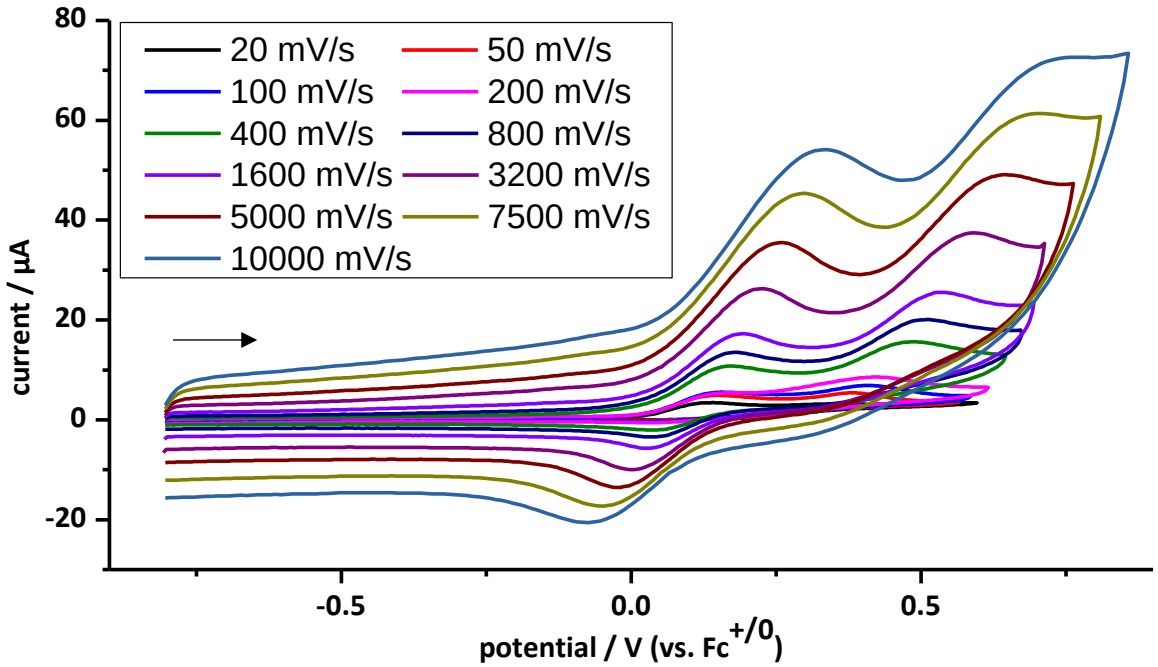

Fig. S59 Cyclic voltammogram of complex **3c** (1 mM) at a Pt electrode in a 0.2 M $^{n}Bu_4PF_6$/THF solution at various scan rates; measurement with anodic initial scan direction (denoted with an arrow) of the first and second redox process; potentials are referenced against $Fc^{+/0}$.

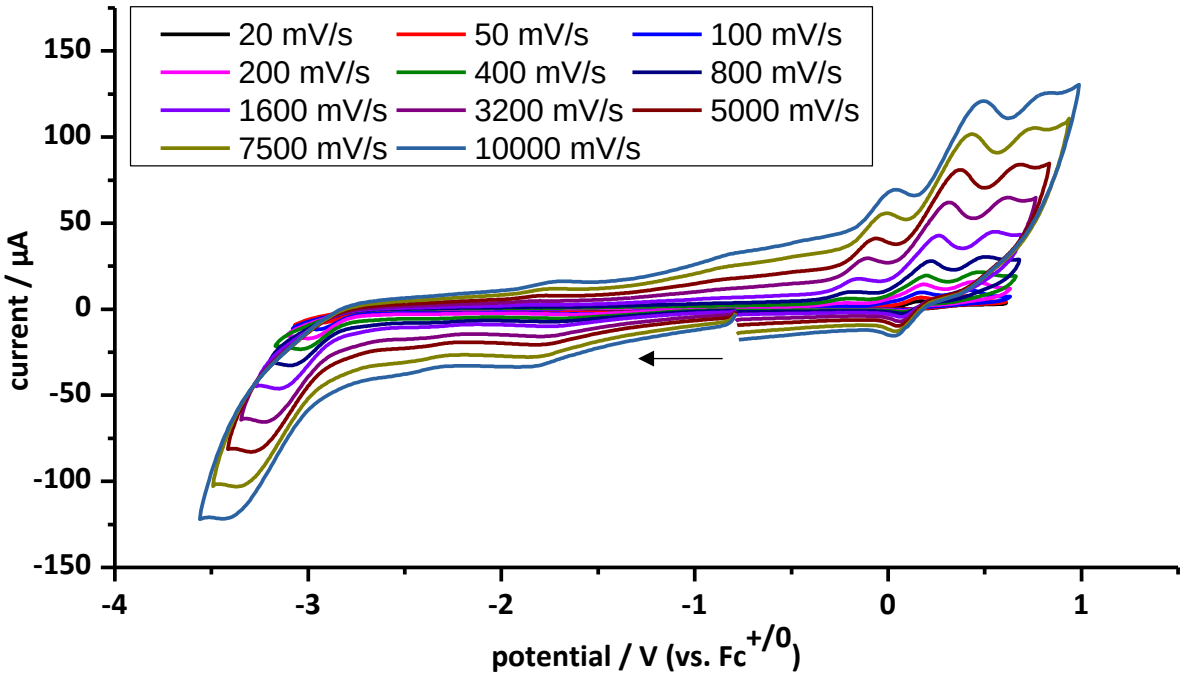

Fig. S60 Cyclic voltammogram of complex **3c** (1 mM) at a Pt electrode in a 0.2 M $^{n}Bu_4PF_6$/THF solution at various scan rates; measurement with cathodic initial scan direction (denoted with an arrow) of the first, second and third redox process; potentials are referenced against $Fc^{+/0}$.

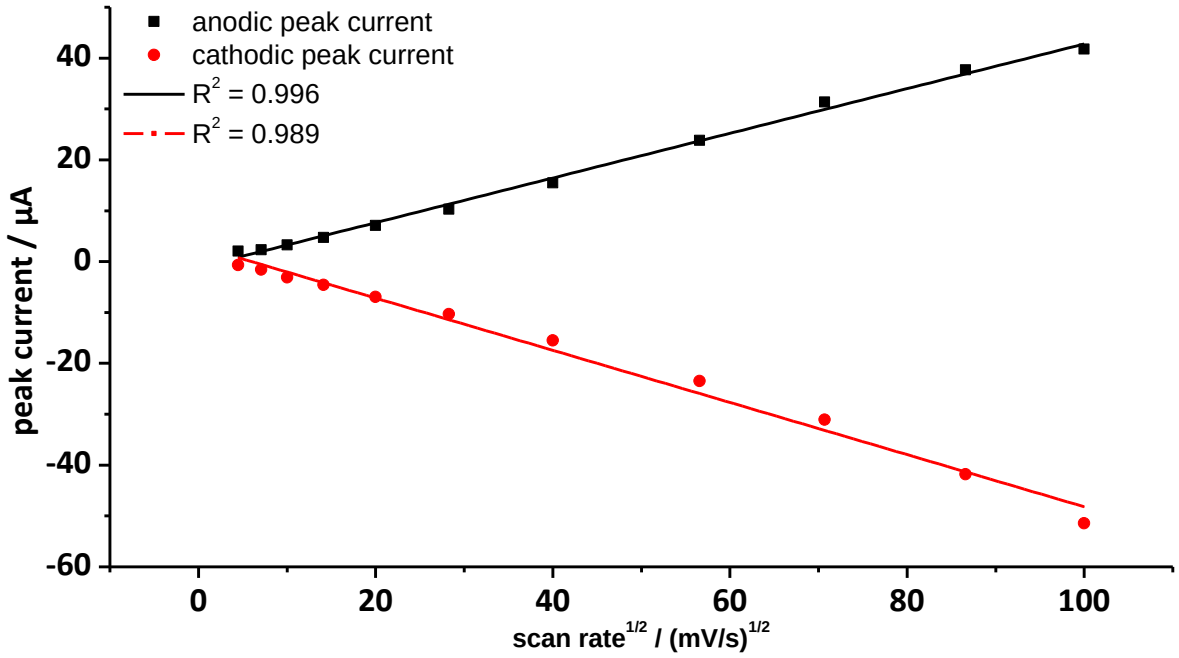

Fig. S61 Plot of the peak currents against the square root of the scan rate $\nu^{1/2}$ for the first redox process of **3c**.

5 X-ray diffraction studies

Compound 3a

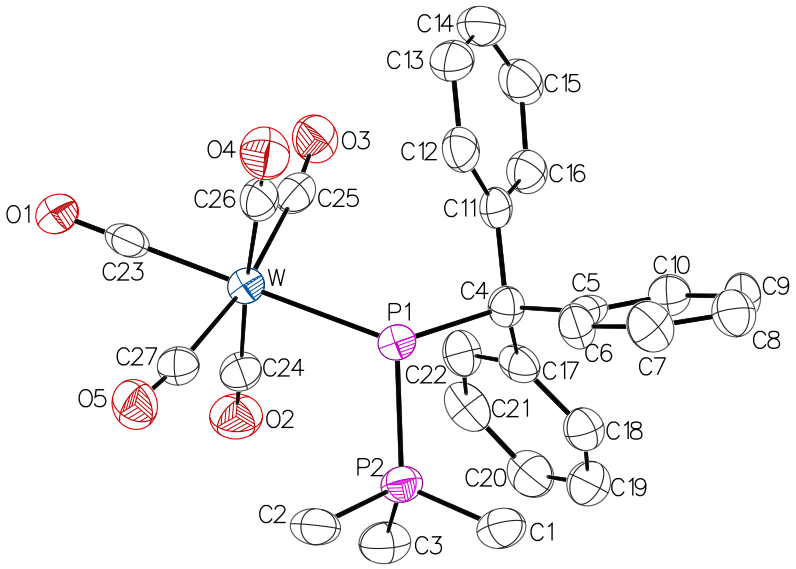

Fig. S62 Molecular structures of **3a** in the single crystal lattice at 123(2) K. Thermal ellipsoids are set at 50% probability level. Hydrogen atoms were omitted for clarity. Suitable single crystals were obtained as clear yellow plates by slowly evaporating a solution of 2.4 mg of **3a** in 3 mL of a 2:1 diethyl ether/THF mixture at ambient temperature in a glovebox. CCDC-2282404.

Table S6 Crystal data and structure refinements for **3a**.

Identification code	GSTR758, DB-491 // GXray6857
Crystal habitus	clear yellow plate
Device type	STOE IPDS-2T
Empirical formula	$C_{27}H_{24}O_5P_2W$
Moiety formula	$C_{27}H_{24}O_5P_2W$
Formula weight / g/mol	674.25
T / K	123(2)
Crystal system	Triclinic
Space group	$P\bar{1}$
a / Å	9.1192(4)
b / Å	9.4046(5)
c / Å	16.0948(8)
α / °	88.489(4)
β / °	76.363(4)
γ / °	70.182(4)
V / Å^3	1259.80(11)
Z	2
ρ_{calc} / g/cm^3	1.777
μ / mm^{-1}	4.748
F(000)	666.0
Crystal size / mm^3	0.21 × 0.15 × 0.1

Absorption correction	integration
Min. and max. transmission	0.2582 and 0.5544
Radiation	Mo-K_α (λ = 0.71073 Å)
2Θ range for data collection / °	4.892 to 56
Completeness to Θ	0.993
Index ranges	$-12 \le h \le 12$, $-12 \le k \le 10$, $-21 \le l \le 21$
Reflections collected	11644
Independent reflections	6004 (R_{int} = 0.0455, R_σ = 0.0648)
Data / restraints / parameters	6004 / 0 / 319
Goodness-of-fit on F^2	0.955
Final R indexes ($I \ge 2\sigma(I)$)	R_1 = 0.0316, ωR_2 = 0.0689
Final R indexes (all data)	R_1 = 0.0432, ωR_2 = 0.0709
Largest diff. peak and hole / e/Å^3	1.62 and −1.83

Table S7 Bond lengths for **3a**.

Atom	Atom	Length / Å	Atom	Atom	Length / Å
W	P1	2.6151(11)	C5	C6	1.384(6)
W	C23	1.978(5)	C5	C10	1.384(6)
W	C24	2.052(5)	C6	C7	1.394(6)
W	C25	2.047(4)	C7	C8	1.383(7)
W	C26	2.054(5)	C8	C9	1.390(7)
W	C27	2.031(4)	C9	C10	1.379(6)
P1	P2	2.1584(14)	C11	C12	1.402(6)
P1	C4	1.958(4)	C11	C16	1.395(6)
P2	C1	1.804(5)	C12	C13	1.384(6)
P2	C2	1.807(5)	C13	C14	1.377(7)
P2	C3	1.811(5)	C14	C15	1.394(7)
O1	C23	1.161(5)	C15	C16	1.393(6)
O2	C24	1.139(5)	C17	C18	1.399(6)
O3	C25	1.147(5)	C17	C22	1.404(6)
O4	C26	1.132(5)	C18	C19	1.382(6)
O5	C27	1.138(5)	C19	C20	1.376(7)
C4	C5	1.560(6)	C20	C21	1.399(6)
C4	C11	1.545(6)	C21	C22	1.381(6)
C4	C17	1.536(6)			

Table S8 Bond angles for **3a**.

Atom	Atom	Atom	Angle / °	Atom	Atom	Atom	Angle / °
C23	W	P1	171.70(14)	C6	C5	C4	123.3(4)
C23	W	C24	90.88(17)	C6	C5	C10	118.5(4)
C23	W	C25	87.66(17)	C10	C5	C4	118.1(4)
C23	W	C26	91.99(17)	C5	C6	C7	120.8(4)
C23	W	C27	83.17(17)	C8	C7	C6	120.3(4)
C24	W	P1	95.87(12)	C7	C8	C9	118.8(4)
C24	W	C26	176.59(18)	C10	C9	C8	120.5(4)
C25	W	P1	97.38(12)	C9	C10	C5	121.1(4)
C25	W	C24	88.07(17)	C12	C11	C4	120.2(4)
C25	W	C26	90.21(17)	C16	C11	C4	122.0(4)
C26	W	P1	81.43(12)	C16	C11	C12	117.6(4)
C27	W	P1	91.45(12)	C13	C12	C11	121.2(4)
C27	W	C24	94.52(17)	C14	C13	C12	120.5(4)
C27	W	C25	170.51(16)	C13	C14	C15	119.3(4)
C27	W	C26	87.65(17)	C16	C15	C14	120.1(4)
P2	P1	W	109.87(5)	C15	C16	C11	121.1(4)
C4	P1	W	119.36(13)	C18	C17	C4	123.4(4)
C4	P1	P2	102.93(13)	C18	C17	C22	117.2(4)
C1	P2	P1	112.21(15)	C22	C17	C4	119.4(4)
C1	P2	C2	103.8(2)	C19	C18	C17	121.2(4)
C1	P2	C3	106.5(2)	C20	C19	C18	120.8(4)
C2	P2	P1	107.49(15)	C19	C20	C21	119.3(4)
C2	P2	C3	103.2(2)	C22	C21	C20	119.8(4)
C3	P2	P1	121.89(16)	C21	C22	C17	121.6(4)
C5	C4	P1	111.1(3)	O1	C23	W	179.1(4)
C11	C4	P1	106.3(3)	O2	C24	W	177.1(4)
C11	C4	C5	105.1(3)	O3	C25	W	173.4(4)
C17	C4	P1	108.7(3)	O4	C26	W	177.8(4)
C17	C4	C5	112.8(3)	O5	C27	W	173.5(4)
C17	C4	C11	112.7(3)				

Table S9 Torsion angles for **3a**.

A	B	C	D	Angle / °	A	B	C	D	Angle / °
P1	C4	C5	C6	−9.1(5)	C10	C5	C6	C7	−1.5(6)
P1	C4	C5	C10	174.9(3)	C11	C4	C5	C6	105.4(4)
P1	C4	C11	C12	44.2(4)	C11	C4	C5	C10	−70.6(4)
P1	C4	C11	C16	−140.9(4)	C11	C4	C17	C18	133.7(4)
P1	C4	C17	C18	−108.8(4)	C11	C4	C17	C22	−48.9(5)
P1	C4	C17	C22	68.6(4)	C11	C12	C13	C14	−2.9(7)
C4	C5	C6	C7	−177.5(4)	C12	C11	C16	C15	−1.7(6)
C4	C5	C10	C9	178.4(4)	C12	C13	C14	C15	−0.5(7)
C4	C11	C12	C13	179.1(4)	C13	C14	C15	C16	2.8(7)
C4	C11	C16	C15	−176.8(4)	C14	C15	C16	C11	−1.7(7)
C4	C17	C18	C19	174.9(4)	C16	C11	C12	C13	4.0(6)
C4	C17	C22	C21	−175.8(4)	C17	C4	C5	C6	−131.4(4)
C5	C4	C11	C12	−73.7(5)	C17	C4	C5	C10	52.6(5)
C5	C4	C11	C16	101.3(4)	C17	C4	C11	C12	163.1(4)
C5	C4	C17	C18	14.9(5)	C17	C4	C11	C16	−21.9(6)
C5	C4	C17	C22	−167.7(4)	C17	C18	C19	C20	0.9(7)
C5	C6	C7	C8	−0.7(6)	C18	C17	C22	C21	1.8(6)
C6	C5	C10	C9	2.2(6)	C18	C19	C20	C21	1.6(7)
C6	C7	C8	C9	2.3(7)	C19	C20	C21	C22	−2.3(7)
C7	C8	C9	C10	−1.7(6)	C20	C21	C22	C17	0.6(7)
C8	C9	C10	C5	−0.6(6)	C22	C17	C18	C19	−2.6(6)

Compound 3a-Cr

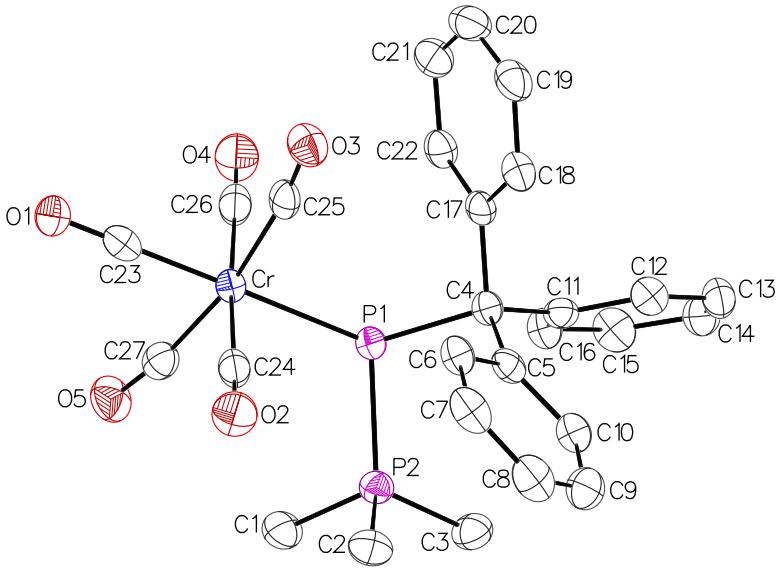

Fig. S63 Molecular structures of **3a-Cr** in the single crystal lattice at 100(2) K. Thermal ellipsoids are set at 50% probability level. Hydrogen atoms were omitted for clarity. Suitable single crystals were obtained as clear light yellow prisms by slowly evaporating a solution of **3a-Cr** in diethyl ether at ambient temperature in a glovebox. CCDC-2282405.

Table S10 Crystal data and structure refinements for **3a-Cr**.

Identification code	GSTR771, DB-565 // GXray6923
Crystal habitus	clear light yellow prisms
Device type	STOE STADIVARI
Empirical formula	$C_{27}H_{24}O_5P_2Cr$
Moiety formula	$C_{27}H_{24}O_5P_2Cr$
Formula weight / g/mol	542.42
T / K	100
Crystal system	triclinic
Space group	$P\bar{1}$
a / Å	9.06234(20)
b / Å	9.31754(23)
c / Å	15.9532(3)
α / °	88.1908(19)
β / °	76.3409(17)
γ / °	70.2330(18)
V / Å^3	1230.12(5)
Z	2
ρ_{calc} / g/cm^3	1.464
μ / mm^{-1}	5.38
F(000)	560.0
Crystal size / mm^3	0.3 × 0.177 × 0.08
Absorption correction	multi-scan
Min. and max. transmission	0.1558 and 0.2633

Radiation	Cu-K_α (λ = 1.54186 Å)
2Θ range for data collection / °	10.102 to 141.05
Completeness to Θ	0.988
Index ranges	$-11 \le h \le 9$, $-11 \le k \le 5$, $-19 \le l \le 18$
Reflections collected	24426
Independent reflections	24037 (R_{int} = 0.0176, R_σ = 0.0122)
Data / restraints / parameters	24037 / 0 / 319
Goodness-of-fit on F^2	1.038
Final R indexes ($I \ge 2\sigma(I)$)	R_1 = 0.0290, ωR_2 = 0.0784
Final R indexes (all data)	R_1 = 0.0297, ωR_2 = 0.0789
Largest diff. peak and hole / e/Å^3	0.56 and −0.47

Table S11 Bond lengths for **3a-Cr**.

Atom	Atom	Length / Å	Atom	Atom	Length / Å
Cr	P1	2.5025(5)	C5	C6	1.405(2)
Cr	C23	1.8332(18)	C5	C10	1.398(2)
Cr	C24	1.9105(18)	C6	C7	1.388(2)
Cr	C25	1.9047(17)	C7	C8	1.384(3)
Cr	C26	1.9080(18)	C8	C9	1.386(3)
Cr	C27	1.8895(18)	C9	C10	1.390(3)
P1	P2	2.1621(6)	C11	C12	1.401(2)
P1	C4	1.9586(16)	C11	C16	1.390(2)
P2	C1	1.8095(17)	C12	C13	1.387(2)
P2	C2	1.8116(17)	C13	C14	1.381(3)
P2	C3	1.8058(18)	C14	C15	1.383(3)
O1	C23	1.165(2)	C15	C16	1.395(2)
O2	C24	1.143(2)	C17	C18	1.398(2)
O3	C25	1.148(2)	C17	C22	1.401(2)
O4	C26	1.139(2)	C18	C19	1.389(3)
O5	C27	1.146(2)	C19	C20	1.390(3)
C4	C5	1.535(2)	C20	C21	1.389(3)
C4	C11	1.549(2)	C21	C22	1.395(3)
C4	C17	1.542(2)			

Table S12 Bond angles for **3a-Cr**.

Atom	Atom	Atom	Angle / °	Atom	Atom	Atom	Angle / °
C23	Cr	P1	172.36(5)	C6	C5	C4	119.30(15)
C23	Cr	C24	91.10(7)	C10	C5	C4	123.34(15)
C23	Cr	C25	87.52(7)	C10	C5	C6	117.27(16)
C23	Cr	C26	92.30(7)	C7	C6	C5	121.29(17)
C23	Cr	C27	83.68(7)	C8	C7	C6	120.46(17)
C24	Cr	P1	94.64(5)	C7	C8	C9	119.09(16)
C25	Cr	P1	97.67(5)	C8	C9	C10	120.65(17)
C25	Cr	C24	88.32(7)	C9	C10	C5	121.17(16)
C25	Cr	C26	90.76(7)	C12	C11	C4	118.05(14)
C26	Cr	P1	82.06(5)	C16	C11	C4	124.28(14)
C26	Cr	C24	176.43(7)	C16	C11	C12	117.56(15)
C27	Cr	P1	90.85(5)	C13	C12	C11	121.30(15)
C27	Cr	C24	94.36(7)	C14	C13	C12	120.31(16)
C27	Cr	C25	170.84(7)	C13	C14	C15	119.35(16)
C27	Cr	C26	87.08(7)	C14	C15	C16	120.37(16)
P2	P1	Cr	110.72(2)	C11	C16	C15	121.06(16)
C4	P1	Cr	119.91(5)	C18	C17	C4	122.53(15)
C4	P1	P2	102.45(5)	C18	C17	C22	117.65(16)
C1	P2	P1	107.38(6)	C22	C17	C4	119.67(14)
C1	P2	C2	103.32(8)	C19	C18	C17	121.11(17)
C2	P2	P1	122.58(6)	C18	C19	C20	120.62(17)
C3	P2	P1	111.93(6)	C21	C20	C19	119.14(17)
C3	P2	C1	103.80(8)	C20	C21	C22	120.15(17)
C3	P2	C2	106.01(9)	C21	C22	C17	121.21(16)
C5	C4	P1	109.07(10)	O1	C23	Cr	178.96(16)
C5	C4	C11	112.63(13)	O2	C24	Cr	176.18(15)
C5	C4	C17	112.52(13)	O3	C25	Cr	172.33(14)
C11	C4	P1	111.30(10)	O4	C26	Cr	178.60(16)
C17	C4	P1	106.53(11)	O5	C27	Cr	172.35(15)
C17	C4	C11	104.58(13)				

Table S13 Torsion angles for **3a-Cr**.

A	B	C	D	Angle / °	A	B	C	D	Angle / °
P1	C4	C5	C6	−67.98(16)	C10	C5	C6	C7	−0.9(2)
P1	C4	C5	C10	108.38(15)	C11	C4	C5	C6	167.92(14)
P1	C4	C11	C12	−175.56(12)	C11	C4	C5	C10	−15.7(2)
P1	C4	C11	C16	8.3(2)	C11	C4	C17	C18	−102.42(17)
P1	C4	C17	C18	139.63(14)	C11	C4	C17	C22	72.96(17)
P1	C4	C17	C22	−44.99(17)	C11	C12	C13	C14	1.2(3)
C4	C5	C6	C7	175.63(15)	C12	C11	C16	C15	2.1(3)
C4	C5	C10	C9	−174.34(15)	C12	C13	C14	C15	0.9(3)
C4	C11	C12	C13	−179.03(16)	C13	C14	C15	C16	−1.4(3)
C4	C11	C16	C15	178.22(16)	C14	C15	C16	C11	−0.1(3)
C4	C17	C18	C19	178.23(15)	C16	C11	C12	C13	−2.6(3)
C4	C17	C22	C21	−179.78(15)	C17	C4	C5	C6	50.01(19)
C5	C4	C11	C12	−52.7(2)	C17	C4	C5	C10	−133.63(16)
C5	C4	C11	C16	131.17(17)	C17	C4	C11	C12	69.79(18)
C5	C4	C17	C18	20.1(2)	C17	C4	C11	C16	−106.33(18)
C5	C4	C17	C22	−164.47(14)	C17	C18	C19	C20	0.1(3)
C5	C6	C7	C8	−1.3(3)	C18	C17	C22	C21	−4.2(2)
C6	C5	C10	C9	2.1(2)	C18	C19	C20	C21	−1.6(3)
C6	C7	C8	C9	2.5(3)	C19	C20	C21	C22	0.2(3)
C7	C8	C9	C10	−1.3(3)	C20	C21	C22	C17	2.8(3)
C8	C9	C10	C5	−1.0(3)	C22	C17	C18	C19	2.8(2)

Compound 3b

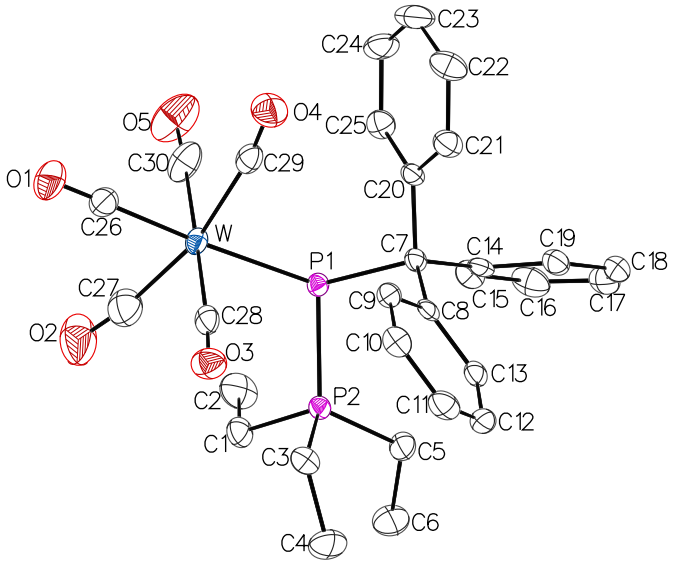

Fig. S64 Molecular structures of **3b** in the single crystal lattice at 100(2) K. Thermal ellipsoids are set at 50% probability level. Hydrogen atoms were omitted for clarity. Suitable single crystals were obtained as clear yellow blocks by slowly evaporating a solution of 3.3 mg of **3b** in 4 mL of diethyl ether at ambient temperature in a glovebox. CCDC-2282406.

Table S14 Crystal data and structure refinements for **3b**.

Identification code	GSTR759, DB-495 // GXraymo_6858f
Crystal habitus	clear yellow block
Device type	Bruker D8 Venture
Empirical formula	$C_{30}H_{30}O_5P_2W$
Moiety formula	$C_{30}H_{30}O_5P_2W$
Formula weight / g/mol	716.33
T / K	100.0
Crystal system	monoclinic
Space group	$P2_1/c$
a / Å	9.5507(4)
b / Å	14.6045(5)
c / Å	20.9543(7)
α / °	90
β / °	101.0820(10)
γ / °	90
V / Å^3	2868.27(18)
Z	4
ρ_{calc} / g/cm^3	1.659
μ / mm^{-1}	4.176
F(000)	1416.0
Crystal size / mm^3	0.28 × 0.25 × 0.24
Absorption correction	empirical
Min. and max. transmission	0.5165 and 0.7461

Radiation	Mo-K_α (λ = 0.71073 Å)
2Θ range for data collection / °	4.346 to 51.998
Completeness to Θ	0.939
Index ranges	−11 ≤ *h* ≤ 11, −18 ≤ *k* ≤ 18, −25 ≤ *l* ≤ 25
Reflections collected	30521
Independent reflections	5325 (R_{int} = 0.0421, R_σ = 0.0242)
Data / restraints / parameters	5325 / 18 / 346
Goodness-of-fit on F^2	1.209
Final *R* indexes ($I \geq 2\sigma(I)$)	R_1 = 0.0204, ωR_2 = 0.0476
Final *R* indexes (all data)	R_1 = 0.0206, ωR_2 = 0.0477
Largest diff. peak and hole / e/Å^3	0.61 and −0.82

Table S15 Bond lengths for **3b**.

Atom	Atom	Length / Å	Atom	Atom	Length / Å
W	P1	2.6373(6)	C7	C14	1.545(3)
W	C26	1.984(2)	C7	C20	1.545(3)
W	C27	2.022(3)	C8	C9	1.403(3)
W	C28	2.037(3)	C8	C13	1.403(3)
W	C29	2.062(3)	C9	C10	1.386(3)
W	C30	2.051(3)	C10	C11	1.394(4)
P1	P2	2.1747(8)	C11	C12	1.387(4)
P1	C7	1.945(2)	C12	C13	1.391(3)
P2	C1	1.815(2)	C14	C15	1.390(4)
P2	C3	1.824(2)	C14	C19	1.405(3)
P2	C5	1.833(2)	C15	C16	1.389(4)
O1	C26	1.150(3)	C16	C17	1.388(4)
O2	C27	1.146(4)	C17	C18	1.386(4)
O3	C28	1.147(3)	C18	C19	1.391(4)
O4	C29	1.138(3)	C20	C21	1.398(3)
O5	C30	1.135(4)	C20	C25	1.396(3)
C1	C2	1.527(4)	C21	C22	1.390(4)
C3	C4	1.531(3)	C22	C23	1.387(4)
C5	C6	1.534(3)	C23	C24	1.388(4)
C7	C8	1.533(3)	C24	C25	1.391(4)

Table S16 Bond angles for **3b**.

Atom	Atom	Atom	Angle / °	Atom	Atom	Atom	Angle / °
C26	W	P1	175.02(7)	C14	C7	C20	104.01(18)
C26	W	C27	85.30(11)	C20	C7	P1	105.75(15)
C26	W	C28	89.55(10)	C9	C8	C7	120.4(2)
C26	W	C29	83.38(10)	C13	C8	C7	122.2(2)
C26	W	C30	89.90(10)	C13	C8	C9	117.3(2)
C27	W	P1	94.17(8)	C10	C9	C8	121.3(2)
C27	W	C28	92.19(11)	C9	C10	C11	120.6(2)
C27	W	C29	167.67(10)	C12	C11	C10	119.0(2)
C27	W	C30	87.30(12)	C11	C12	C13	120.4(2)
C28	W	P1	95.42(7)	C12	C13	C8	121.4(2)
C28	W	C29	92.61(10)	C15	C14	C7	123.8(2)
C28	W	C30	179.28(10)	C15	C14	C19	117.4(2)
C29	W	P1	96.68(7)	C19	C14	C7	118.6(2)
C30	W	P1	85.12(7)	C16	C15	C14	121.4(2)
C30	W	C29	87.80(11)	C17	C16	C15	120.4(3)
P2	P1	W	109.25(3)	C18	C17	C16	119.2(2)
C7	P1	W	116.69(7)	C17	C18	C19	120.2(2)
C7	P1	P2	103.45(8)	C18	C19	C14	121.2(2)
C1	P2	P1	105.15(8)	C21	C20	C7	122.1(2)
C1	P2	C3	105.08(12)	C25	C20	C7	119.8(2)
C1	P2	C5	104.72(12)	C25	C20	C21	117.8(2)
C3	P2	P1	117.60(8)	C22	C21	C20	121.0(2)
C3	P2	C5	108.88(12)	C23	C22	C21	120.5(2)
C5	P2	P1	114.11(8)	C22	C23	C24	119.2(2)
C2	C1	P2	113.97(18)	C23	C24	C25	120.2(2)
C4	C3	P2	116.32(18)	C24	C25	C20	121.2(2)
C6	C5	P2	116.62(18)	O1	C26	W	179.2(2)
C8	C7	P1	109.17(15)	O2	C27	W	172.1(3)
C8	C7	C14	112.09(19)	O3	C28	W	176.2(2)
C8	C7	C20	113.69(19)	O4	C29	W	171.3(2)
C14	C7	P1	111.93(16)	O5	C30	W	177.3(2)

6 Computational Details

Quantum chemical calculations were performed with the ORCA electronic structure program package.[10] All geometry optimizations were run in redundant internal coordinates with tight convergence criteria, using the B3LYP[12] functional together with the powerful speeding up RIJCOSX algorithm[13] and the Ahlrichs' segmented def2-TZVP basis set.[14] For W atoms the [SD(60,MWB)] effective core potential (ECP) was used, as obtained from Turbomole basis set library (ftp://ftp.chemie.uni-karlsruhe.de/pub/basen/).[15] In all optimizations and energy evaluations, the 2010 Grimme's semiempirical atom-pair-wise correction (DFT-D3 methods), taking into account the major part of the contribution of dispersion forces to the energy, was included.[16] Harmonic frequency calculations verified the nature of the computed species as minima structures, featuring none negative eigenvalues. From these geometries, all reported electronic data were obtained by means of single-point (SP) calculations using (unless otherwise indicated) the same functional as well as the more polarized def2-TZVPP basis set. Basis sets may be obtained from the Basis Set Exchange (BSE) software and the EMSL Basis Set Library (https://bse.pnl.gov/bse/portal).[17] Reported energies were corrected for the Gibbs energy term at the optimization level and obtained by means of the double-hybrid-meta-GGA functional PWPB95[18] with Grimme's D3 correction (PWPB95-D3) and the def2-QZVPP[19] basis set. Solvent effects (toluene) were included using the Conductor-like Polarizable Continuum Model (CPCM).[20] Isotropic values (σ_{iso}) for the ^{31}P NMR magnetic shielding tensor were computed using the Gauge Including Atomic Orbital (GIAO) method,[21] using the PBE0[22] functional and the def2-TZVP(ecp) basis set. The expected chemical shifts δ^P were estimated through a linear equation $\delta^P = 237.68 - 0.8628 \cdot \sigma_{iso}$, which in turn was obtained from a linear regression ($R^2 = 0.997$) of nine reference compounds spanning a wide range of chemical shifts, as reported elsewhere.[7,23] Diamagnetic and paramagnetic contributions were scaled using the same linear equation. Data of the Laplacian of the electron density along the P-P bond path were obtained using Multiwfn.[24]

Table S17 Computed diamagnetic and paramagnetic contributions (ppm) to the chemical shift from the isotropic value of the magnetic shielding tensor for **3a–c**.

	3a	**3b**	**3c**
Diamagnetic	−608.8	−611.9	−616.3
Paramagnetic	828.1	843.0	814.0

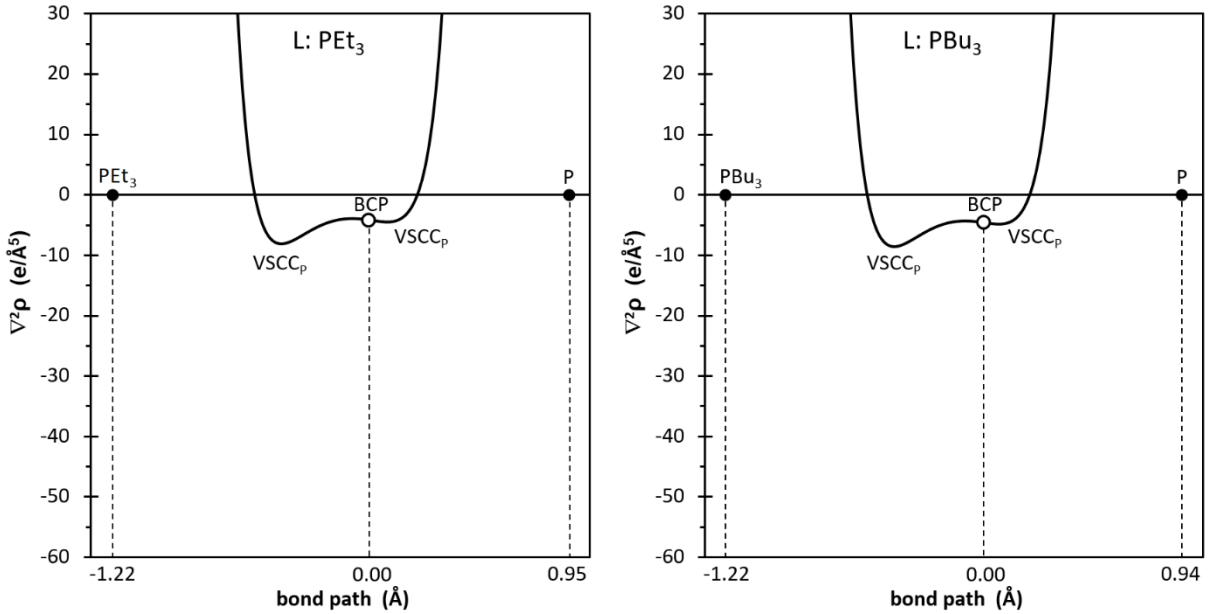

Fig. S65 Computed [B3LYP-D3/def2-TZVPP(ecp)//B3LYP-D3/def2-TZVP(ecp)] variation of the Laplacian of the electron density $\nabla^2\rho$ for complex **3b** (left) and **3c** (right) along the P-P bond path.

7 Calculated structures

Cartesian coordinates (in Å) and energies (in hartrees) for all computed species. Geometries, zero-point energy correction (ZPE) and Gibbs energy correction (G_{corr}) at the optimization level (*vide supra*), whereas electronic energies are computed at the CPCM(toluene)/PWPB95-D3/def2-QZVPP(ecp) level.

PMe_3

E = -461.022182251620 au [$CPCM_{to}$/PWPB95-D3/def2-QZVPP]
ZPE = 0.11189177 au [$CPCM_{to}$/B3LYP-D3/def2-TZVP]
G_{corr} = 0.08262959 au [$CPCM_{to}$/B3LYP-D3/def2-TZVP]

P	-0.803610	-1.099068	-0.916435
C	-0.779107	-2.922124	-0.611656
H	-1.179137	-3.130381	0.382105
H	-1.369085	-3.466778	-1.353751
H	0.250550	-3.282398	-0.643115
C	-0.338120	-1.078588	-2.705217
H	-0.958629	-1.758701	-3.294991
H	0.708188	-1.369623	-2.812399
H	-0.448682	-0.066575	-3.098381
C	-2.626803	-0.835315	-1.068875
H	-2.819867	0.185945	-1.401695
H	-3.081135	-1.532189	-1.778353
H	-3.096448	-0.966342	-0.092543

PEt_3

E = -578.913511631710 au [$CPCM_{to}$/PWPB95-D3/def2-QZVPP]
ZPE = 0.19779148 au [$CPCM_{to}$/B3LYP-D3/def2-TZVP]
G_{corr} = 0.16257736 au [$CPCM_{to}$/B3LYP-D3/def2-TZVP]

P	-1.126047	-0.996549	-1.025433
C	-1.388348	-2.832000	-0.901998
H	-2.134552	-2.991817	-0.119974
H	-1.821613	-3.199083	-1.838361
C	-0.112937	-3.602058	-0.558817
H	0.643150	-3.495354	-1.338967
H	0.322705	-3.242963	0.376009
H	-0.319876	-4.668511	-0.445716
C	-0.274861	-0.907510	-2.674564
H	-0.885409	-1.420361	-3.425217
H	0.655967	-1.471873	-2.579424
C	0.035701	0.522815	-3.116606
H	0.580180	0.528759	-4.063405
H	-0.875793	1.106612	-3.258369
H	0.647491	1.038934	-2.373670
C	-2.836002	-0.464437	-1.520924
H	-2.749536	0.552824	-1.910331
H	-3.186220	-1.094642	-2.345193
C	-3.833700	-0.486322	-0.362522
H	-3.973231	-1.495746	0.029096

H	-3.492371	0.144348	0.461094	H	-4.811568	-0.120539	-0.683305

PBu_3

E = -814.704532370161 au [$CPCM_{to}$/PWPB95-D3/def2-QZVPP]
ZPE = 0.36829327 au [$CPCM_{to}$/B3LYP-D3/def2-TZVP]
G_{corr} = 0.32312945 au [$CPCM_{to}$/B3LYP-D3/def2-TZVP]

P	0.011644	0.076242	0.021528	H	0.951275	-5.473195	-0.218584
C	0.076297	-0.127723	1.871409	H	-0.616584	-6.284684	-0.237726
C	1.800397	-0.129997	-0.437794	H	-0.749505	1.790591	2.366189
C	-0.673596	-1.574122	-0.495048	H	0.995705	1.787901	2.290829
H	0.919149	-0.769082	2.139161	C	0.207490	1.045050	4.148993
H	-0.833281	-0.662058	2.163550	H	-0.636302	0.434135	4.488052
C	0.134701	1.202523	2.627145	H	0.078265	2.029537	4.608706
H	2.201030	-1.031055	0.030574	C	1.516469	0.432863	4.646303
C	2.665432	1.082689	-0.088816	H	1.656795	-0.583362	4.273047
H	1.822257	-0.292549	-1.520910	H	1.541246	0.388714	5.737125
C	-0.020975	-2.848401	0.040722	H	2.372529	1.028089	4.316649
H	-0.658092	-1.579198	-1.589865	H	2.191412	1.986772	-0.482373
H	-1.731233	-1.554120	-0.212149	C	4.098238	0.994208	-0.623533
H	-0.009876	-2.829498	1.134379	H	2.704206	1.204546	0.997978
H	1.024513	-2.894203	-0.276342	H	4.067435	0.881886	-1.712637
C	-0.734927	-4.117704	-0.425777	C	4.919987	-0.140938	-0.014588
H	-1.782690	-4.076241	-0.109889	H	4.602323	1.945251	-0.426612
C	-0.088750	-5.393615	0.108637	H	4.502278	-1.119272	-0.259456
H	-0.746469	-4.141529	-1.520582	H	4.950854	-0.056949	1.075370
H	-0.093228	-5.406574	1.201768	H	5.948842	-0.121247	-0.379943

Trt-P=W$(CO)_5$

E = -1707.928486428092 au [$CPCM_{to}$/PWPB95-D3/def2-QZVPP]
ZPE = 0.32127084 au [$CPCM_{to}$/B3LYP-D3/def2-TZVP]
G_{corr} = 0.26404347 au [$CPCM_{to}$/B3LYP-D3/def2-TZVP]

P	0.283935	-0.462649	0.269493	H	-1.857192	0.812139	-0.955394
C	-1.066190	-0.045938	1.530263	C	-0.941162	1.221097	2.352244
C	-0.682311	-1.357274	2.200146	C	-1.259944	1.258783	3.709369
C	0.193001	-1.425561	3.301309	C	-1.201111	2.451480	4.421069
C	0.581259	-2.644262	3.820578	C	-0.839489	3.632259	3.782982
C	0.137309	-3.834534	3.240291	C	-0.560036	3.613804	2.420790
C	-0.698325	-3.792850	2.135077	C	-0.618927	2.419781	1.716438
C	-1.106385	-2.568938	1.616530	H	-1.556939	0.353680	4.220987
H	0.562980	-0.517014	3.747402	H	-1.439803	2.455556	5.477143
H	1.246306	-2.673252	4.673553	H	-0.785241	4.559066	4.339415
H	0.452817	-4.785847	3.648729	H	-0.293464	4.527602	1.905240
H	-1.039021	-4.709105	1.671399	H	-0.420238	2.420682	0.654334
H	-1.778119	-2.540772	0.771496	W	2.579879	0.343652	0.634423
C	-2.461477	-0.056682	0.911772	C	2.099619	2.171175	-0.211775
C	-3.552385	-0.501702	1.659840	O	1.850356	3.188494	-0.670504
C	-4.840129	-0.438896	1.143674	C	2.291155	1.182842	2.503930
C	-5.059166	0.079975	-0.129373	O	2.200891	1.644071	3.546232
C	-3.979722	0.532313	-0.879052	C	3.118178	-1.451420	1.539783
C	-2.691382	0.462004	-0.359435	O	3.424590	-2.433157	2.033525
H	-3.392981	-0.903008	2.652675	C	2.890532	-0.504732	-1.221004
H	-5.673769	-0.793511	1.736693	O	3.076212	-0.978740	-2.245345
H	-6.062499	0.129880	-0.532550	C	4.553991	0.925603	0.619100
H	-4.136761	0.937789	-1.870491	O	5.653617	1.246960	0.601398

3a

E = -2169.025294905502 au [$CPCM_{to}$/PWPB95-D3/def2-QZVPP]
ZPE = 0.43819108 au [$CPCM_{to}$/B3LYP-D3/def2-TZVP]
G_{corr} = 0.37495598 au [$CPCM_{to}$/B3LYP-D3/def2-TZVP]

P	0.202542	0.358029	0.092111	O	2.588067	-3.347912	0.305497
W	2.807581	-0.168542	0.013139	C	2.782160	-0.270595	-2.033293
C	2.982072	1.887201	-0.125761	O	2.887618	-0.312823	-3.177615
O	3.095633	3.023339	-0.207059	C	4.790445	-0.368314	-0.167160
C	3.187207	-0.036203	2.042784	O	5.932979	-0.492011	-0.277130
O	3.542663	0.009291	3.129677	C	-0.679136	0.357807	1.840594
C	2.631488	-2.204881	0.192732	C	-0.924822	-1.084005	2.278615

C	0.158910	-1.918912	2.580979
C	-0.022791	-3.244443	2.938484
C	-1.304796	-3.786267	3.003009
C	-2.392020	-2.976300	2.706879
C	-2.202826	-1.642100	2.352471
H	1.159252	-1.521930	2.528010
H	0.840595	-3.858641	3.160025
H	-1.449799	-4.822577	3.279487
H	-3.397479	-3.375811	2.750783
H	-3.070369	-1.035748	2.141225
C	-1.975653	1.200311	1.832493
C	-2.703661	1.301404	3.025530
C	-3.846376	2.081085	3.109415
C	-4.288340	2.799457	2.000320
C	-3.564932	2.728065	0.819421
C	-2.419221	1.938080	0.740421
H	-2.367160	0.765722	3.902736
H	-4.388948	2.135730	4.044940
H	-5.177637	3.413481	2.064356
H	-3.882838	3.291619	-0.049078
H	-1.853768	1.912631	-0.179313
C	0.258890	1.122808	2.789824
C	0.479496	0.720411	4.105614
C	1.254530	1.490108	4.966914
C	1.828475	2.675424	4.527482
C	1.601775	3.097079	3.221045
C	0.814856	2.334577	2.370885
H	0.049233	-0.200515	4.470748
H	1.414987	1.152215	5.982977
H	2.442541	3.266890	5.194327
H	2.035084	4.021910	2.862187
H	0.621651	2.692694	1.368052
P	-0.883757	-1.164744	-0.988495
C	-0.742647	-2.932255	-0.596777
H	-1.164567	-3.143222	0.381051
H	-1.288323	-3.492623	-1.358270
H	0.301224	-3.230812	-0.608947
C	-0.330166	-1.049672	-2.711261
H	-1.070468	-1.543719	-3.341612
H	0.625887	-1.550604	-2.832445
H	-0.234674	-0.007466	-3.008611
C	-2.669858	-0.847577	-1.065722
H	-2.845769	0.127616	-1.514532
H	-3.132488	-1.622972	-1.677976
H	-3.106278	-0.864085	-0.071709

3b

E = -2286.913779754087 au [CPCM$_{to}$/PWPB95-D3/def2-QZVPP(ecp)]
ZPE = 0.52515392 au [CPCM$_{to}$/B3LYP-D3/def2-TZVP(ecp)]
G_{corr} = 0.45902181 au [CPCM$_{to}$/B3LYP-D3/def2-TZVP(ecp)]

P	0.239355	0.241649	0.176129
W	2.843506	-0.367988	0.054533
C	2.925698	1.598927	-0.567268
O	2.977188	2.689327	-0.914428
C	3.244492	0.197835	2.005170
O	3.627500	0.454252	3.052995
C	2.799854	-2.329436	0.680489
O	2.879239	-3.422569	1.018066
C	2.854539	-1.010221	-1.886485
O	3.000337	-1.384166	-2.965409
C	4.829487	-0.501011	-0.095169
O	5.978356	-0.577586	-0.185470
C	-0.569707	0.260611	1.947694
C	-0.635790	-1.177447	2.455760
C	0.501862	-1.805795	2.975341
C	0.479352	-3.131808	3.381275
C	-0.688204	-3.880419	3.277645
C	-1.827035	-3.276845	2.761477
C	-1.797558	-1.946401	2.358336
H	1.420550	-1.250788	3.067566
H	1.382958	-3.582387	3.770878
H	-0.707619	-4.915775	3.592412
H	-2.747886	-3.839435	2.668270
H	-2.700546	-1.508988	1.963563
C	-1.928434	0.992889	1.959355
C	-2.816144	0.802630	3.023654
C	-4.004443	1.516318	3.105776
C	-4.326114	2.460267	2.135570
C	-3.431710	2.693331	1.099067
C	-2.245543	1.972496	1.019506
H	-2.578654	0.091349	3.801478
H	-4.676513	1.338486	3.935981
H	-5.253151	3.015791	2.197310
H	-3.652282	3.440656	0.346944
H	-1.553387	2.171072	0.213909
C	0.316400	1.177386	2.818066
C	0.442176	0.962910	4.191025
C	1.151528	1.849995	4.991573
C	1.745784	2.977417	4.437241
C	1.604085	3.218169	3.076043
C	0.888841	2.332591	2.281300
H	-0.015370	0.096987	4.646924
H	1.239669	1.655003	6.053008
H	2.306886	3.662678	5.059495
H	2.050653	4.096223	2.626958
H	0.771270	2.549705	1.228438
P	-1.062694	-0.974719	-1.053706
C	-1.356661	-2.768669	-0.810728
H	-2.098304	-2.883394	-0.024786
H	-1.816757	-3.106800	-1.744676
C	-0.108995	-3.574182	-0.474232
H	0.681867	-3.435135	-1.211455
H	0.276698	-3.288199	0.499389
H	-0.352681	-4.636716	-0.440913
C	-0.303335	-0.914106	-2.717562
H	-1.032415	-1.404981	-3.367328
H	0.573771	-1.554651	-2.697956
C	0.041261	0.473818	-3.249758
H	0.444182	0.386006	-4.259674
H	-0.837958	1.117688	-3.290781
H	0.786763	0.964603	-2.627859
C	-2.738759	-0.274841	-1.366400
H	-2.622821	0.807195	-1.401775
H	-2.972157	-0.605074	-2.382336
C	-3.881028	-0.663921	-0.432499
H	-4.015341	-1.744349	-0.383231
H	-3.732338	-0.281554	0.573112
H	-4.809168	-0.233492	-0.811441

3c

E = -2522.716868655404 au [CPCM$_{to}$/PWPB95-D3/def2-QZVPP(ecp)]
ZPE = 0.69533149 au [CPCM$_{to}$/B3LYP-D3/def2-TZVP(ecp)]
G_{corr} = 0.62169089 au [CPCM$_{to}$/B3LYP-D3/def2-TZVP(ecp)]

P	-1.084098	0.543898	-1.445306
P	-0.400588	1.952363	0.042880
C	-2.117222	-0.752935	-0.392937
W	-2.394860	1.896315	-3.331990
C	-3.934541	0.527071	-3.550804
C	-3.210373	2.779749	-4.929889
C	-3.599064	3.039962	-2.120611
C	-1.054993	3.438603	-3.400056
C	-1.182097	0.739287	-4.542705
O	-4.846990	-0.123741	-3.781418
O	-3.679988	3.294365	-5.850978
O	-4.293977	3.720963	-1.510565
O	-0.376523	4.358908	-3.536432
O	-0.509107	0.096248	-5.209551
H	0.934705	-4.546928	2.037256
C	0.340810	-3.777961	1.559867
C	-1.013152	-3.646243	1.858189
H	-1.482836	-4.319106	2.564790
C	-1.771990	-2.661276	1.243769
H	-2.826353	-2.592251	1.472729
C	-1.200745	-1.766167	0.330362
C	0.146384	-1.930106	0.022030
H	0.599508	-1.279937	-0.711498
C	0.912390	-2.920081	0.631667
H	1.959948	-3.015298	0.374262
H	-1.981860	-0.432278	2.375429
C	-2.809487	0.095717	1.929545
C	-3.623617	0.863644	2.757054
H	-3.398371	0.923503	3.814500
C	-4.713810	1.545279	2.234205
H	-5.346736	2.146353	2.874083
C	-4.982153	1.439496	0.872302
H	-5.825312	1.963031	0.440999
C	-4.163922	0.677516	0.053445
H	-4.387103	0.618905	-0.998909
C	-3.050228	-0.006051	0.556266
H	-1.194186	-1.727993	-2.770581
C	-2.204998	-2.059831	-2.573689
C	-2.864248	-1.623666	-1.421060
C	-4.145435	-2.115314	-1.174191
H	-4.676368	-1.818869	-0.281436
C	-4.759591	-2.988929	-2.064648
H	-5.757470	-3.351120	-1.851340
C	-4.104204	-3.390521	-3.221469
H	-4.587220	-4.061932	-3.919676
C	-2.818389	-2.922992	-3.470184
H	-2.288295	-3.230694	-4.362601
C	0.865340	3.020929	-0.734472
C	0.403872	1.162687	1.487830
C	-1.631020	3.142280	0.684615
H	1.444089	3.426601	0.097543
H	0.334315	3.862395	-1.178495
C	1.780844	2.372272	-1.774400
H	0.315556	1.873335	2.309466
C	1.862910	0.741242	1.303544
H	-0.194292	0.294908	1.752119
C	-1.158536	4.097688	1.780262
H	-2.498710	2.579962	1.019196
H	-1.944314	3.706546	-0.194339
H	-0.246299	4.617104	1.472925
H	-0.911970	3.536739	2.685305
C	-2.236787	5.128388	2.117361
H	-2.480961	5.697983	1.215614
C	-1.813083	6.079550	3.232569
H	-3.151584	4.601338	2.404836
H	-0.913882	6.635288	2.954510
H	-1.594468	5.532304	4.153176
H	-2.598408	6.804747	3.453697
H	1.173262	1.998629	-2.598400
H	2.280065	1.501132	-1.347935
C	2.832140	3.345249	-2.314233
H	2.330039	4.223993	-2.728890
H	3.344116	2.860506	-3.149827
C	3.866831	3.778756	-1.276910
H	3.413317	4.339244	-0.456503
H	4.625597	4.421150	-1.727516
H	4.375699	2.911733	-0.847077
H	1.959004	0.126377	0.409383
C	2.390497	-0.048929	2.504388
H	2.488509	1.623994	1.150669
H	1.784889	-0.951227	2.627250
C	2.415317	0.741829	3.810798
H	3.403150	-0.387946	2.268791
H	1.410593	1.013292	4.141075
H	2.991083	1.664833	3.700248
H	2.873337	0.156925	4.610443

8 References

1 W. L. E. Armarego, *Purification of Laboratory Chemicals*, Elsevier, Amsterdam, 5th edn., 2003.

2 G. R. Fulmer, A. J. M. Miller, N. H. Sherden, H. E. Gottlieb, A. Nudelman, B. M. Stoltz, J. E. Bercaw and K. I. Goldberg, *Organometallics*, 2010, **29**, 2176–2179.

3 a) R. K. Harris, E. D. Becker, S. M. Cabral de Menezes, P. Granger, R. E. Hoffman and K. W. Zilm, *Pure Appl. Chem.*, 2008, **80**, 59–84; b) R. K. Harris, E. D. Becker, S. M. Cabral de Menezes, R. Goodfellow and P. Granger, *Pure Appl. Chem.*, 2001, **73**, 1795–1818.

4 R. H. Blessing, *Acta Crystallogr., Sect. A: Found. Crystallogr.*, 1995, **51**, 33–38.

5 G. M. Sheldrick, ShelXS97 and ShelXL97, University of Göttingen, Germany, 1997.

6 O. V. Dolomanov, L. J. Bourhis, R. J. Gildea, J. A. K. Howard and H. Puschmann, *J. Appl. Crystallogr.*, 2009, **42**, 339–341.

7 D. Biskup, G. Schnakenburg, R. T. Boeré, A. Espinosa Ferao and R. K. Streubel, *submitted*.

8 R. S. Stojanovic and A. M. Bond, *Anal. Chem.*, 1993, **65**, 56–64.

9 G. Gritzner and J. Kuta, *Pure Appl. Chem.*, 1984, **56**, 461–466.

10 ORCA -An *ab initio*, DFT and semiempirical SCF-MO package. Written by F. Neese, Max Planck Institute for Bioinorganic Chemistry, D-45470 Mülheim/Ruhr, 2019. Version 4.2.1. Website: https://orcaforum.kofo.mpg.de/index.php.[11]

11 a) F. Neese, *WIREs Comput. Mol. Sci.*, 2012, **2**, 73–78; b) F. Neese, *WIREs Comput. Mol. Sci.*, 2018, **8**, e1327.

12 a) C. Lee, W. Yang and R. G. Parr, *Phys. Rev. B*, 1988, **37**, 785–789; b) A. D. Becke, *J. Chem. Phys.*, 1993, **98**, 5648–5652.

13 F. Neese, F. Wennmohs, A. Hansen and U. Becker, *Chem. Phys.*, 2009, **356**, 98–109.

14 a) A. Schäfer, C. Huber and R. Ahlrichs, *J. Chem. Phys.*, 1994, **100**, 5829–5835; b) F. Weigend and R. Ahlrichs, *Phys. Chem. Chem. Phys.*, 2005, **7**, 3297–3305.

15 D. Andrae, U. Huermann, M. Dolg, H. Stoll and H. Preu, *Theoret. Chim. Acta*, 1990, **77**, 123–141.

16 a) S. Grimme, J. Antony, S. Ehrlich and H. Krieg, *J. Chem. Phys.*, 2010, **132**, 154104; b) S. Grimme, S. Ehrlich and L. Goerigk, *J. Comput. Chem.*, 2011, **32**, 1456–1465.

17 D. Feller, *J. Comput. Chem.*, 1996, **17**, 1571–1586.

18 a) L. Goerigk and S. Grimme, *J. Chem. Theory Comput.*, 2011, **7**, 291–309; b) L. Goerigk and S. Grimme, *Phys. Chem. Chem. Phys.*, 2011, **13**, 6670–6688.

19 F. Weigend, F. Furche and R. Ahlrichs, *J. Chem. Phys.*, 2003, **119**, 12753–12762.

20 a) V. Barone and M. Cossi, *J. Phys. Chem. A*, 1998, **102**, 1995–2001; b) M. Cossi, N. Rega, G. Scalmani and V. Barone, *J. Comput. Chem.*, 2003, **24**, 669–681.

21 G. Schreckenbach and T. Ziegler, *J. Phys. Chem.*, 1995, **99**, 606–611.

22 a) J. P. Perdew, K. Burke and M. Ernzerhof, *Phys. Rev. Lett.*, 1996, **77**, 3865–3868; b) J. P. Perdew, K. Burke and M. Ernzerhof, *Phys. Rev. Lett.*, 1997, **78**, 1396.

23 A. Gese, S. Kermanshahian, G. Schnakenburg, Z. Kelemen, L. Nyulaszi, A. E. Ferao and R. K. Streubel, *Inorg. Chem.*, 2021, **60**, 13029–13040.

24 T. Lu and F. Chen, *J. Comput. Chem.*, 2012, **33**, 580–592.